Nanowire Alignment: Techniques, Quantification, and Applications in Large-Area Devices

by
Jianjin Dong

A thesis
presented to the University of Waterloo
in fulfillment of the
thesis requirement for the degree of
Doctor of Philosophy
in
Electrical and Computer Engineering

Waterloo, Ontario, Canada, 2018

Examining Committee Membership

The following served on the Examining Committee for this thesis. The decision of the Examining Committee is by majority vote.

External Examiner

Name: Jun Yang

Title: Professor of Mechanical & Materials Engineering at Western University

Supervisor

Name: Irene A. Goldthorpe

Title: Professor of Electrical & Computer Engineering at University of Waterloo

Internal Member

Name: Bo Cui

Title: Professor of Electrical & Computer Engineering at University of Waterloo

Internal Member

Name: William Wong

Title: Professor of Electrical & Computer Engineering at University of Waterloo

Internal-external Examiner

Name: Ting Tsui

Title: Professor of Chemical Engineering at University of Waterloo

Author's Declaration

I hereby declare that I am the sole author of this thesis. This is a true copy of the thesis, including any required final revisions, as accepted by my examiners. I understand that my thesis may be made electronically available to the public.

Abstract

Nanowire alignment is essential for their integration into large-area devices, as well as to obtain certain functionality such as the ability to polarize light and increase surface-enhanced Raman scattering. Various nanowire alignment methods have been developed, however, major drawbacks have limited their application such as complex processing, high cost, limited compatible nanowire materials, and limited scalability. In addition, the methods used to quantify the quality of nanowire alignment are lacking in accuracy, speed, and applicability to all kinds of nanowires. In this thesis, two simple and large-area alignment methods are studied that are applicable for nanowires synthesized by any method and compatible with large-area electronic device fabrication processes. The first method is accomplished by depositing nanowires on polyvinyl alcohol films followed by film stretching, which achieves high-quality alignment (with an order parameter S=0.93). Nanowire breakage, which is commonly encountered in similar techniques, is minimized and the average length of nanowires after alignment is nearly the same (~99.3%) as before alignment. The second alignment method is accomplished directly during rod-coating deposition of the nanowires, without the need of any additional step. Two image processing methods based on edge-detection and skeletonication are presented to recognize nanowires from microscopy images. Then an order parameter and an orientational distribution function are used for alignment quantification. Compared with previously reported studies, these methods are fast and automated, reliable without bias, generally applicable, easy to implement, and computationally efficient.

The alignment methods described above are applied in two applications. Firstly, the electrical and optical anisotropy of slightly aligned silver nanowire films, which can be used as transparent electrodes, are investigated. Their transparency to polarized light is increased by 7.3 percentage points compared to typical randomly oriented silver nanowire films, which may benefit end uses such as liquid crystal displays and the touch sensors on top of them. Secondly, a crossed film structure consisting of semiconductor nanowires aligned in one direction and metal nanowires orthogonally aligned is designed. The metal nanowires are intended to act as interconnects to substantially reduce semiconductor nanowire-nanowire junction resistances while avoiding lithographically-defined metal pads, the latter which can have poor mechanically flexibility and involve fabrication processes not desired for large-area electronics. Such a device structure can be developed further for use in large-area flexible devices such as light, strain and chemical sensors and energy generators.

Acknowledgement

First of all, I am extremely grateful to my supervisor, Prof. Irene A. Goldthorpe for her continuous guidance and strong support during my PhD study. The opportunities she granted me are invaluable to my success. Her research style and rigorous attitude will have an influence on me throughout my life. With her help and open-mindedness, I gradually explored my potentials and found my strengths, which is another valuable thing I harvested from my PhD study. I enjoy everyday during my study here since she creates an active and peaceful research atmosphere for me.

I would like to thank Prof. Bo Cui, William Wong, Ting Tsui, and the external committee member, Prof. Jun Yang for all of their contribution to this thesis. Besides, my committee members, I would thank Prof. Nasser Abulkhdeir for all his contribution to my image processing work.

I would thank Waterloo Institute of Nanotechnology (WIN), which provides me a multidiscipline research atmosphere, which contributes to my diversified views and ideas.

I am thankful to all of my colleagues, Marwa Abd-Ellah, Jonathan Atkinson, Mina Abdelmalek, Alexandra Madeira, Geoffery Deignan, Hadi Hosseinzadeh Khaligh, Nupur Maheshwari, Yahya Atwa, Adrian Yabut for their help and discussions.

I would like to thank all my family members, such as my parents and my wife, for their support and patience.

Dedication

This thesis is dedicated to my parents and my wife Qianzhu Wu.

Table of Contents

List of Figures

List of Tables

Chapter 1 Introduction

1.1 Nanowires

Nanowires (NWs) represent a broad class of one-dimensional (1D) nanostructures that have received intense and continually growing interest for more than 20 years [1][2]. NWs have diameters of about 100 nm or less and lengths of several microns or more. NWs are often single-crystalline, and can be semiconducting, insulating, or metallic [3]. NWs of many materials including germanium [4], silicon (Si) [5], indium phosphate [6], gallium arsenide [7], gold [8], silver (Ag) [9], and nickel have been successfully synthesized [10]. They can be rationally and predictably synthesized in single-crystal form with key parameters controlled during growth including chemical composition, length, diameter, growth direction and dopant concentration [11]. NWs represent different advantages compared to the most popular 1D nanostructure, carbon nanotubes, such as the range of available materials, more-controllable morphology and tailored electrical properties. NW applications have been extensively explored in areas such as electronics (e.g. thin film transistors, transparent electrodes), photonics (e.g. polarizers, light emitting diodes), sensors (e.g. ultraviolet light, gas sensors), and photovoltaics. [3][12].

1.2 Nanowire synthesis

NWs can be synthesized in one of two distinct approaches: top-down and bottom-up.

In the top-down approach, small features are patterned in bulk materials by a combination of lithography and etching. However, improvements in resolution are associated with a near-exponential increase in cost and other scientific challenges exist such as making nanostructures with near-atomic perfection [3]. In this thesis, we focus on semiconductor and metallic NWs synthesized using the bottom-up approach, where structures are assembled from their subcomponents in an additive fashion. Below, the bottom-up semiconductor and metallic NW syntheses most pertinent to this thesis are reviewed.

1.2.1 Semiconductor nanowire synthesis

Bottom-up synthesis routes using both gas-phase and solution-phase chemistry have enabled a variety of semiconductor materials systems and morphologies to be obtained with control of the dimensions, composition, crystallinity and chemical properties. [12]. The vapor–liquid–solid (VLS) method is the most widely adopted approach to grow semiconductor NWs because of its flexibility, control over dimensions, and the ability to obtain quality crystalline material [5]. During this process, the metal nanoclusters are heated above the eutectic temperature for the metal–semiconductor system of choice. In the presence of a vapor-phase source of the semiconductor, a liquid droplet of the metal/semiconductor alloy is formed. The continued feeding of the semiconductor reactant into the liquid droplet supersaturates the eutectic mixture, leading to nucleation of the solid semiconductor. The solid–liquid interface forms the growth interface, which acts as a sink causing the continued

semiconductor incorporation into the lattice and, thereby, the growth of the desired NW [5], as shown in figure 1.1.

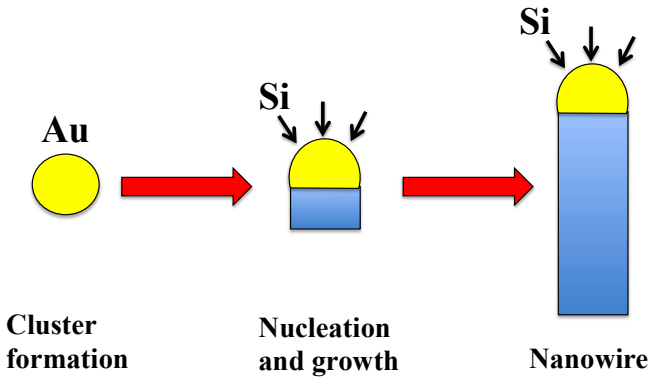

Figure 1.1 Schematic of vapor–liquid–solid growth of a silicon nanowire, where a liquid alloy droplet of gold/silicon is first formed. The continued feeding of silicon from the vapor phase into the liquid alloy causes an oversaturation of the liquid alloy, resulting in solid silicon nucleation and the directional growth of a nanowire.

Various approaches can be executed to allow the gaseous semiconductor reactants to be generated such as chemical vapor deposition (CVD) [13][14], pulsed laser ablation [15], and molecular beam epitaxy (MBE) [16].

1.2.2 Metal nanowire synthesis

Although metal NWs can also be synthesized in the gas phase, they are instead most commonly synthesized by solution-based methods at low temperatures (<200 °C). This makes them easier to be commercialized due to the synthesis being less capital-intensive and significantly easier to scale-up compared to vapor-phase processes [9]. All solution-phase syntheses of NWs are quite similar in that they require a reducing agent to convert metal ions into metal and a capping agent to direct anisotropic assembly of the metal atoms into NWs. Since AgNWs are used

extensively throughout this thesis, their synthesis is summarized below. Other metal NWs, such as gold or copper NWs, can be synthesized using a similar method but with different reducing agents, temperatures, and pH values [17][18].

***Silver nanowires**:* Generally speaking, AgNWs can be synthesized in solution through a one-pot reduction strategy in which Ag precursors are slowly added to a reaction system, or a seed-mediated two-step strategy in which the nucleation and growth steps are well separated [19]. Polyol reduction of $AgNO_3$ with assistance of a polymeric surfactant, most commonly polyvinylpyrrolidone (PVP), developed by Xia et al. represents one of the most successful methods for the synthesis of high quality AgNWs in large quantity and variations of it are widely used for commercial production of AgNWs [20][21].

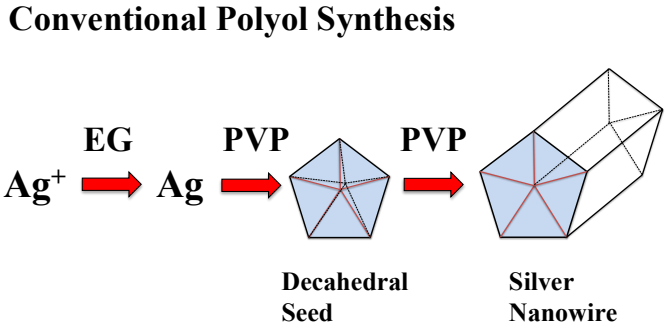

Figure 1.2 Conventional polyol synthesis of silver nanowires. EG = ethylene glycol, PVP = polyvinylpyrrolidone.

This synthesis involves the reduction of Ag ions using hot ethylene glycol (EG) in the presence of PVP, a polymeric capping agent (figure 1.2). PVP is thought to preferentially adhere to the sides of the nanorods, leaving their ends open to atomic addition [22]. Ag atoms add to the end facets which then leads to the rapid anisotropic growth of NWs. The resulting NW has a pentagonal cross-section, consisting of 5

crystalline regions separated by a twin boundary.

1.3 Nanowire applications in flexible large-area electronics

Because of the use of high-throughput, lower-cost deposition processes (compared to conventional Si electronics), large-area electronics can dramatically lower the cost of electronic devices as well as permit them to be integrated with mechanically flexible substrates. As such, it is a growing area which enables new applications from personal wearable devices (e.g. wearable health monitoring devices) [23] to wearable sensors (e.g. electronic skin, biomedical devices) [24] and smart tagging of products with radio-frequency identification tags [25]. Major interest has appeared specifically in the display industry, with one goal to develop flexible and/or rollable displays deployable on demand to be integrated with portable devices (e.g., smartphones and tablets) [26]. The requirements for flexibility and compatibility with plastic substrates limit the process temperature to be lower than 300°C, a formidable challenge for the fabrication techniques especially in the choice and quality (e.g. crystallinity, electrical properties) of materials [27].

A single crystalline substrate is required to deposit crystalline semiconductor thin films and thus crystalline films cannot generally be achieved on plastic substrates. Thus materials such as amorphous Si are used which have far lower electronic mobility than their crystalline counterparts, resulting in lower performing devices than conventional electronics. Single-crystalline semiconductor NWs, on the other hand, can be synthesized directly on plastic, or grown in solution or on a different substrate

and easily transferred to plastic (or textiles [28] or paper [29]). Because they are crystalline, SiNWs, for example, have an electron mobility of ~500 cm^2/Vs versus ~0.5 cm^2/Vs of amorphous Si thin films [30][31]. Therefore, NWs represent an opportunity to obtain crystalline and high quality semiconductor material on plastic. Furthermore, NWs provide much more mechanical flexibility than thin films, including amorphous Si thin films, and are thus more suitable for bendable and flexible devices [32]. Likewise, crystalline metal NWs, which can be used as electrical interconnects, can also be synthesized in solution in large volumes at low cost. In both the semiconductor and metallic cases, very small feature sizes can be obtained without lithography. Deposition of NWs can be done using high-throughput roll-to-roll compatible methods like rod coating [33], spray coating [34] and inkjet printing [35]. And importantly, NWs and films of NWs are mechanically flexible [36], unlike most of their thin-film counterparts, and if sparse enough can be optically transparent [37]. With the wide variety of NWs materials available, nearly any electronic device can be constructed with NWs. Therefore, bottom-up synthesized NWs are well suited for flexible large area electronics. However, to be able to integrate NWs into such devices, developing a cost-effective NW alignment/assembly method over large areas is of high need.

1.3.1 Large-area semiconductor nanowire devices

Up to now, semiconductor NWs have been used as the active region in field-effect transistors (FETs) [38][39], computational circuits [40], light emitting diodes (LEDs)

[41], a wide variety of sensors [42][43], nanolasers [44], nanogenerators [45], and nanoresonators [46]. Many devices in the literature are based on a single NW. A typical fabrication method of single semiconductor NW devices is described in the following text. Contact pads are predefined on substrate using photolithography. After dispersing NWs on the substrate, NWs can be located using a microscope and connections from the NWs to the contact pads can be formed using electron beam lithography or a focused ion beam [47]. Figure 1.3 is a schematic diagram of a zinc oxide (ZnO) single NW device for a chemical sensor application. Chemisorbed gas molecules on a metal-oxide surface may withdraw or donate electrons to the conduction channel, resulting in a measurable change in the conductivity of the NW [48].

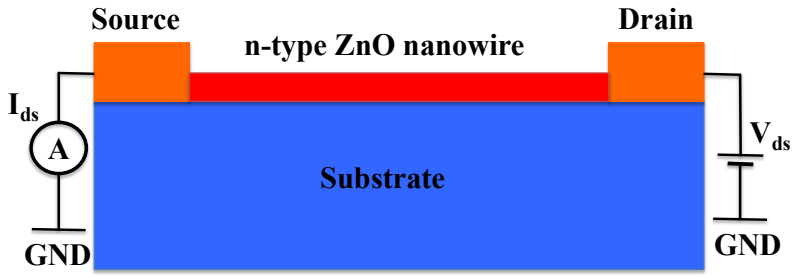

Figure 1.3 Schematic diagram of a single nanowire device.

Fabricating single NW devices as described above may be suitable for studying NW physical or chemical properties, or for testing proof-of-concept devices. However, the fabrication methods of single-NW devices are not suitable for scalable large-area devices or scalable devices using solution-synthesized NWs at low cost. Moreover, due to a large variability between NW properties, there is a lack of reproducibility

from one single NW device to another which is problematic for applications [49]. There are two main approaches for assembling devices with multiple NWs working in tandem as the active area [32][50]. Firstly, an inexpensive, scalable method is to deposit the NWs as a random mesh, as shown in figure 1.4.

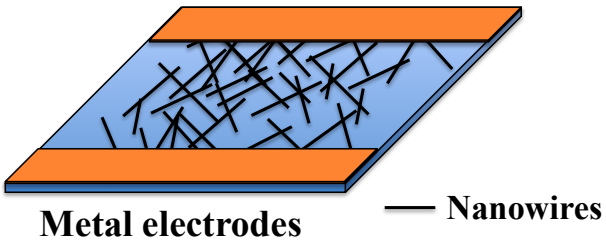

Figure 1.4 Schematic of a large-area nanowire mesh device.

The NW mesh in the middle of the device is used as the active region. These random NW networks can be deposited by various solution-deposition techniques such as rod coating, spray coating, slot-die coating, and inkjet printing [33][34][35][51]. Metal electrodes can be deposited by thermal evaporation [52]. Unlike single NW devices, of which signals are low and susceptible to environmental conditions, NW mesh devices, which have also been called NW networks or nanonets, produce higher and steady signals [32]. Their fabrication is relatively cheap as no lithography is required, and it is scalable to large areas. Comparing with typical thin film devices, NW mesh devices provide a wide-range of crystalline material to choose from while also having higher surface area, more mechanical flexibility and optical transparency.

Even though large-area NW mesh devices have been used for UV sensors [52], chemical sensors [53][54], biological sensors [55][56], and thin-film transistors (TFTs) [57][58][59], the utilization of these devices faces several limitations. First, the sheet

resistance is high due to the high junction resistance of overlapping individual semiconductor NWs. A mesh of degenerately-doped SiNWs, for example, is non-conductive due to the junction resistances [60]. Unlike metal NWs, semiconductor NWs cannot be easily fused to achieve a low contact resistance. This results in a small current for a given voltage, which is undesirable for device applications because it is hard to measure and easily susceptible to environmental conditions or equipment. A sintering process has been reported to reduce the junction resistances in a SiNW network used in a TFT [58]. However, the sintering temperature is 400 °C, exceeding the thermal budget of most commonly flexible substrates, for example, polyethylene terephthalate (PET). Because a major advantage of NW meshes is their flexibility, the ability to process the film on plastics is important. Secondly, the random NW networks are not suitable for some applications such as piezoelectric energy generation devices which are strongly dependent on NW orientation [45].

In order to realize a more functional device on a large scale in a cost effective way, assembly of NWs with controlled orientations is required [61]. And metal contacts are needed between single NWs to avoid high semiconductor-semiconductor NW junction resistance. One previous study implemented this by utilizing aligned SiNWs as a strain sensor [50], which is shown in figure 1.5. From the image we can see that the metal contacts take up a large portion of the total device area (54%), and only about half the NWs are connected on either end by the metal pads.

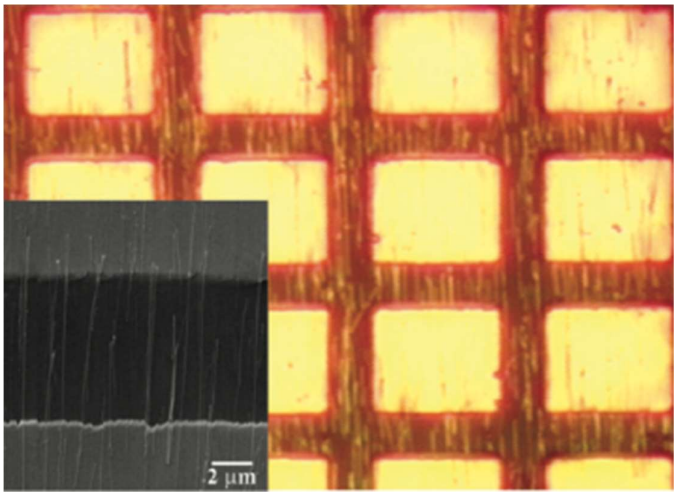

Figure 1.5 Optical microscopy image of a large-area aligned silicon nanowire device where metal pads are used for interconnections between nanowires. Inset: a scanning electron microscopy image of the nanowires between two metal electrodes [50]. (Reprint permitted by American Chemical Society)

In general, to fabricate such an aligned NW device, NWs are first synthesized in solution or on a substrate and aligned using one of the various methods of alignment to be discussed in chapter 1.4. Second, aligned NWs are transferred to the desired substrate if needed. Third, metal pads are defined by lithography and deposited by thermal evaporation to make electrical connections between NWs. This kind of device suffers several drawbacks. First, a common challenge of NW devices on polymer substrates is the contact between the NW and the evaporated electrodes; the contact resistance can change under stretching or bending [62][63]. If a tensile or compressive strain greater than 3% was applied to the sensors, the I-V curve did not return to its original state. The metal pads, which have dimensions on the order of 20 × 15 μm^2, likely cannot tolerate bending, causing some delamination and thus degradation of the NW-metal contact. Therefore, these devices cannot be used in flexible device applications which is one of the main areas where large-area NW devices excel.

Second, the lithography and metal deposition requires expensive facilities and a complicated fabrication process, which is not desired for large-area device applications. Third, electrical signals are measured between adjacent metal pads, limiting device size to be smaller than the length of a nanowire and not relevant to large-area.

To overcome the drawbacks with both NW meshes and aligned NW devices, in chapter 5, I design and fabricate another kind of device. The semiconductor NWs are aligned, but metal NWs instead of lithographically defined metal pads are used as interconnects. Because the metal NWs are very mechanically flexible, the devices will be as well, and the process of synthesizing and depositing the NW contacts is also simpler and less expensive than lithographically-defined metal pads.

1.3.2 Metal nanowire transparent electrodes

Transparent electrodes are films that are both optically transparent and electrically conductive. They are required in many optoelectronic devices such as liquid crystal displays (LCDs), organic solar cells, and organic light emitting diodes (OLEDs) [64]. Transparency and sheet resistance are the two most important factors of transparent electrodes. An electrode with a high transparency and a low sheet resistance is desirable. To efficiently evaluate and compare the performance of transparent electrodes, figures of merit (FoM) are often used. The classic FoM definition of Haacke is described in the following formula [65]:

$$FoM=\frac{T^{10}}{R_s} \tag{1.1}$$

where T is the electrode optical transparency at 550 nm and R_s is the sheet resistance. The larger the FoM value, the better the performance is.

At this time, the most common materials used for transparent electrodes are metal oxides, most particularly indium tin oxide (ITO). However, ITO is expensive, and because it has limited mechanical flexibility and requires high temperatures and vacuum for deposition, it is a problematic material for use in large-area flexible electronics. Random meshes of metal NWs, in a configuration depicted in figure 1.4, can be utilized as an alternative transparent electrode material since the connected metal NWs form conductive pathways and the mesh is transparent to visible light if it is sparse enough [66][67]. Unlike in semiconductor NW meshes, the junctions of metal NWs can be welded through annealing or mechanical pressure, resulting in relatively low junction resistances and thus a low sheet resistance of the film [36][68]. AgNW transparent electrodes can achieve conductivity and transparency values similar to or even better than ITO, especially on plastic substrates. At the same time, unlike ITO, metal NW films can be deposited at room temperature without the requirement for vacuum using roll-to-roll compatible techniques such as rod or spray coating or printing. They are also mechanically flexible and can even be made to be stretchable [9][69]. Therefore, AgNW electrodes have received intense interest in the past few years as an enabling material for flexible, printable optoelectronic devices.

The vast majority of studies on AgNW transparent electrodes involve randomly placed NWs. However, it has been shown that NW alignment can decrease electrode

sheet resistance [70]. This is because imparting some NW alignment results in a lower number of overlapping NW junctions which although relatively low compared to the junction resistance of semiconductor NWs, is still higher than the resistance of the metal NWs themselves. While previous studies showed that alignment can increase electrical conductivity, in chapter 4, I study how alignment can also be utilized to achieve a higher transparency to linear polarized light within visible wavelength range, applicable to devices such as LCDs and the touchscreens on top of them.

1.4 Nanowire alignment methods

Essential for the large-area integration of NW based devices, whether the active area is based on a single NW or multiple NWs, is the assembly of these 1D nanomaterials using alignment techniques that are controllable and scalable. Generally, such techniques should enable assembly of uniform, large-area NW arrays with control of density [71]. Ideally, such techniques should be applicable to NWs synthesized by both wet and dry methods, compatible with transfer processes and ideally roll-to-roll processes. Moreover, such techniques are recommended to be simple, cheap, not destructive to the NW structure and require no complicated fabrication steps. Till now, researchers have developed a variety of NW assembly methods. The advantages and disadvantages of each technique are briefly reviewed below then summarized in table 1.1.

1.4.1 Microfluidic alignment

The motion of a fluid can create a shear force against a solid boundary, and this effect

results in aligning NWs suspended in a solution [72]. The orientations of the NWs will be aligned according to the flow direction of the fluid through microfluidic channels, commonly made of polydimethylsiloxane (PDMS), as shown in figure 1.6. One of the critical disadvantages of this method is that the fluidic-directed alignment can only extend over several hundreds of micrometers, as it is restricted by the size of the microfluidic channels, and thus it is not suitable for large-area devices.

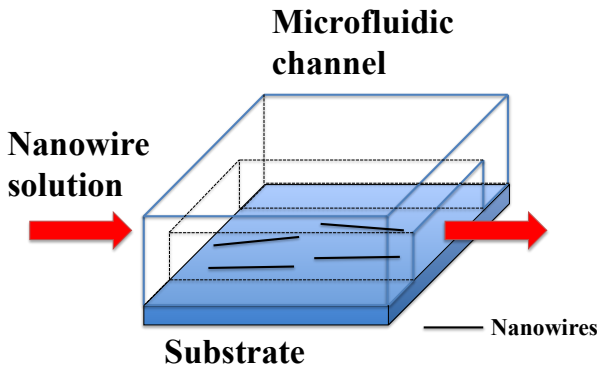

Figure 1.6 Schematic of parallel nanowire arrays obtained by passing nanowire solution through a microfluidic channel on a substrate.

1.4.2 Langmuir-Blodgett alignment

The Langmuir Blodgett (LB) technique is usually utilized to deposit organic monolayers from the surface of a liquid onto a solid substrate by immersing a substrate into the liquid to form films with a high degree of ordering [73]. To perform assembly of NWs using this technique, NWs are typically functionalized by surfactants in order to form stable suspensions in an organic solvent [74]. The process of the LB technique, as shown in figure 1.7, can be briefly described as follows [75]. A NW surfactant monolayer is first formed on a liquid surface in a LB trough (figure 1.7(a)). Then a barrier compresses the NW monolayer, as shown in figure 1.7(b). The

NWs are aligned as parallel arrays with their longitudinal axes perpendicular to the compression direction. A dipping technique is then used to deposit the monolayer of aligned NWs onto a substrate [76][77]. Although the LB technique has demonstrated its versatility for NW alignment, the disadvantages of this technique rest in several aspects: the difficulty of the NWs surface functionalization, the LB slow process, the need for rigid control of conditions, and the non-uniform density of the resulting aligned NW arrays.

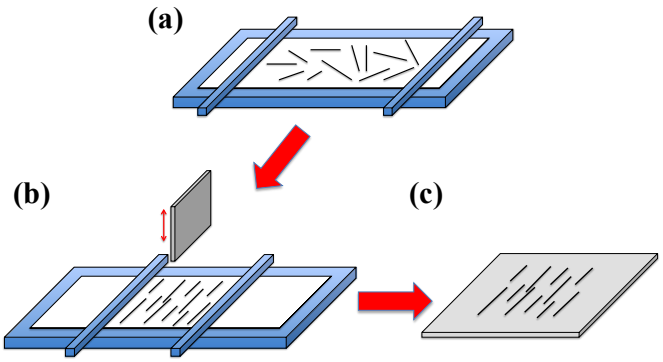

Figure 1.7 Schematic diagram of Langmuir Blodgett assembly of a paralleled nanowire film. (a) Random nanowires suspended in the Langmuir Blodgett trough. (b) Wafer being pulled vertically from the suspension in parallel with the lateral motion of the barrier. (c) Resulting parallel nanowire array on the substrate.

1.4.3 Bubble-blown technique

The shear force created by the expansion of a bubble-blown film can also be utilized for assembly of NWs. Briefly, a polymer suspension of NWs is first prepared then dispersed on a circular dye followed by blowing the NW suspension into a bubble at a controlled pressure and expansion rate (figure 1.8) [78]. During this process, the expansion triggers the shear force to align more than 85% of the NWs along the upward expansion. Then the NWs can be transferred to rigid or flexible substrates by

bringing them in contact with the bubble. However, due to the bubble expansion, it is challenging to achieve a close pack of NWs; for example, in one study the NW density was modest at □0.04 NWs/μm^2 [78]. This technique is not scalable to very large areas and requires functionalization of the NW surfaces.

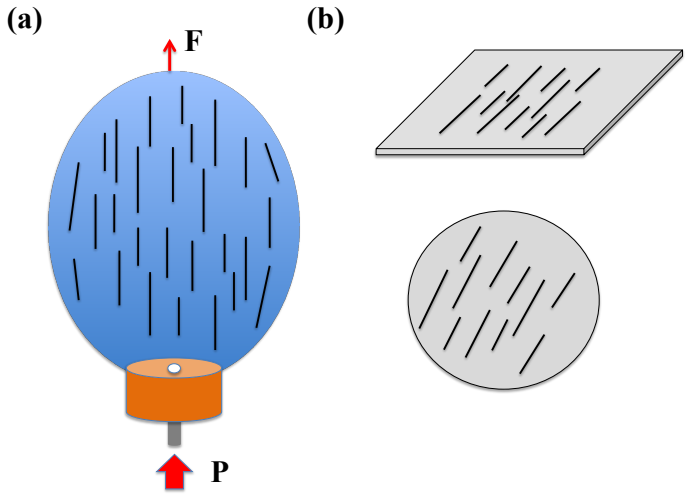

Figure 1.8 Schematic diagram of the blown bubble film process. (a) Bubble expansion over a circular die and (b) films transferred to arbitrary substrates, such as thin films or wafers.

1.4.4 Electric/magnetic field-assisted alignment

Both electric and magnetic fields have been successfully utilized to direct the alignment of the suspended NWs within a solution as illustrated in figure 1.9 [79][80][81]. An applied electric field can be used to attract and align NWs normally through dielectrophoresis forces, which are exerted on dielectric NWs through induced dipoles [82]. For the magnetic field alignment technique, NWs composed of ferromagnetic and superparamagnetic materials can be guided by external magnetic fields. A major disadvantage of these techniques is that they are only appropriate for certain kinds of NWs (e.g. metallic or ferromagnetic NWs). While alignment of

non-magnetic NWs has been demonstrated by attaching iron oxide nanoparticles to the surface of the NWs [83], for example, introducing additional material is often not desired as it can interfere with the performance of the end device. Also, these techniques require prefabricated micro-electrode arrays to generate the electric or magnetic field; this can increase the complexity of the process and limits its scalability.

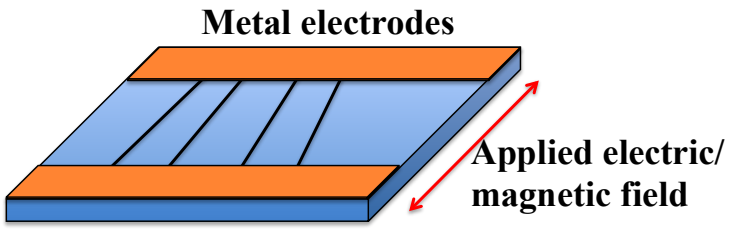

Figure 1.9 Schematic of nanowire alignment driven by an electric or magnetic field.

1.4.5 Contact printing

A convenient contact printing technique for wafer-scale assembly of aligned and high-density NW arrays has been reported [84][85]. As shown in figure 1.10, NWs that have been grown on a substrate are placed upside-down on a receiver substrate. During contact sliding of the NW substrate, the NWs are realigned by the sliding shear force and detach from the donor substrate. This results in the NWs being highly aligned parallel to one another on the receiver substrate. However, a major disadvantage of the contact printing method is that it is only applicable for alignment of NWs grown on substrates, which is not the case for most metal NW syntheses and some semiconductor syntheses as well. Scalability to large areas is also an issue.

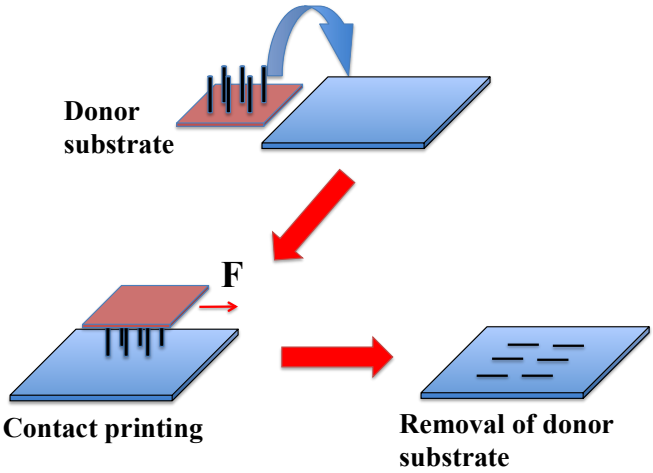

Figure 1.10 Schematic of the process flow for contact printing of nanowire arrays.

1.4.6 Stretching nanowire-polymer composites

A simple method for alignment of NWs by unidirectional stretching has been developed as illustrated in figure 1.11 [86][87]. Similar to fluidic-assisted NWs alignment and contact printing techniques, this method also uses shear forces to align NWs, which are embedded in a polymer. As the stretching ratio increases, NWs embedded in the transparent polymer film tend gradually toward directional alignment by the external force [88]. The disadvantage of this alignment method is that NWs are all embedded in the polymer rather than on the surface. Thus, it is impossible to access those aligned NWs for further device integration, limiting applications.

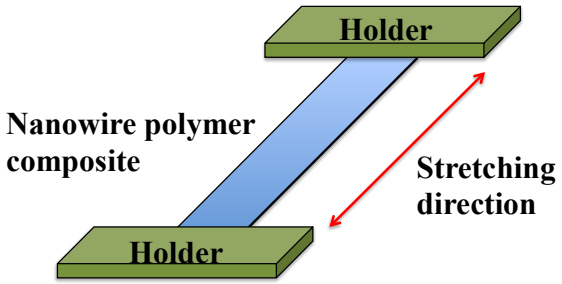

Figure 1.11 Schematic of nanowire alignment by stretching nanowire-polymer

composites.

1.4.7 Substrate contraction/stretching

To avoid the limitation of stretching NW-polymer composites, in which NWs are embedded in the composite and thereby cannot be utilized for device integration, a strain-release assembly method has been reported which utilizes a PDMS surface to align NWs as shown in figure 1.12 [50][61]. The NWs were deposited on top of a pre-strained substrate. When the strained substrate was released, the NWs aligned in the transverse direction and the areal coverage of the NWs on the substrate increased. The elasticity of the substrates and the static friction between the NWs and the substrates play important roles in this alignment process. However, the alignment result is moderate and a second strain release which also requires a NW transfer process is needed for a good alignment, which makes this alignment technique complex.

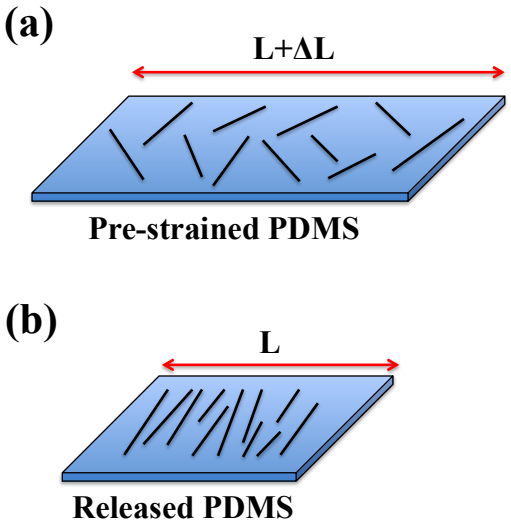

Figure 1.12 Schematic of strained-substrate nanowire alignment process. (a) Polydimethylsiloxane was mechanically stretched followed by nanowire deposition on it. (b) The strain of the substrate was released to achieve nanowire alignment.

Unlike the above strain-release assembly of NWs, which relies on repeated operation of material transfer to pre-strained substrates and strain release to obtain good alignment, another simple alignment method has been developed. This method is based on a simple one-step stretching of a PDMS substrate coated with NWs (figure 1.13) [89]. During the stretching process, the randomly orientated nanostructures gradually transform to aligned arrays. Subsequently, these stretching-aligned 1D nanostructures can be transferred to other rigid or flexible substrates. This inexpensive method can be applied to NWs of all materials synthesized either in solution or on a substrate. The disadvantage of this alignment method is that PDMS is only capable of a small stretching ratio which limits the quality of alignment. Also, strained PDMS films tend to shrink back to its original state, which makes their alignment even worse.

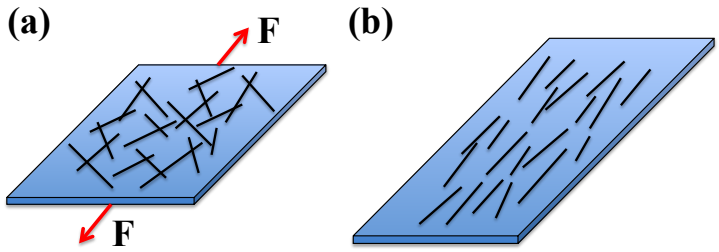

Figure 1.13 Schematic of the process flow of using substrate stretching to align nanowires. (a) Nanowires deposited on an elastic polydimethylsiloxane films without stretching. (b) Nanowire alignment after substrate stretching.

1.4.8 Capillary printing

Another example of a simple NW alignment method is the capillary method, where NW solution is deposited at one end of a substrate, then aligned by dragging a nanopatterned PDMS stamp overtop (figure 1.14) [90]. Alignment is achieved both

through the shear forces of the NW solution flow between the PDMS nanochannels and an evaporating air-liquid-meniscus line. However, the aligned NWs may suffer from non-uniform distribution because NWs forced through channels would lead to striped patterns. And this alignment technique requires fabrication of nanopatterned PDMS stamps, which is complicated, expensive, and not compatible with roll-to-roll process.

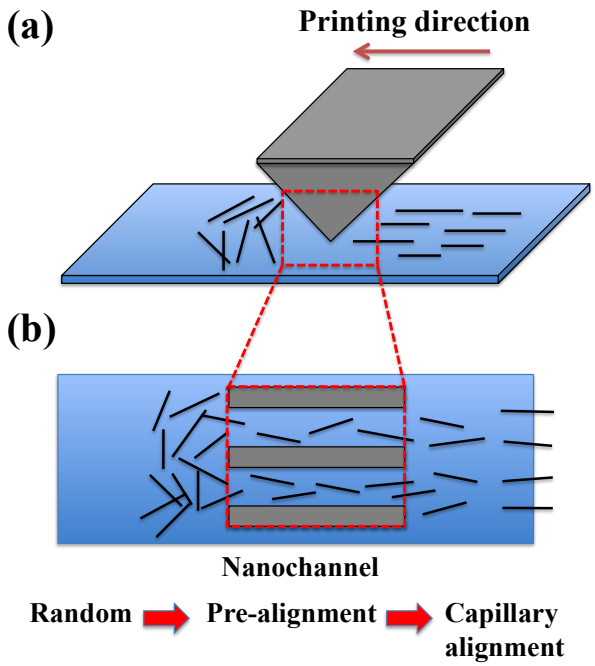

Figure 1.14 Schematic of the capillary printing process using a nanopatterned polydimethylsiloxane stamp to produce highly aligned nanowire arrays. (a) Side view. (b) Top view.

1.4.9 Summary of nanowire alignment methods

The advantages and disadvantages of the primary NW alignment methods are summarized in Table 1.1.

Table 1.1 A summary of the advantages and disadvantages of various nanowire alignment methods.

NW assembly technology	Advantages	Disadvantages	Ref.

Flow-assisted alignment	Parallel and crossed NWs arrays can be assembled Applicable to many NW materials	NWs only assembled over small areas Requires microfluidic channel fabrication Difficult to achieve high density of NW arrays	[40], [72]
Langmuir-Blodgett alignment	Large area alignment Applicable to many NW materials	The assembly process is slow and has to be precisely controlled NWs need to be functionalized with surfactant	[76], [91]
Bubble-blown technique	Compatible with both rigid and flexible substrates	Requires functionalization of NW surface Not scalable to very large areas Complicated set-up	[78]
Electric/magnetic field-assisted alignment	NW can be placed at specific locations	Not scalable Need to pre-pattern electrodes NW materials are limited Alignment poorer than other method since field-lines are curved	[79], [81]
Contact printing	Large area Simple and economical	Not applicable to NWs grown in solution NW breakage occurs even with the use of lubricant	[84]
Stretching NW-polymer composites	Uncomplicated fabrication process	NWs are embedded in nanocomposite and cannot be accessed	[86], [87]
Substrate contraction/ stretching	Large area Density controllable Applicable to many NW materials Uncomplicated fabrication process	Alignment result is not good due to the low stretching ratio of PDMS Substrate returns to the undeformed state without applied force,	[50], [89]

		necessitating a transfer step. NW breakage	
Capillary printing	Large area Simple method without releasing or stretching substrate	Non-uniform NW area density Requires fabrication of PDMS nanochannel	[90]

According to the above drawbacks, there is a critical need to have an alignment method which is: (i) applicable to both substrate-grown and solution-grown NWs, (ii) economical and appropriate for large areas, (iii) compatible with a roll-to-roll process and requires no complicated fabrication processes, and (iv) minimal NW breakage. Based on these requirements, two simple and large-area alignment methods are developed illustrated in chapter 3.

1.5 Nanowire alignment quantification

Since NW alignment is becoming more crucial for applications, a method of determining whether the NW alignment is good or not is in demand. Not only important for device integration, the quality of the NW alignment has been shown to also affect many useful materials properties such as the ability to polarize light and increase surface-enhanced Raman scattering [92][93]. A standard, fast, and generally applicable NW alignment quantification method is required for comparing alignment quality between different methods, optimizing alignment process/parameters within one method, and for quality control in a manufacturing process. Till now, researchers have developed a few NW alignment characterization methods, which are briefly introduced below.

1.5.1 Manual measurement

Most commonly, NW alignment in the literature is characterized by taking a microscopy image and measuring each individual NW angle in the image manually (i.e. by hand) using an angle protractor. The alignment result is typically presented in an angular distribution histogram [72][78][89]. Obviously, measuring NW alignment manually one-by-one is time consuming, which limits the number of NWs that can be measured. It is also inaccurate, being nearly impossible to execute without bias.

1.5.2 Polarization method

The fact that aligned metal NWs can polarize light has been utilized to characterize NW alignment, which is faster than measuring NW alignment angles manually [86]. As shown in figure 1.15, transmittance of a AgNW-polymer composite after stretching by 100%, 150% and 200% showed a slight transparency difference of up to 5–10% [86]. These differences of transmittance can be used for determining the quality of alignment. However, the polarization method works only for metal NWs and NW alignment is not the only aspect that affects the polarization result. Other factors such as NW length, diameter, and material affect the extent of polarization which makes this alignment quantification method unusable for comparing samples of different NWs.

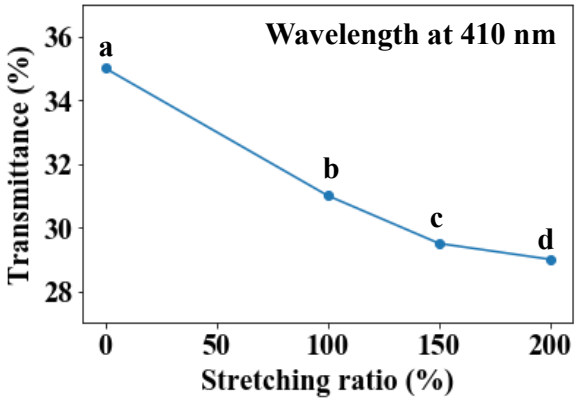

Figure 1.15 Optical transmittance of silver nanowire-polymer composite film. (a) Before stretching, and after stretching by (b) 100%, (c) 150% and (d) 200%. Data from [75].

1.5.3 Pattern analysis

To avoid the drawbacks of the alignment quantification methods mentioned above, another method based on pattern analysis of NWs in an image was developed by Jeon et al. [94]. Autocorrelation functions (ACF) used in this study provide a measure of the degree to which an image is correlated with itself, and consequently the orientation and symmetry within the image can be measured [95]. ACF permits a qualitative analysis of the image properties, such as the presence of strong ordering (figure 1.16). However, an ACF needs to calculate the correlation between an image and itself, which requires a huge amount of calculations. Secondly, ACF only provides the probably of NW angle distribution rather than the actual number counts. Thirdly, ACF cannot provide a single-value metric for alignment comparison between different samples. Fourthly, it is hard to implement, especially for NW researchers, and most of the functions needed are not provided by an open source library. Researchers themselves have to realize these functions which increases the difficulty

of program development and further maintenance.

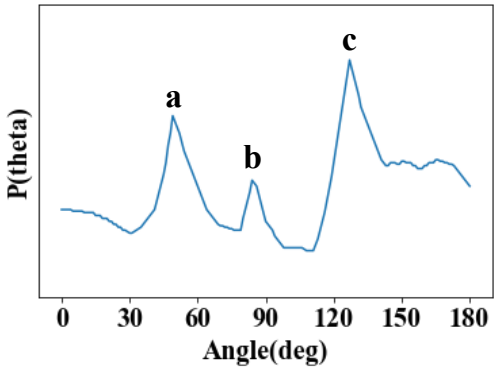

Figure 1.16 Nanowire angle probability distribution determined by an autocorrelation function. Data from [94].

1.5.4 Desired nanowire alignment quantification

After a brief review of previous studies on how to quantify NW alignment, a desired NW alignment quantification method should have the following features: (i) fast and accurate, (ii) compatible with all kinds of NWs, (iii) easy to be implemented and computationally efficient, and (iv) provides a standard parameter or function to quantify the alignment results mathematically to be used for alignment result comparison. In Chapter 2, image processing method based on convolution operations are presented which satisfy all the above requirements.

1.6 Outline of this thesis

This thesis continues with four main chapters. Firstly, two fast, accurate, generally applicable, and computationally efficient image processing methods based on edge detection and skeletonization convolution operations are used to recognize NWs from microscopy images. Then, an order parameter and an orientational distribution function are used for standard alignment quantification (chapter 2). These methods

will subsequently be used throughout the remainder of the thesis to quantify the NW alignment in my experiments. In chapter 3, two simple, large-area, and cost-efficient NW alignment methods based on substrate stretching and rod coating are studied, which can be used for NWs of any material and synthesized by any method. These two NW alignment processes will be used in the fabrication of devices in chapter 4 and 5. In chapter 4, the electrical and optical anisotropy of slightly aligned AgNW films are investigated, which can be used as transparent electrodes. Their optical transparency to linearly polarized light can be increased compared to typical randomly oriented AgNW films within the visible wavelength range, which is desirable for LCD applications. In chapter 5, a crossed film structure consisting of semiconductor NWs aligned in one direction and metal NWs orthogonally aligned is postulated. Metal NWs are used as interconnects to reduce semiconductor NW-NW junction resistances as well as provide more mechanical flexibility and a lower cost than metal pad interconnects which are lithographically defined. The device fabrication process may be further developed for use in large-area flexible devices such as sensors, thin-film transistors and energy generators. Lastly, a conclusion and future work are documented in chapter 6.

Chapter 2 Nanowire alignment quantification

This project was done in collaboration with Prof. Nasser Abulkhdeir from the Department of Chemical Engineering at the University of Waterloo. Prof. Abulkhdeir participated in the design of the study, edge detection convolution operation, skeletonization convolution operation, and code implementation. I participated in the design of the study, preparation of appropriate microscopy images of NWs (overlapped/non-overlapped ones), math deduction, and analysis of results including the order parameter (*S*) and orientational distribution function (ODF) values.

Portions of this work were published in two first-authored journal papers [96][97], and the code used in this chapter was provided in the supplementary data of the journal papers.

2.1 Introduction

In the literature, the predominant method for NW alignment quantification is by measuring the orientation angle of individual NWs in scanning electron microscopy (SEM) images by hand [72][98]. However, this technique is time consuming, inaccurate, and difficult to implement without bias. Another method involves measuring the polarization effect of aligned metal NWs, but it likewise can be inaccurate and time consuming and is limited to characterization of metal NWs only [86]. Moreover, polarization is not only affected by metal NW alignment, but also

NW materials and dimensions. Given that more than 100 research studies have been conducted on NW alignment methods and the applicability of alignment for NW-based manufactured devices, there is a need for more accurate, rapid, and generally applicable alignment quantification methods. Furthermore, the metrics used to assess alignment across the literature is not consistent, making it difficult to compare the quality of alignment within a single study or between different studies. For example, some studies use NW angle distribution histograms to evaluate their alignment result and count the percentage of NWs aligned within a certain angle (e.g. ±10° or ±15°) and some others use polarization results. No matter whether it is for optimization of a single alignment method, alignment comparison between different methods, or quality control in a manufacturing process, a standard alignment quantification metric (e.g. a well-defined value) is needed.

The use of image processing is an ideal quantification method as it is fast, generally applicable to all NWs, lends itself to the use of a comparable metrics, and can be accurate. A few studies in the literature have used image processing tools and standardized metrics, however, they employ the complicated autocorrelation function (ACF) which is computationally inefficient and only provides the probability of NW angle distribution rather than the actual number counts [94]. It also does not provide a metric that can be easily used for comparison across studies. Furthermore, the implementation of ACF is particularly difficult to implement for NW researchers because it requires researchers to realize most of the functions themselves since there is no well-developed open-source library to call. In this chapter, two fast, accurate,

generally applicable, and computationally efficient NW alignment quantification techniques based on image processing/computer vision are presented. Furthermore, two standard and quantitative metrics are defined which can be used across all studies. From the view of NW recognition, the first technique is based on an edge detection convolution operation (section 2.2) and the second one is based on a skeletonization convolution operation (section 2.3). From the view of alignment quantification, the first technique utilizes the *S* parameter (section 2.2), and the second one utilizes an ODF (section 2.3). The methods of alignment quantification are discussed in this chapter, and will be applied to experimental work in chapters 3, 4, and 5.

2.2 Image processing based on edge detection

2.2.1 Motivation

In this subchapter a rapid and accurate image processing method is presented which can recognize NWs automatically from optical microscopy (OM) or SEM images using an edge detection convolution operation. It is shown that this method can be used for recognizing both metal and semiconductor NWs. In order to quantify the presence of orientational order, or alignment, of the NWs, an *S* parameter is used. *S* is defined as a statistical mean of each NW angle to the average alignment angle. For this method, sparse NW networks with no overlapping NWs in the microscopy images is utilized for simplicity.

2.2.2 Computational methods

Image processing is performed using the Python programming language interface to the Open Computer Vision Library (OpenCV) [99] and Numpy Library [100]. The image processing method consists of four sequential tasks all implemented using the OpenCV library methods: filtering, thresholding, object detection/recognition, and shape fitting.

The filtering task involves removing measurement "noise" from the image, where noise refers to variations of the image brightness localized to one or a few pixels. For example, for the case where there is a single pixel with high brightness in an area of the image where the intensity is otherwise low, the filtering task will reduce the outlier pixel brightness. A raw input gray-scale SEM image (figure 2.1(a)) is first normalized ($0 \rightarrow 1$) and then filtered using a Gaussian filter function or "kernel" with the kernel size chosen to be smaller than the NW diameter to avoid loss of information (figure 2.1(b)). In this particular example, AgNWs with a diameter of 35 nm were aligned using substrate stretching (discussed in chapter 3.2) and a kernel size of 7 pixels was used for the filtering task.

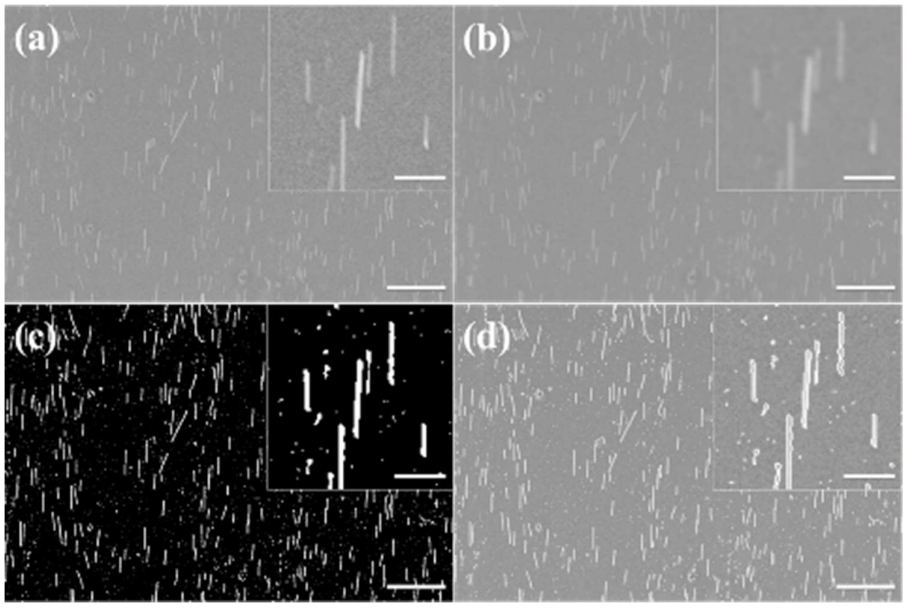

Figure 2.1 Images resulting from each task of the image processing method: (a) sample raw SEM image, (b) filtered image, (c) thresholded binary image, and (d) object contours superimposed on the raw image. Scale bar: 10 and 2.5 μm (inset).

The thresholding task involves digitizing the filtered image into pixel values corresponding to either foreground (NW) or background (substrate). The output of this task is a binary image with pixel values being either foreground (1) or background (0). Global thresholding methods typically fail for images with significant noise or varying background intensity, thus an adaptive thresholding method is used [99]. The method determines a threshold for every pixel in the image based upon a localized calculation, which means only neighbour pixels are taken into consideration to determine the threshold for each centre pixel. Localized calculations are commonly used in image processing because a pixel has more relations with its neighbour pixels rather than pixels far away from it. A Gaussian kernel is used as the localization function for the thresholding task here. Values above the threshold are assigned a 1, and values below the threshold are assigned a 0.

Object detection is achieved using a convolution operation. Convolution operations are commonly used in image processing. There are many kinds of operations, and each of them implements a specific modification (e.g. smooth, sharpen, intensify, edge detection, skeletonization, etc.) for input images. A specific kernel/filter is first applied to an input image, each pixel value in the input image is then modified depending on its neighbour pixel values and the kernel/filter, and finally a modified image is output [101][102]. In this subchapter, the object detection/recognition task involves inputting the binary image to determine the presence of objects in the image by using an edge detection convolution operation. Objects are essentially connected areas in the foreground of the binary image, which could include individual NWs, collections of non-overlapping NWs, or any other connected foreground feature (such as non-NW structures) resulting from the thresholding task. These regions are detected through the utilization of an edge-detection convolution operation [103] where the kernel/filter below is used:

$$\text{Filter (Edge detection)}=\begin{bmatrix} -1 & 0 & 1 \\ -1 & 0 & 1 \\ -1 & 0 & 1 \end{bmatrix} \tag{2.1}$$

Vertical edges can be detected using the above kernel/filter, and horizontal edges or ±45° edges can be detected by rotating the kernel/filter correspondingly. In general, an object can be roughly recognized using its vertical, horizontal, and ±45° edges. Of course, objects will be presented more clearly if more detailed edges are used however this will increase the computational time. Given the fact that we just need to recognize NWs, which are very simple in morphology, vertical, horizontal, and ±45°

edges are quite enough. After that, a set of contours, which enclose each of the objects in the image, is determined.

Given a set of candidate NW objects in the form of contour lines determined from the previous task, the shape-fitting task involves determining which of these candidate objects could be real individual NWs through morphological analysis, since some of them might be nanoparticles or just image noise. A least-squares method [104] is used to find the minimum size ellipse which encloses each of the candidate NW objects. Then, if the aspect ratio of the ellipse is greater than a specific value, it is considered a NW. This specific value, 7 in this particular case, was determined through a convergence analysis of the orientational order parameters for the set of images. In other words, if the calculated *S* parameter is not converged, another aspect ratio value needs to chosen according to the images. The orientation and lengths of the ellipses are used to approximate the alignment vectors and lengths of the NWs, respectively.

In order to quantify the presence of orientational order, or alignment, of the NWs, the use of an alignment metric or set of metrics is needed. In past work [105] the use of an orientational order parameter *S* is formulated to characterize two-dimensional nematic liquid crystalline phases. *S* ranges from 0 (random alignment) to 1 (perfect alignment) and is calculated according to the expression below,

$$S = < 2\cos^2\theta_i - 1 > \tag{2.2}$$

where <> is the statistical mean, and θ_i is the angle between the average orientation vector (***n***) and the axis of each elongated object *i* (***m****i*). A simple method to compute both *S* and ***n*** simultaneously is presented [106], which involves computing a tensor

order parameter,

$$< \boldsymbol{Q} >=< \boldsymbol{m}_i \boldsymbol{m}_i - \frac{1}{2} > \tag{2.3}$$

and then finding $\boldsymbol{n}$ from the eigenspace associated with the largest eigenvalue λ_1 and $S = \lambda_1 - \lambda_2$, where λ_2 is the smaller eigenvalue. S values range between 0 and 1, with values closer to 1 meaning the objects are more aligned. Unlike other alignment quantification methods, such as angle distribution histogram or polarization results, the S parameter provides a standard and well-defined metric with which different NW alignment results can be simply compared with a single value.

2.2.3 Results and discussion

Given a raw SEM image with non-overlapping aligned AgNWs with a diameter of 35 nm (figure 2.2(a)), our image processing technique can accurately recognize NW objects and filter non-NW objects. Comparing the raw image with the corresponding processed image with all the object contours (figure 2.2(b)), all the NWs are accurately recognized and none of the non-NW objects (e.g. nanoparticles) are incorrectly recognized since they are filtered after applying an appropriate object aspect ratio threshold (of 7). Moreover, our quantification metric can accurately quantify the alignment quality since it can calculate the average orientation vector ($\boldsymbol{n}$). This vector represents the main alignment direction of all the NWs on the image, and further analysis such as NW angle distribution and S value are calculated using this vector as a reference. Without the average orientation vector, it is hard to manually find the main alignment direction based on all the NWs from a SEM image with many

NWs, for example in figure 2.1. In the previous pattern analysis study using ACF, the exact angle difference between each NW and the average orientation vector (***n***) cannot be calculated either, because ACF can only calculate the angle probability for each NW instead of the exact angle value [94]. Based on our quantification metric, an *S* value (in this case 0.97) can be calculated, and the NW angular distribution (figure 2.2(c)) and length distribution (figure 2.2(d)) can also be amassed from the image processing data and presented as histograms. The angular distribution histrogram can be used compare alignment results to studies where *S* parameter is not used. For example, the angular distribution in figure 2.2(c) indicates that more than 85% of the NWs were aligned within ±10° of the alignment direction.

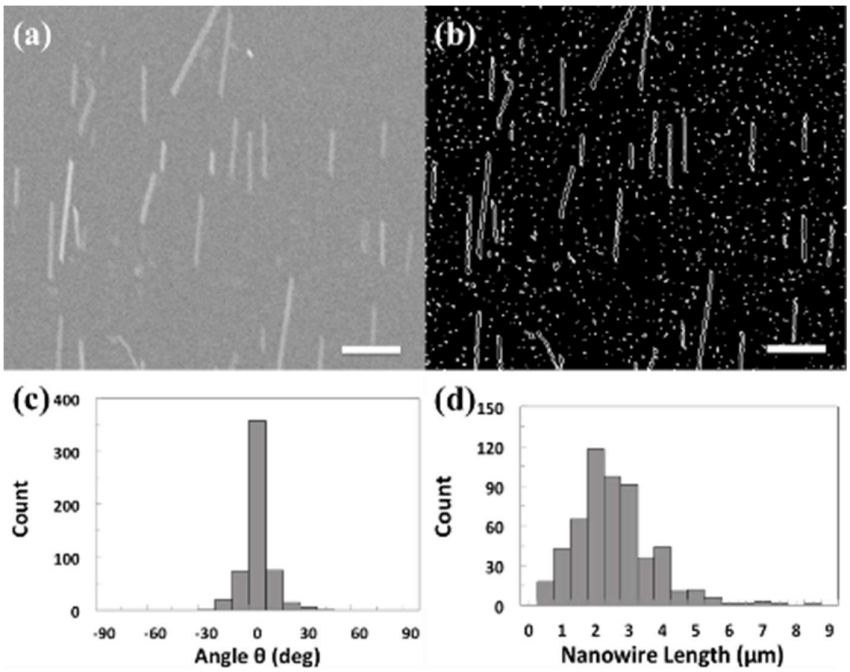

Figure 2.2 (a) Sample raw SEM image with non-overlapping aligned silver nanowires. (b) Object contours superimposed on the raw image. (c) Angular distribution of aligned nanowires amassed from image processing data. (d) Length distribution of aligned nanowires amassed from image processing data. Scale bar: 2.5 μm.

Our method works for NWs of any material, as long as the NW can be imaged.

The above results were for metal NWs. Figure 2.3 shows the method applied to semiconductor NWs. ZnONWs with a diameter of 50 nm were aligned using substrate stretching (discussed in chapter 3.2) and a kernel size of 7 was used. The *S* value was calculated to be 0.90.

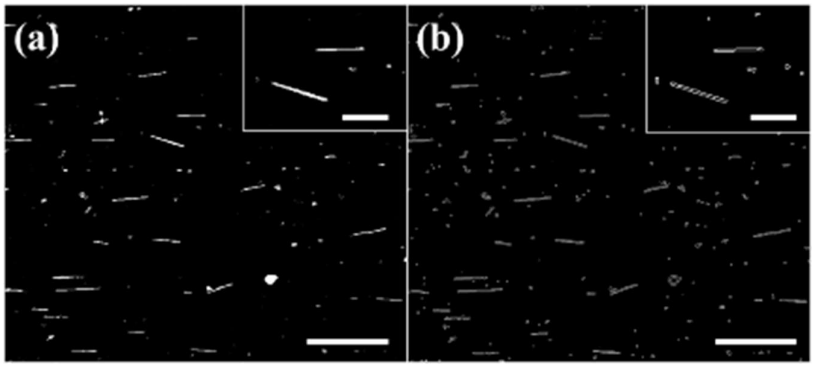

Figure 2.3 (a) Sample raw SEM image of aligned zinc oxide nanowires. (b) Object contours superimposed on the raw image. Scale bar: 15 and 5 μm (inset).

Image processing based on edge detection was shown to provide an effective and rapid way to recognize NWs from sparser NW networks. The previously used pattern analysis method (i.e. ACF) requires a huge amount of computation since it needs to calculate the correlation between an image and itself, while our method based on a convolution operation substantially reduces the computational cost since it only takes neighbour pixels into account during calculations. Given an image of n × n pixels, ACF takes ~n^4 calculations, and our method only takes ~n^2 calculations to process each image. For example, it only takes ~30 seconds to process and analyze an image with 1500 × 1000 pixels, which is faster than all other methods. In the case of quality control in manufacturing, a huge amount of images need to be processed, and the time advantage of our method would be magnified. Moreover, our method can be easily implemented and maintained since most of the functions have been developed and

tested in the OpenCV Library. However, edge detection fails to recognize NWs from denser networks which contain overlapping NWs. And the S parameter is not adequate to quantify the alignment of very highly aligned NW networks since the S value approaches 1 in these cases, making it hard to compare the difference between highly aligned NW networks.

2.3 Image processing based on skeletonization

2.3.1 Motivation

Denser NW networks are desirable in some large-area electronic applications including different kinds of displays and sensing devices [26][107]. Sparser semiconductor or metal NW networks have a smaller active region than denser ones, yielding lower detection sensitivity (e.g. optoelectronic signals or polarization effects). And sparser metal NW films do not achieve a connected, conductive network, which limits their usage as transparent electrodes. The image processing method based on an edge detection convolution operation (discussed in chapter 2.2) doesn't work with denser NW networks with overlapping NWs because the method recognizes NWs based on their contours. Given a crossed NW structure, it can't be recognized as two crossed NWs but instead it would be recognized as a cross. Previous reported pattern analysis based on ACF can work with denser NW films, however it suffers from computational complexity and implementation issues, as discussed in chapter 2.1. Thus, significant challenges still exist for NW recognition and, with the merging of highly dense NW devices and applications, advances in image processing methods are

required for denser NW films [61][70][83]. Also, in chapter 2.2 the *S* parameter was introduced as a standard alignment quantification metric, however, it is not adequate for highly aligned NW films. This is because the *S* parameter can saturate to 1 and thus make it difficult to compare the differences between highly aligned NW films. Furthermore, the definition of the *S* parameter in chapter 2.2 doesn't take NW length into account; however, good alignment of longer NWs may have more importance than shorter NWs from the view of device applications.

In this section, we will address two significant current challenges in automated alignment quantification of NWs on surfaces: (i) image processing of dense (overlapping) NW films and (ii) alignment quantification metric formulation for highly aligned NW films with consideration of different NW lengths. The *S* parameter will be shown to be a coarse approximation for the ODF of the NWs, especially for high-alignment cases (e.g. figure 2.4(b) and (c)). Thus, the first objective of this subchapter is the derivation of a complete set of order parameters which enable the reconstruction of the ODF, and thus rigorously quantify alignment. The second objective of this subchapter is to develop an enhanced image processing method which is able to robustly and seamlessly handle both disperse (non-overlapping) (e.g. figure 2.4(a) and (b)) and dense (overlapping) NW films (e.g. figure 2.4(c)).

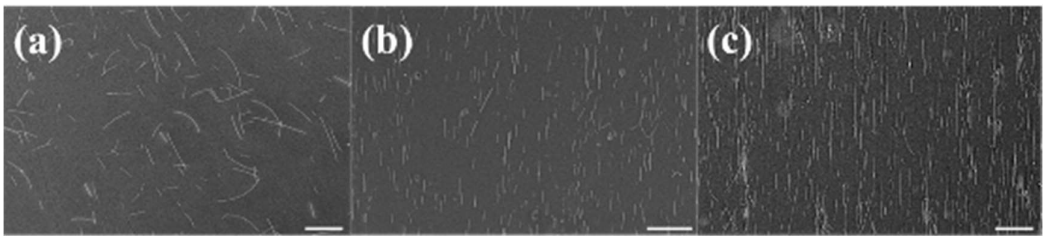

Figure 2.4 SEM images of nanowire films with (a) sparse (non-overlapping) coverage and low alignment (scale bar: 50 μm), (b) sparse coverage and high alignment (scale

bar: 10 μm), and (c) dense (overlapping) coverage and high alignment (scale bar: 40 μm).

2.3.2 Theory

Quantification of alignment of materials through the introduction of appropriate orientational order parameters has been rigorously addressed in the area of liquid crystal physics [108]. Orientational order in liquid crystal phases is traditionally quantified by a finite set of orientational order parameters [105]:

$$S_{2n} = < P_{2n}(\cos\theta_i) > \tag{2.4}$$

where n is a positive integer, P_{2n} is the Legendre polynomial of order $2n$, and θ_i is the angle between the average alignment vector **n** and the ith molecular alignment vector $\boldsymbol{m}_i$. These order parameters are derived from the ODF, which is used for 3D representation of crystallographic texture in materials science and a full statistical representation of three-dimensional uniaxial molecular alignment. The ODF in spherical coordinates is given by:

$$\int_0^{\pi} f(\theta)\sin\theta d\theta = 1 \tag{2.5}$$

where the ODF can be shown to also have the form [105]:

$$f(\theta) = \frac{1}{2} + \sum_{n=1}^{\infty} \frac{4n+1}{2} S_{2n} P_{2n}(\cos\theta) \tag{2.6}$$

and thus a finite set of scalar order parameters defined by equation (2.4) can be interpreted as a reduced-basis approximation of the exact ODF.

Since liquid crystal phases are composed of molecules whose orientation is inherently three-dimensional, equations (2.4)–(2.6) cannot be used for NWs on a substrate where only 2 orientation dimensions are applicable. Past research has been

performed on liquid crystal phases constrained to two-dimensions in which a two-dimensional orientational order parameter $S = <\cos 2\theta_i >$ was first introduced by Straley in [109]. This can be shown to be equivalent to equation (2.2) using simple trigonometric identities. For two-dimensional liquid crystal phases, the scalar order parameter was later expanded on in [110] introducing a two-dimensional alignment tensor:

$$\boldsymbol{Q} =< 2\boldsymbol{m}_i\boldsymbol{m}_i - 1 > \tag{2.7}$$

which provides a simple approach to compute the average molecular alignment vector $\boldsymbol{n}$ through eigenvalue decomposition of $\boldsymbol{Q}$.

The derivation of a suitable set of two-dimensional orientational order parameters in this work closely follows that of Zannoni in [105] where the three-dimensional case of the derivation was studied. An ODF for a set of non-polar cylindrically symmetric objects constrained to two-dimensions must obey the following constraints:

$$f(\theta) = f(\theta + i\pi) \tag{2.8}$$

where i is an integer, and the normalization condition:

$$\int_0^{2\pi} f(\theta) d\theta = 1 \tag{2.9}$$

An appropriate orthogonal expansion for $f(\theta)$ exists in terms of a Fourier cosine series,

$$f(\theta) = \frac{1}{2\pi} + \frac{1}{\pi}\sum_{n=1}^{\infty} S_n \cos n\theta \tag{2.10}$$

which is further constrained by equation (2.8) to include terms with only even integers:

$$f(\theta) = \frac{1}{2\pi} + \frac{1}{\pi}\sum_{n=1}^{\infty} S_{2n}\cos 2n\theta \tag{2.11}$$

As with the three-dimensional orientational order case, this expansion defines a consistent set of orientational order parameters:

$$S_{2n} = <\cos 2n\theta_i> = N^{-1}\sum_{i=1}^{N}\cos 2n\theta_i \tag{2.12}$$

the first of which $S \equiv S_2$ is consistent with equation (2.2). Through computation of these order parameters the ODF (equation (2.11)) may be reconstructed with increasing accuracy, as higher order S_{2n} terms are included. In the cases of highly aligned NWs, ODF is superior to S to quantify alignment because the S value approaches 1 in such cases, making it hard to compare different alignment results. The ODF includes higher order parameters (S_{2n}), which can magnify the subtle difference between highly aligned NW networks for further alignment quality comparison. This is the first time ODF has been used to quantify NW alignment.

2.3.3 Computational methods

As in chapter 2.2, the filtering and thresholding tasks are still used to remove measurement noise from the raw microscopy image and segment the grayscale image into a binary image, respectively. A non-local denoising filter is used with a length scale chosen to be smaller than the smallest characteristic NW [99][111]. More advanced than chapter 2.2 where only adaptive Gaussian thresholding was used, Otsu's method is also implemented for the thresholding task here, which is preferable if the background intensity variation is not large [112]. Depending on the variation of

the background intensity in the image, either Otsu's method or adaptive thresholding is used on the filtered grayscale image to generate a binary image where each pixel is either foreground (1) or background (0). This binary image is the starting point for automated identification of NWs. Sample binary images resulting from filtering and thresholding of a sub-region of figure 2.4(c) are shown in figures 2.5(a) and (b), respectively. In this particular example, AgNWs with diameters of 90 nm were aligned using substrate stretching.

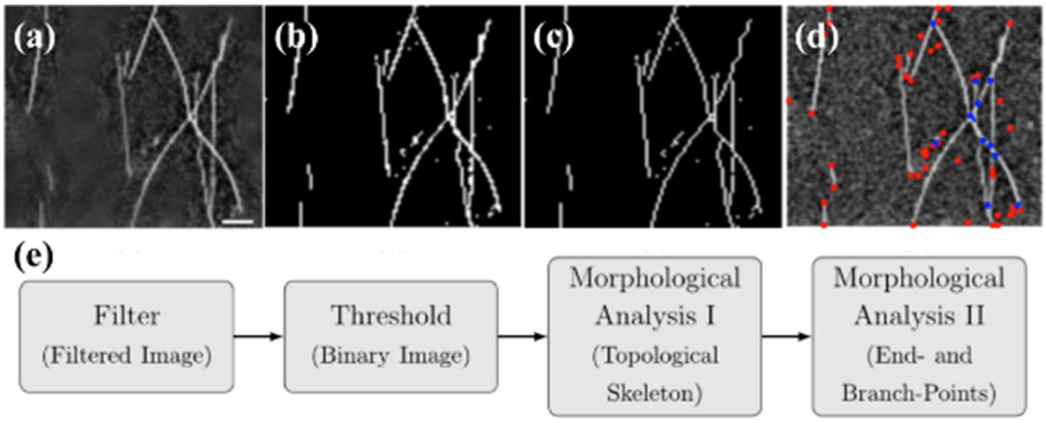

Figure 2.5 (a) A denoised sub-region of the SEM image from figure 2.4(c) (rotated, scale bar is 5 μm), (b) the binary image generated through thresholding of the sub-region using Otsu's method, (c) the topological skeleton generated through morphological analysis of the binary image, (d) end-point (red) and branch-point (blue) pixels identified through further morphological analysis of the topological skeleton (superimposed on the original image), and (e) a flow chart summarizing the image processing tasks and corresponding outputs (in parenthesis).

Given a binary image, the method discussed in chapter 2.2 used least-squares fitting of ellipses to foreground objects to recognize candidate NWs. This single operation both uniquely identifies foreground objects and provides approximations of their morphological quantities such as major axis length, minor axis length, aspect ratio, eccentricity, and axes orientations. This approach has limited applicability in that NWs need to be non-overlapping and thus is useful only for dispersed samples

like those shown in figures 2.4(a) and (b).

In order to robustly and seamlessly process images with both non-overlapping and overlapping NW films, a topological skeleton [113][114] generated from the binary image is used in the presented method which is based on a skeletonization convolution operation [101][102]. A topological skeleton preserves foreground object shapes, but reduces its representation to a simple set of discretized curves which are more amenable to characterization. There are many methods for generating topological skeletons from a binary image; in this work morphological operators are used, specifically using the hit-and-miss transform [114]. This approach is chosen in that morphological operators are also used to determine end-points and branch-points (overlapping areas) of NWs from the topological skeleton. Given the binary image in figure 2.5(b), the resulting topological skeleton is shown in figure 2.5(c).

Characterization of the NWs is facilitated by identification of end-points and branch-points in the topological skeleton. End-points in the topological skeleton correspond to end-points of the NWs in the image, while branch-points correspond to overlap areas of individual NWs. These points are efficiently identified through the use of mathematical morphology operations on the topological skeleton (figure 2.5(c)); sample output is shown in figure 2.5(d). For each object in the binary image, end-points and branch-points located within them may then be grouped together for further analysis (chapter 2.3.4), including a second level of filtering to exclude features below a certain length threshold which results from the presence of noise and non-NW structures (e.g. nanoparticles) in the source image.

Through the use of the topological skeleton, the presented image processing method does not directly use the diameter (or minor length scale) of the NW, which will be much smaller than the length (or major length scale) for a NW. Thus, given that the resolution of the imaging method is sufficient to resolve the NW length accurately, increasing the resolution beyond that threshold will not have a significant effect on the resulting topological skeleton.

2.3.4 Results and discussion

***Dispersed (non-overlapping) nanowire films**:* A distinguishing feature of NW-covered films is that they are able to be fabricated with an extremely high degree of alignment with $S > 0.9$, like those shown in figures 2.4(b) and (c). Conversely, orientational order found in liquid crystalline materials is typically low, where $S \approx 0.3 - 0.6$. In high alignment regimes, single orientational order parameter measures of alignment [82] are insufficient for accurate reconstruction of the ODF, $f(\theta_i)$, and thus not adequate for rigorous quantification of alignment. In order to demonstrate this, SEM images of disperse (non-overlapping) NW-covered films were analyzed using the image processing method presented in chapter 2.2. Figure 2.4(a) was used for the low alignment case and figure 2.4(b) for the high alignment case; order parameters (equation (2.12)) up to order 50 were computed. Figures 2.6(a) and (b) show histograms of the angle θ_i between the orientation of individual NWs and the average orientational axis. The y-axis, $f(\theta_i)$, is the ODF. As observed in figure 2.6(a), the single order parameter approximation (dashed blue line) is adequate for the low

alignment case in that higher order parameters quickly approach zero, shown in figure 2.6(c). However, the single order parameter approximation fails for the high alignment case, where a relatively complex ODF is reconstructed (figure 2.6(b)) and higher order parameters are non-zero up to order 30 (figure 2.6(c)). Given that the ODF is smooth, convergence of the reconstructed ODF is found as higher order parameters approach zero. This is qualitatively shown in figure 2.6(c) for both the low and high alignment cases. Sample size also affects the quality of the ODF reconstruction. Oscillations are observed in figures 2.6(a) and (b) at larger values of θ_i. And oscillations in the higher order parameters in figure 2.6 (c) are also observed. These are both due to the relatively small sample size.

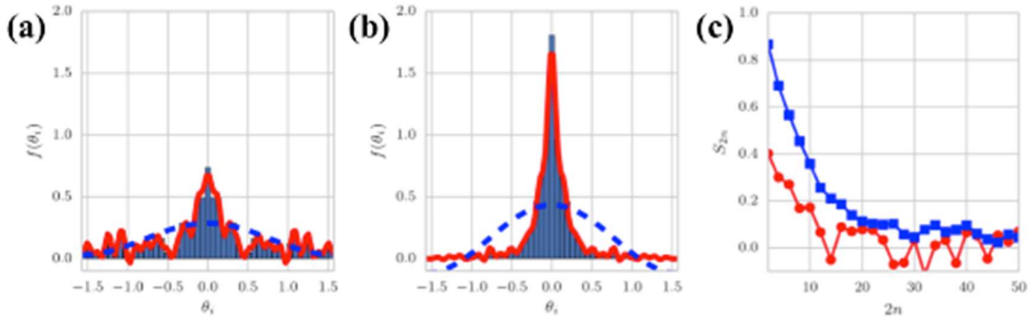

Figure 2.6 Single (dashed line) and multiple (red solid line) orientational order parameter reconstructions of the ODF $f(\theta_i)$ superimposed over histogram plots of the NW orientations (θ_i) in the SEM images shown in (a) figure 2.4(a), and (b) figure 2.4(b). (c) Plots of the magnitude of the orientational order parameters S_{2n} from the image in figures 2.4(a) (red circles) and (b) (blue squares).

These results show that a single orientational parameter (i.e. S) is useful to determine if order is present (or not) and its approximate degree, but it does not reveal details of the orientational distribution of the NWs. Two well-aligned samples with the same S could have a very different composition of NW orientations, and this composition can affect the properties of the aggregate film. An example of two

images with similar *S* values but different higher order parameters is discussed in the sub-section *Dense (overlapping) nanowire films* on page 49.

***Optimized image processing method**:* Given the combination of image segmentation and mathematical morphology image processing methods reviewed in chapter 2.3.3, for a given image of NWs, sets of end points and branch points for each contiguous feature can be computed. For dispersed films (figures 2.4(a) and (b)), NW orientation and length can be easily approximated from this data in that each feature should have only two end-points and no branch-points since there are no overlapping NWs. Given for each feature a pair of end points $\{\mathbf{r_1}, \mathbf{r_2}\}$, the NW alignment vector is $\mathbf{m_i} = l_i^{-1}(\mathbf{r_1} - \mathbf{r_2})$ with the NW length $l_i = \left|\left|\mathbf{r_1} - \mathbf{r_2}\right|\right|_2$.

In the frequent case of overlapping NWs, the identification of end points for each of them becomes significantly more difficult. Instead of developing a complex iterative method to determine end points, a more simple method is proposed. Given the case where two or more NWs overlap, a single feature in the raw image (figure 2.7(a)) will contain multiple NWs and at least one branch-point will be identified within it. The addition of an intermediate step is proposed where branch points within the topological skeleton computed from the binary image are removed and treated as if they are background pixels. The modified topological skeleton now has no branch points and, for example, a feature that originally had two NWs overlapping now corresponds to three or four separate non-overlapping NWs. The method for non-overlapping NWs may now be applied in that each feature in the modified topological skeleton has no branch points and only two end points. The result of

applying this image processing method to the SEM image is shown in figure 2.7(b). Comparing the raw SEM image with the corresponding processed image with all the object skeletons, ~98% the NWs can be accurately recognized and none of the non-NW objects (e.g. nanoparticles) are incorrectly recognized since they are filtered after applying an appropriate object threshold pixel value (of 5). In this particular example, AgNWs with diameters of 90 nm were aligned using substrate stretching.

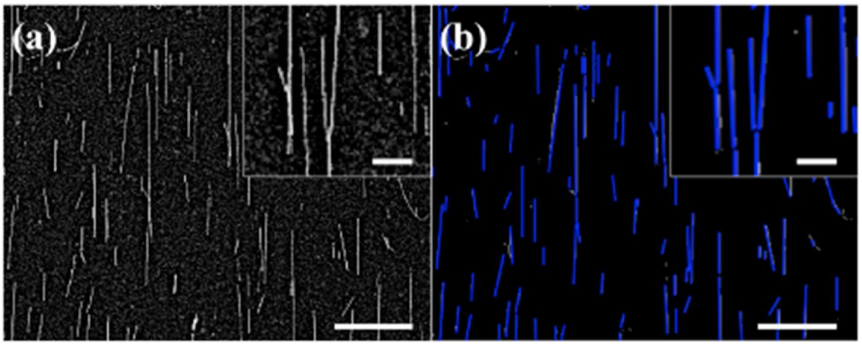

Figure 2.7 (a) Sample raw SEM image of aligned nanowires. (b) The nanowire segments recognized from applying the enhanced algorithm to the topological skeleton and filtering segments below a user-specified threshold (5 pixels). Scale bar: 20 and 5 μm (inset).

This approach does result in a loss of information in that the original topological skeleton is modified such that contiguous NWs are now non-contiguous. The implication of this is that determination of original NW length is not possible, but the orientation is unaffected. Within the present context of quantifying alignment of the NWs, this can be resolved through a reformulation of equation (2.12). Assuming that each NW has an equal length l and, thus, equal contribution to the orientational order of the film:

$$S_{2n} = (lN)^{-1} \sum_{i=1}^{N} l \cos 2n\theta_i = N^{-1} \sum_{i=1}^{N} \cos 2n\theta_i \qquad (2.13)$$

Now, taking into account that each NW can have different lengths l_i a weighted

average can be used:

$$S_{2n}^{w} = L^{-1}\sum_{i=1}^{N} l_i \cos 2n\theta_i \tag{2.14}$$

where $L = \sum_i l_i$ is the total length of NWs present in the image and, as with the unweighted case, $S^w \equiv S_2^w$. This approach both accounts for the differing length of NWs in the orientational order parameter formulation (i.e. the alignment of a short NW is now no longer of equal weight to an aligned long NW) and circumvents the need for identification of a unique set of NWs in the image.

Any NW or combination of NWs may be decomposed into an arbitrary set of smaller NWs without any effect on the order parameters computed through equation (2.14), unlike with equation (2.12), which weights each NW orientation equally. Furthermore, even for non-overlapping samples, equation (2.14) might be more appropriate than equation (2.12) if one desires the alignment of longer NWs to be weighted more heavily than shorter ones, which is desirable in transparent electrode and polarizer applications for example.

It should be noted that if any of the NWs are tilted out-of-plane of the surface, the measured lengths from the image are actually projected lengths of the NWs on the surface. While this possible measurement inaccuracy will have a small effect on the weighting of the length-weighted order parameters, the measured orientations of the nanostructures will be unaffected.

Dense (overlapping) nanowire films*:* Combining the ODF and image processing methods elaborated above results in a highly robust and descriptive method for quantification of NW alignment. The combined approach was applied to the dense

NW film shown in figure 2.4(c) (where AgNWs with diameters of 90 nm were aligned using substrate stretching) in order to both demonstrate its application and compare the use of non-weighted (equation (2.12)) and weighted (equation (2.14)) order parameters to reconstruct the ODF. As in chapter 2.2, the average orientation vector (***n***) was calculated first and the ODF was reconstructed using that as a reference, which as discussed previously is impossible to be realized by manual measurement. Figures 2.8(a) and (b) show reconstructions of the ODF using single and multiple order parameters for the unweighted (S_{2n}) and weighted (S^{w}_{2n}) formulations, respectively. The NWs in the SEM image shown in figure 2.4(c) are highly aligned and, thus, the single order parameter approximation again is found to be insufficient in reconstructing the ODF. Instead, orientational order parameters up to order 200 were required to reconstruct the ODF due to the extremely high alignment, where $S \rightarrow 1$.

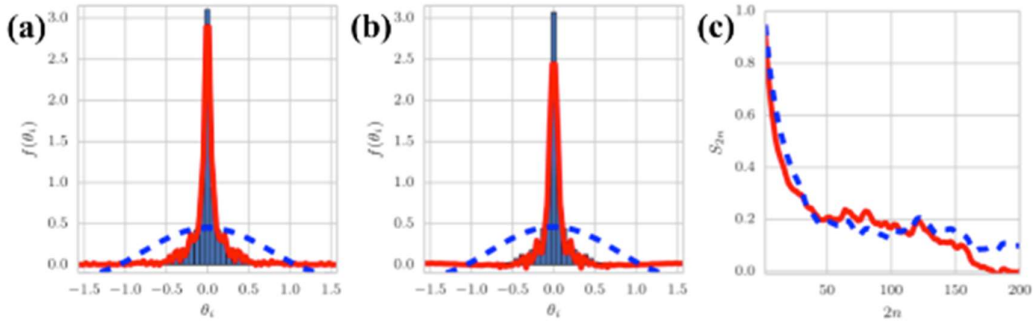

Figure 2.8 Single (dashed line) and multiple (red solid line) orientational order parameter reconstructions of the ODF $f(\theta_i)$ superimposed over histogram plots of the nanostructure orientation θ_i values from the SEM image shown in figure 2.4(c) using the ODF reconstruction with (a) the standard order parameters S_{2n} and (b) the length-weighted order parameters S^{w}_{2n}. (c) Plots of the magnitude of orientational order parameters S_{2n} (red solid line) and S^{w}_{2n} (blue dashed line).

Comparing the multiple order parameter reconstructions, a non-negligible

difference is found between the peak value of unweighted ODF (figure 2.8(a)) and that of the weighted ODF reconstruction (figure 2.8(b)). The unweighted ODF is calculated without consideration of NW length (i.e. the alignment of long and short NWs contribute equally. On the other hand, the weighted ODF is calculated with the consideration of different NW length contribution to the alignment, in which case long NWs have more contribution to their corresponding alignment direction. The weighted ODF reconstruction (figure 2.8(b)) is preferable in many cases to the unweighted ODF (figure 2.8(a)), especially when the skeletonization method is used where NWs are split into segments for image processing purposes. Figure 2.8(c) shows the magnitude of the orientational order parameters of increasing order, which also shows a non-negligible difference between the unweighted and weighted approaches.

In order to further support the use of multiple orientational order parameter quantification of alignment, length weighted order parameters were also computed for the non-overlapping NW images shown in figures 2.4(a) and (b). These images were already shown to have NWs with low and high alignment, respectively. Figure 2.9 shows the length-weighted orientational order parameter plots for each of these images.

Focusing on the single order parameter metric S^{w} (i.e. where S_{2n}^{w} crosses the y-axis and is the same parameter as S described in chapter 2.2), there is a clear difference in its magnitude for the poorly aligned nanostructure image (figure 2.4(a)) compared to those for the highly aligned nanostructure images (figures 2.4(b) and (c)).

However, for the two highly aligned nanostructure images, the difference in S^w is very small. This implies that the single order parameter quantification of orientational order is not suitable for distinguishing between different highly aligned samples. Taking into account multiple orientational order parameters enables this comparison, with the caveat that the orientational order parameters and ODF quantify alignment only. Other metrics such as NW shape or morphology could be included in the comparison, but would require the introduction of additional metrics.

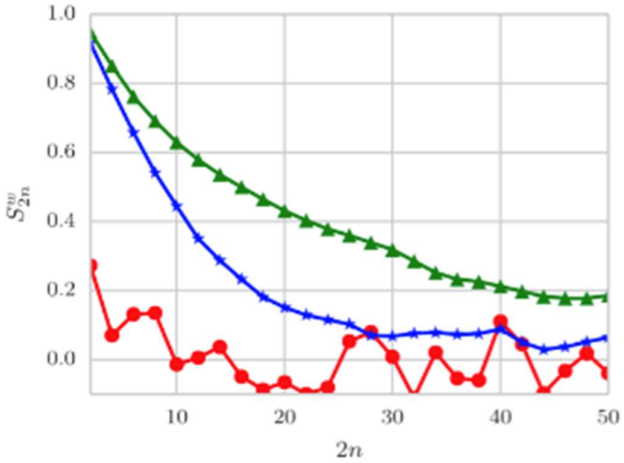

Figure 2.9 Plots of the magnitude of the length-weighted orientational order parameters S^w_{2n} for the SEM images shown in figures 2.4(a) (red circles), (b) (blue stars), and (c) (green triangles).

Table 2.1 Similarity metric values from the comparison of SEM images in figure 2.4.

	Figure 2.4(a) and (b)	Figure 2.4(a) and (c)	Figure 2.4(b) and (c)
$\left\|S^w - S^{w'}\right\|$	0.65	0.68	0.031
$\left\|\left\|\boldsymbol{S}^w - \boldsymbol{S}^{w'}\right\|\right\|$	1.5	2.2	1.0

A simple way to compare the ODFs from each image is through treating the set of

orientational order parameters (for each image) as a vector $\boldsymbol{S}^{\mathrm{w}} = [S_{2n}^{w}]$ and compute the Euclidean dean distance between vectors from pairs of images. This value can be interpreted as a similarity metric; the smaller its value the more similar the orientational character of the NWs shown in the pair of images is, the larger the more different.

Table 2.1 shows the similarity metric values resulting from comparing each of the three SEM images for both the single and multiple order parameter cases. Both the single and multiple order parameter similarity metrics are found to result in large values comparing the poorly aligned image to both highly aligned images. While this is correct in both cases, when comparing the highly aligned images to each other the single order parameter similarity metric is very small, which incorrectly implies that these images have very similar alignment characteristics. The multiple order parameter similarity metrics performs well for all cases, indicating that the poorly aligned sample is less similar to the aligned samples and the aligned samples are similar but distinct.

Besides dense metal NW film alignment, this enhanced image processing algorithm works for NWs of other materials as well. For example, dense semiconductor NWs, in this case ZnONWs, were quantified. The NWs had diameters of 50 nm and were aligned using substrate stretching (figure 2.10(a)). Figure 2.10(c) shows the reconstructions of the ODF using single and multiple order parameters for the weighted (S_{2n}^{w}) formulation. Figure 2.10(d) shows both non-weighted and length-weighted orientational order parameter plots up to order 50.

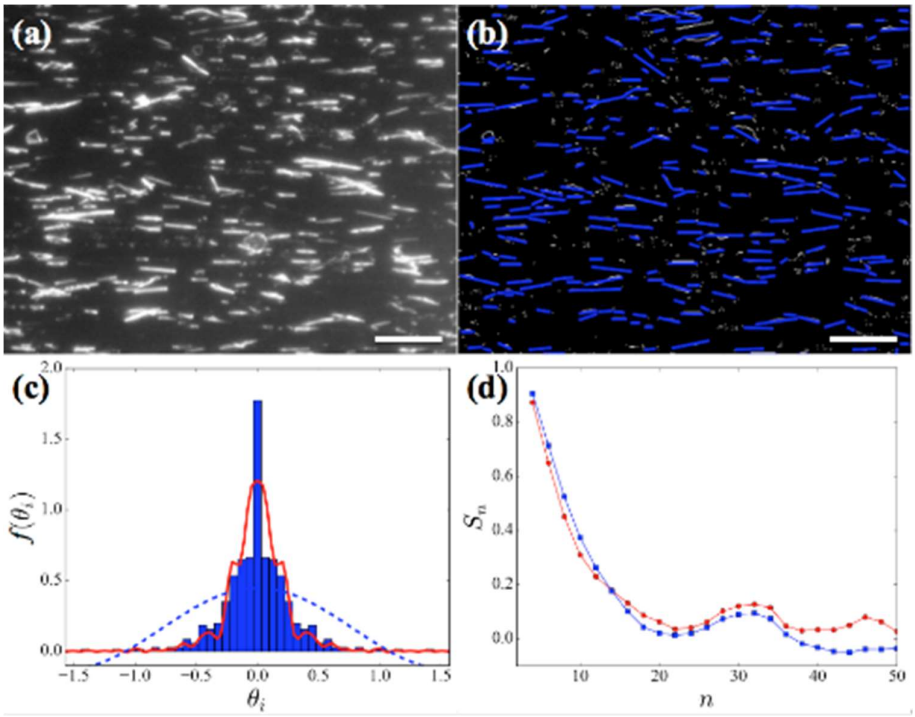

Figure 2.10 (a) Sample raw optical microscopy image of aligned zinc oxide nanowires. (b) The nanowire segments recognized from image processing based on skeletonization. (c) Single (dashed line) and multiple (red solid line) orientational order parameter reconstructions of the ODF $f(\theta_i)$ for the length-weighted (S^w_{2n}) formulation, superimposed over histogram plots of the nanostructure orientation θ_i values . (d) Plots of the magnitude of orientational order parameters S_{2n} (red circles) and S^w_{2n} (blue squares). Scale bar: 25 μm.

Since the enhanced image processing method is based on a convolution operation, which only takes neighbour pixels into account during calculation, it is also computationally efficient like the method discussed in chapter 2.2. Given an image with 1500 × 1000 pixels, this enhanced image processing method and ODF quantification metric takes ~30 seconds to process and analyze, which doesn't take any additional time compared with the method in chapter 2.2 and is also more efficient than all other NW alignment quantification methods.

2.4 Conclusions

Image processing methods based on edge detection and skeletonization convolution operations were presented and applied to recognize NWs from microscopy images. Alignment quantification metrics based on the *S* parameter and the ODF reconstructed from two-dimensional orientational order parameters were developed with which NW alignment is rigorously quantified. Edge detection convolution operation is adequate for non-overlapping NW recognition while skeletonization convolution operation can be used for denser films were there exist overlapping NWs.

The use of high-order orientational order parameters (i.e. ODF) is shown to be necessary for quantification of highly aligned NWs, while the single parameter (i.e. *S*) method is shown to be insufficient. Both image processing and alignment quantification techniques provide researchers in nanoscience and nanotechnology with a fast, accurate, generally applicable, and computationally efficient method for the determination of structure/property relationships where alignment of NWs is significant. These methods can be used for NWs of any material, as long as they can be imaged, and can be used to quantify alignment of other 1D nanostructures as well such as nanotubes, nanorods and nanobelts.

The methods presented in this chapter will be used in the following chapters (3-5) to quantify NW alignment. The code used in this chapter can be accessed from the supplementary data of our published journal papers [96][97]. To set up the computational environment, researchers need to install Python 2.7, Homebrew, and Pip on their own computers. (This work is done under a Mac operation system. For a

Windows/Linux operating system, the installation and configuration may be different). To run the code, researchers need to install Numpy, OpenCV, Scipy, and Matplotlib open source libraries under the pre-installed Python 2.7.

Chapter 3 Large-area, cost-effective, one-step nanowire alignment

3.1 Introduction

Over the past decade, NW alignment has been extensively studied and multiple methods have been developed including: microfluidic flow [72], the Langmuir-Blodgett technique [91], electric and magnetic fields [3][4], bubble-blown films [78], and contact printing [84]. While past works have achieved successful NW alignment, various limitations have been observed either due to the complicated fabrication processes or incompatibility for large-scale alignment. In addition, some of the above mentioned methods do not work for NWs synthesized in solution (contact printing), or require certain electrical/magnetic characteristics of the NWs. In this chapter, two simple, low-cost, large-area, one-step NW alignment methods are presented. Both are compatible with flexible, printable electronic device fabrication techniques. The first one is based on substrate stretching (chapter 3.2), and the second is based on Mayer rod coating (chapter 3.3). Parts of this work were published in two first-author publications [68][96].

3.2 Nanowire alignment based on substrate stretching

3.2.1 Motivation

To overcome the drawbacks of previous alignment methods as mentioned above and

discussed in chapter 1.4, an alternative method was investigated by both Lee et al and Zhao et al where NWs were mixed with the polymer polyvinyl alcohol (PVA) and stretched to align the NWs [86][92] (as discussed in chapter 1.4.6). However, this method is not applicable for device integration as the NWs are embedded in the polymer and cannot be electrically accessed. Recently, a few reports have deposited NWs on the surface of a plastic substrate, followed by a contraction or stretching of the substrate (as discussed in chapter 1.4.7). This achieves NW alignment by the shear force of the underlying substrate [50][61][89]. However, the substrate materials that have been used so far, PDMS and polyvinylidene fluoride (PVDF) [87][89], are elastomers with relatively low stretching ratios, and the maximum strains employed were limited to 120%. Consequently, the low stretching ratio means that either high-quality alignment (e.g. S>0.90) cannot be achieved or multiple transfer/stretching cycles are required which substantially complicates the process [50]. Furthermore, these substrates return to the undeformed state without an applied force and thus the NWs must be transferred to another substrate while maintaining the stress on the original substrate, which adds complexity. Additionally, NW breakage during the substrate's stretching process is a critical problem that has not yet been addressed. For example, in the study where AgNWs were aligned by stretching PVA/AgNW nanocomposites [86], the average NW length after stretching is only 61% of the original length. Longer NWs are usually highly desirable for applications since they require a lower density of contacts and thus allowing for more active device area. Breakage is also a challenge for NW assembly by contact printing and has been

addressed by oil lubrication [84]. However, even with lubrication, the assembled NW lengths in that work are still only 50% of their original lengths.

In this section, a substrate stretching NW alignment technique with minimal NW breakage and a high degree of alignment is demonstrated. This method can be utilized for NWs grown on a substrate or in solution, and is shown to work for both metallic and semiconductor NWs. For the first time, PVA films are used as the underlying stretchable substrate for NW alignment (i.e. not mixed with the NWs); they can be stretched up to 450% of the original size without shrinking back after stretching which allows us to obtain an alignment quality superior to other substrate stretching/contracting methods in the literature. Also for the first time, a lubricant, in this case poly[oxy(methyl-1,2-ethanediyl)], is employed during stretching to nearly eliminate NW breakage while maintaining good alignment. Moreover, the feasibility of large-area NW transfer from PVA to a PET substrate is demonstrated for industry.

3.2.2 Experimental

Nanowire deposition: Two different sizes of AgNWs dispersed in ethanol were purchased from Blue Nano Inc. (Charlotte, NC). The average NW diameters were 35 nm and 90 nm with average lengths of 7 μm and 16 μm, respectively. Ethanol was used to further dilute the as-received solution. ZnONWs with average diameters and lengths of 50 nm and 4.6 μm, respectively, were purchased from M K Impex Corp. (Mississauga, Canada). For the purpose of minimizing NW breakage, a lubricant polymer poly[oxy(methyl-1,2-ethanediyl)] with various percentages were then added

to the Ag and ZnO NW solutions. PVA films, obtained from Kuraray Co. (Tokyo, Japan, 70 µm thick) were sonicated in methanol for 30 min and dried under nitrogen atmosphere. The NW/polymer solutions were then uniformly dispersed on 3 × 5 cm PVA films using Mayer rod coating (figure 3.1(a) and (b)) [36][66][115].

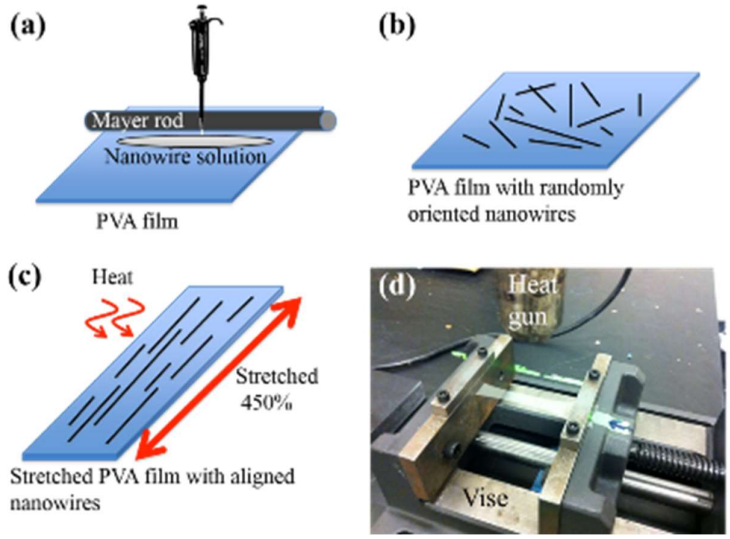

Figure 3.1 Nanowire alignment process. Schematic of (a) Nanowire/polymer deposition on a polyvinyl alcohol film by Mayer rod coating, (b) Nanowires after deposition, (c) Nanowire alignment by stretching the polyvinyl alcohol film under heat. (d) Photograph of the experimental setup.

Alignment method: The PVA films were immobilized in a vice and slowly stretched to 450% of their original lengths (figure 3.1(c) and (d)). 450% is the manufacturer-specified maximum stretch ratio of the PVA. Larger stretching ratios led to a film breakdown and smaller stretching ratios led to inferior alignment [86]. A heat gun set at 140 °C was directed at the substrate to facilitate stretching and prevent shrinkage post-stretching. Higher temperatures (e.g. 200 °C) could not be used due to a visible breakdown of the film. Films were stretched at a constant strain rate of 0.002 s^{-1} along the PVA film machine direction (MD) [116]. This rate was chosen since slower stretching rates did not improve the alignment process and at significantly

higher rates the film deformation was partially elastic (i.e. the films shrunk in length once the stretching force was released which is not preferred).

Lubricant removal: The lubricant poly[oxy(methyl-1,2-ethanediyl)] is soluble in ethanol at room temperature [117][118] and can be easily removed post-alignment if desired. The removal process can be summarized as follows; firstly, the NW samples were mechanically pressed at room temperature using an electric rolling press (MSK-HRP-01, MTI Corporation, Richmond, CA) in order to increase adhesion of the NWs to the PVA surface. The samples were then immersed in ethanol for 5 minutes and then dried using a heat gun at 85 ºC for 15 s; a fast evaporation time was necessary to prevent distortion of the PVA film. If the transfer of the aligned NWs to another substrate such as PET is desired, lubricant removal can be done after the transfer process.

Nanowire transfer: PET films, obtained from Dupont Inc. (Tianjin, China, 127 µm thick), were sonicated for 30 s in isopropyl alcohol (IPA) then in deionized (DI) water. The PET was subsequently immersed in a 1 mol/L sodium hydroxide (NaOH) solution for 4 hours at room temperature to render the surface hydrophilic (this process can be shortened to 8 mins if the NaOH solution temperature is raised to 70 °C) [119]. The chemically modified PET was then rinsed with DI water and dried under nitrogen atmosphere. The aligned NWs on PVA films were pressed against the PET films (figure 3.2(a)) using the rolling press. The optimized parameters of the rolling process were: rolling speed = 5 mm/s, temperature of rollers = 70 °C, and distance between the two rollers = 115 µm.

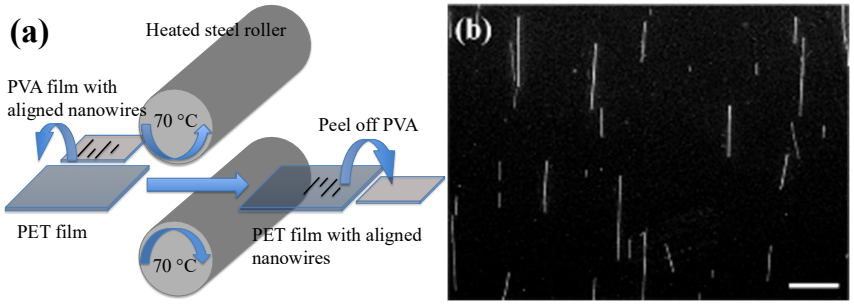

Figure 3.2 Nanowire transfer process. (a) Schematic of aligned nanowires transferred from polyvinyl alcohol to polyethylene terephthalate films using a hot-rolling machine. (b) SEM image of the nanowires on a polyethylene terephthalate film after transfer (scale bar: 25 µm).

Characterization: To investigate the NW alignment and lengths before and after stretching, SEM (LEO 1550, ZEISS Corporation) images were taken of the samples, which were coated with a 10 nm thick layer of gold to prevent electron charging.

Nanowire alignment quantification: Image processing based on edge detection convolution operation was used to identify and assess the NW alignment through OpenCV, implemented by the Python programming language, which was described in chapter 2.2. An orientational order parameter S is used to quantitatively assess the quality of alignment, also discussed in chapter 2.2.

3.2.3 Results and discussion

Aligning nanowires: Figure 3.3(a) is an SEM image of 35 nm AgNWs prior to stretching, showing that the NWs are randomly oriented. Figure 3.3(b) and (c) show SEM images of AgNWs on a PVA film stretched to 450%, without and with the addition of the polymer lubricant to the NW solution before deposition, respectively. In either case, it can be seen that almost all the AgNWs were aligned along the stretching direction due to the large shear force from the PVA film [86]; the PVA

compression in the orthogonal direction improves NW alignment as well [50].

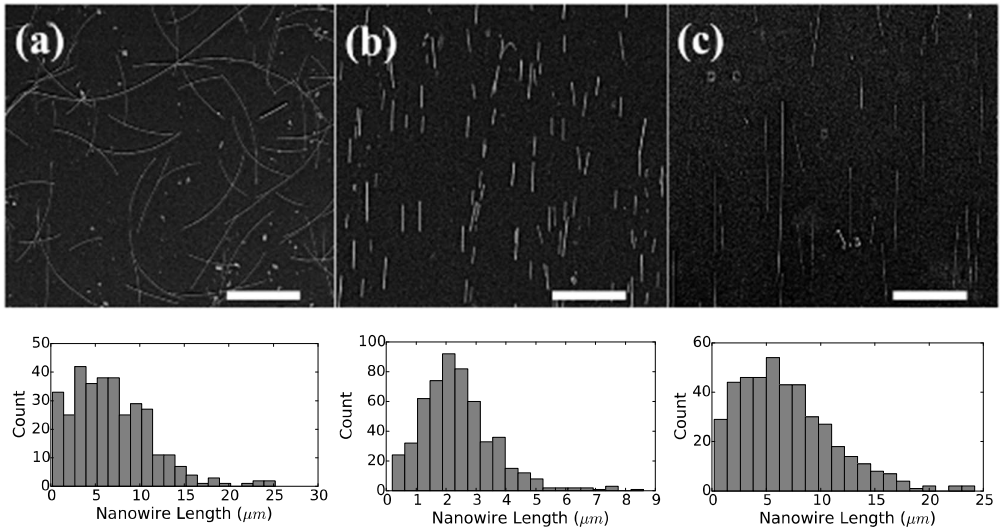

Figure 3.3 SEM images and histograms of silver nanowire lengths (a) before substrate stretching, (b) after substrate stretching without lubricant, and (c) after substrate stretching with lubricant (scale bar: 10 µm).

It clearly can be seen that the NWs stretched without the use of the lubricant (figure 3.3(b)) broke into several short pieces after stretching, which is typically undesirable for device applications. The average NW length is 2.4 µm after stretching, compared to the 6.8 µm average length before stretching. When comparing the histograms in figure 3.3(b) to that of 3.3(a), we noticed that the length distribution is compressed to lower values with nearly all NWs being less than 5 µm. The major reason of the NW's breakage is due to the attachment force between the NWs and the PVA surface. Consequently, as the PVA is stretched, the NWs get pulled apart into multiple pieces as shown in figure 3.3(b).

When the polymer lubricant is used, good NW alignment is achieved with minimal NW breakage. In figure 3.3(c), where a volume ratio of poly[oxy(methyl-1,2-ethanediyl)] to AgNW solution of 1:1300 was used and the NW

density is 3 NWs/100 μm^2, the average NW length after stretching was 6.8 μm and the length distribution, as seen in the histogram, appears similar to that before stretching. The polymer reduces friction between the AgNWs and the PVA film as well as acts as a shear force medium that will transfer the shear force from PVA film to AgNWs.

To achieve a good alignment with a minimal NWs breakage, the properties of the polymer lubricant should be chosen carefully. If the polymer viscosity is too low, the NW breakage will still occur since the NWs will still have a significant friction force with the substrate surface. If the polymer viscosity is too high, the alignment will degrade since the polymer does not flow easily with substrate stretching. Furthermore, because the PVA is stretched at an elevated temperature, the lubricant cannot harden or evaporate under heat. It was found that poly[oxy(methyl-1,2-ethanediyl)] has an appropriate level of viscosity and can flow (on the substrate) when the substrate underneath is stretched. It does not solidify or evaporate quickly, and can be removed post-alignment with ethanol. Through the use of this lubricant, the NWs do not have a strong attachment force to either the substrate or the lubricant and therefore they do not break easily. The NWs become aligned with the flowing force of the polymer, similar to NW assembly using microfluidics.

NWs of various densities were aligned as observed. Figure 3.4 shows the alignment of NWs with a density of 20 NWs/100 μm^2. With such high density, good alignment is still achieved and the average NW length is 6.6 μm, nearly the same average length as at a density of 3 NWs/100 μm^2. However, for samples denser than

shown in figure 3.4 (e.g. 100 NWs/100 μm^2), more NWs become tangled and alignment is degraded.

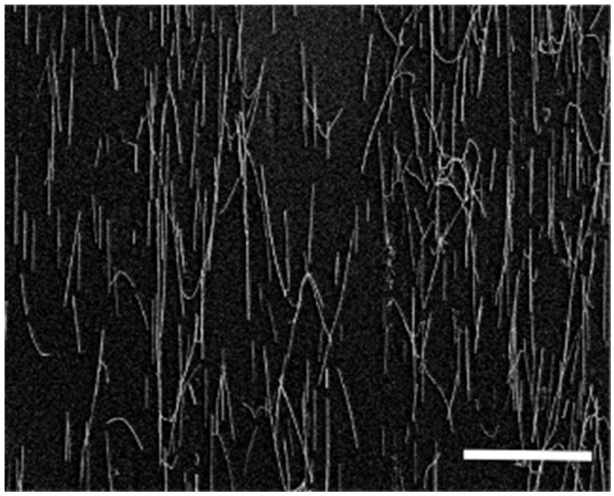

Figure 3.4 SEM image of higher density silver nanowires after aligning using lubricant (scale bar: 10 μm).

To demonstrate the versatility of our alignment method, semiconductor NWs (ZnO) grown on a substrate were also aligned. ZnO is a widely known semiconductor with a bandgap of (3.4 eV) and has broad applications specifically in optoelectronic applications. Unlike the AgNWs used in this work, which are synthesized in solution [22], the ZnONWs were grown on a substrate using chemical vapor deposition (after which they were removed from the substrate as a powder and dispersed in solution). SEM images of the ZnONWs before and after alignment are shown in figure 3.5. The volume ratio of polymer lubricant to ZnONW solution was 1:600. Similar to the AgNWs, the ZnONWs were well aligned after PVA stretching, with minimal breakage. The average NW length after alignment was 4.4 μm, only slightly less than the original 4.6 μm average length.

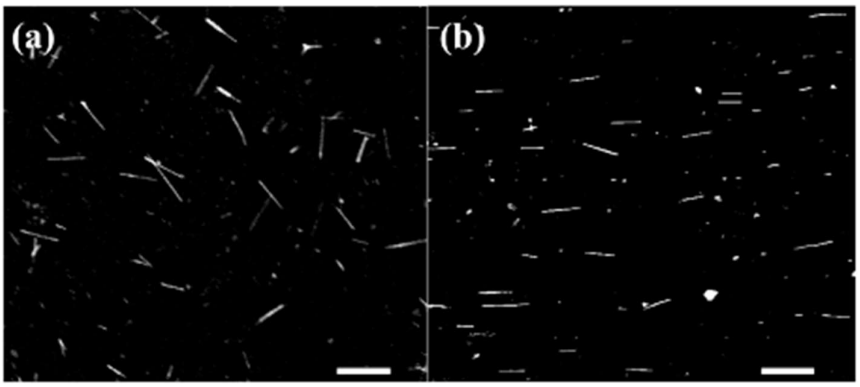

Figure 3.5 SEM images of zinc oxide nanowires (a) before substrate stretching, and (b) after substrate stretching with lubricant (scale bar: 10 μm).

In this study the order parameter *S*, defined as the statistical mean of the cosine of the angle difference between each NW and the main alignment direction, was calculated for both the 35 nm diameter AgNWs and 90 nm diameter AgNWs aligned with various polymer lubricant concentrations (table 3.1). The densities of the aligned NWs were (3 NWs/100 μm^2) and (1 NW/500 μm^2) for the 35 nm and 90 nm NWs diameter, respectively. The *S* parameter was calculated from a minimum of 400 NWs in each case. It can be seen that when the polymer concentration is too low, the average NW length is relatively small. However, if the polymer lubricant concentration is too high (e.g. 1:130 in the 35 nm diameter AgNW alignment case), the *S* parameter is as low as 0.90, indicating their poorer alignment compared to lower lubricant concentration case. The optimal balance between minimizing breakage and maximizing their alignment for the 35 nm diameter NWs occurred at a polymer lubricant/AgNW solution volume ratio of 1:1300, and 1:400 for the 90 nm diameter NWs. For the Mayer rod used, it can be calculated that the thickness of the deposited polymer film in each of these cases is 35 nm and 114 nm, respectively. Therefore, the thickness of the polymer lubricant in the optimal case is approximately equal to the

diameter of the NWs.

Table 3.1 (a) Average length and orientational order parameter, *S*, of 35 nm diameter silver nanowires aligned using different polymer concentrations

Polymer/AgNW solution volume ratio	Average length (μm)	*S*
No polymer, no stretching	6.81	0.15
No polymer, stretched to 450%	2.40	0.96
1:7800, stretched to 450%	3.52	0.97
1:5200, stretched to 450%	3.97	0.95
1:3900, stretched to 450%	4.18	0.96
1:2600, stretched to 450%	4.99	0.97
1:1300, stretched to 450%	6.76	0.93
1:130, stretched to 450%	6.62	0.90

Table 3.1. (b) Average length and *S* of 90 nm diameter silver nanowires aligned using different polymer concentrations

Polymer/AgNW solution volume ratio	Average length (μm)	*S*
No polymer, no stretching	16.22	0.34
No polymer, stretched to 450%	9.25	0.95
1:3000, stretched to 450%	10.31	0.94
1:400, stretched to 450%	16.14	0.95

Nanowire transfer: Many potential devices such as polarizers can be made using the aligned NWs directly on PVA. Also, the aligned NWs can be transferred, as described in the experimental section, if a different substrate is desired such as PET. Figure 3.2(b) is an SEM image of the aligned 90 nm AgNWs after transferring to a PET film. All the AgNWs remained aligned and there was not obvious breakage after the transfer process. In addition, less than 2% of the NWs were found on the PVA films after transfer, indicating that almost all the NWs had been transferred to the PET films.

Comparison to other alignment methods: In a few previous works, the order parameter (i.e. *S*) was used to quantify NW alignment. The highest value obtained so

far was S = 0.92 where cadmium selenide/cadmium sulfide nanorod alignment was achieved using an electric field [82][120][121]. In this work, we were able to achieve an S value as high as 0.97 (table 3.1(a)), with some NWs breakage, and S = 0.95 with a very minimal NWs damage (table 3.1(b)). In previous studies where substrate stretching or contraction processes [50][87][89] are performed, the order parameter S was never used. However, comparison can be achieved by using the angular distribution data shown in figure 2.2, where AgNWs with a diameter of 35 nm and a density of 15 NWs/100 μm^2 were aligned. The alignment in this work is superior to all these other works since more than 85% of the NWs were aligned within ±10° of the alignment direction. The reason is that the PVA was used as the stretching substrate rather than PDMS or PVDF, which can support much higher strains compared to elastic substrates.

Our newly proposed method can be easily applied on any NW material without specific properties requirements and can be performed for both NWs dispersed in solution or directly grown on a substrate. In the latter case, the NWs can be sonicated and dispersed in a solution for deposition, or they can be transferred to the PVA substrate through mechanical sliding of the growth substrate across the PVA surface. Furthermore, the material deposition and NW transfer process we used in this method are compatible with roll-to-roll processes. A very similar stretching process has been widely applied in the industry where PVA films impregnated with iodine are stretched to manufacture polarizers. These films are very commonly used as the polarizers in LCDs [122]. Thus, all the fabrication processes we used in this method are

industrially compatible.

3.3 Nanowire alignment based on Mayer rod alignment

3.3.1 Motivation

The technique of substrate stretching for NW alignment (chapter 3.2) can provide a supreme alignment result, however, an additional step is still needed for alignment besides NW deposition. Also, if PET or any other substrate is preferred for a specific application, a transfer step needs to be added to transfer the aligned NWs from PVA to the desired substrate. In this section, I demonstrate another alignment method through a rod coating process that does not encounter these drawbacks, since it does not require any extra steps such as substrate stretching and transfer. Furthermore, rod coating or the similar technique of doctor blading are very common methods for depositing materials on thin films over large areas, especially in the printable, flexible electronics industry, and it is also compatible with commercial roll-to-roll processes. Although the alignment achieved is not as high as with other methods, it is desirable for some applications such as transparent electrodes. In the latter, some misalignment is needed to obtain some NW overlap for percolation and thus film conduction (i.e. perfectly parallel NWs do not form a connected network). Though it has been implied that Mayer rod coating can quasi-align 1D nanostructures such as carbon nanotubes and NWs [123][124], a comprehensive study to investigate NW alignment by rod coating is still required for optimizing the alignment process. In this section, a slight preferential alignment is simply accomplished during the rod coating of the NWs and

a study of the pertinent parameters including NW concentration, rod rolling vs. dragging, rod rolling speed, solvent, temperature, and pressing between coats is presented.

3.3.2 Experimental

Nanowire film deposition and alignment: AgNWs dispersed in ethanol were purchased from Novarials (Woburn, MA) with an average diameter and length of 70 nm and 50 μm, respectively. The as-received NW solution was diluted by various amounts using ethanol, deionized water, acetone, and IPA to test the effects of both the concentration and solvent on NW alignment. PET films with a thickness of 127 μm, purchased from Tekra Inc. (New Berlin, WI), were sonicated in IPA for 60 s then deionized water for 30 s, followed by drying under nitrogen. The AgNW solution was then deposited on the PET films using Mayer rod coating [36][66][125]. Different rolling speeds, rod dragging vs. rolling, and temperatures conditions were tested to carefully study their effects on NW alignment. To make denser aligned NWs, mechanical pressure was applied at room temperature using an electric rolling press machine (MSK-HRP-01, MTI Corporation, Richmond, CA) after each NW coating layer, since the pressure increases the adhesion between the NWs and the substrate in order to maintain the alignment when subsequent layers were deposited.

Characterization: Similar to the characterization process used in chapter 3.2.2, SEM (LEO 1550, ZEISS Corporation) images were taken of the electrodes to investigate the NW morphology and alignment. A 10 nm gold layer was sputtered on top of the

samples to prevent electron charging.

Quantification of nanowire alignment: Image processing based on the skeletonization convolution operation (chapter 2.3) was used to characterize the denser overlapping NW alignment. The weighted orientational order parameter *S* is used to quantitatively assess the alignment quality as discussed in chapter 2.3.

3.3.3 Results and discussions

NW films were deposited with various NW solution concentrations, rolling methods, deposition speeds, solvents, and different processing temperatures. Even more, the consequence of the number of coatings and the effect of pressing between coats was also tested. The order parameter *S* was calculated to quantitatively determine the ideal parameters for best alignment. Stated *S* parameters in this work are calculated based on at least 1000 NWs for each sample.

Nanowire concentration: Of all coating variable parameters, the NW solution concentration had the greatest effect on their alignment. One layer of NWs with a solution concentration of 1.0, 3.0, or 5.0 mg/ml was coated on three equivalent PET films using a Mayer rod speed of 2 cm/s. The *S* parameters, calculated from SEM images, were 0.603, 0.546, and 0.403, respectively. With increasing NW concentration the *S* value decreases, indicating their poorer alignment. This degraded alignment behavior is because in denser networks the NWs do not have as much space to rotate towards alignment before impinging upon another NW. Although the sparsest NW films achieve the best alignment, this is not always the most practical

choice if denser films are required because an increased number of coats and mechanical pressings would be required.

Rod rolling vs. dragging technique: Both Mayer rod rolling and dragging (dragging the Mayer rod without rotating it) were found to achieve similar levels of alignment. However, the NW films deposited by dragging the rod results in some non-uniformity where stripes of denser regions of NWs exist along the dragging direction. Thus, in this and further studies (chapter 4), Mayer rod rolling was employed as it resulted in a much more uniform NW density.

Rolling speed effect: Higher rod rolling speeds led to lower *S* parameters. For example, at a NW concentration of 3.0 mg/ml, $S = 0.508$ at a speed of 4 cm/s compared to 0.546 at a speed of 2 cm/s. This is because at higher speeds the shear force on the NWs is shorter and weaker, resulting in poorer alignment. Although lower rod rolling speeds led to slightly higher *S* values (e.g. $S = 0.553$ at 0.2 cm/s for a NW concentration of 3.0 mg/ml), the NW density uniformity was compromised, with NWs being progressively sparser in the direction of the coating. An optimum speed of 2 cm/s was chosen to balance the NW alignment and their film uniformity.

Solvent effect: NWs dispersed in five different solvents were tested to study the solvent effect on the NW's alignment: DI water, IPA, ethanol, acetone, and methanol. Different solvents have different surface energies, which might affect the shear force, resulting in different alignment results. Aggregation of some NWs in the film was observed with the use of DI water due to the higher surface energy of water compared to PET. NW aggregation was also observed when using acetone as the solvent due to

the low solubility of PVP in acetone, which is the polymer that remains on the surface of polyol-synthesized AgNWs [22][126]. In the case of IPA, ethanol, and methanol, both NW alignment and film uniformity can be achieved after deposition, with almost no difference for each solvent. In this and further studies (chapter 4), ethanol was chosen as the solvent.

Temperature effect: A wide temperature range (22 °C-100 °C) was examined to study the impact of increased solvent evaporation rates on alignment. NWs dispersed in ethanol were deposited on PET films which were preheated by a hot plate to 50 °C and 100 °C. The NW solution concentration was 3.0 mg/ml and the rolling speed was 2 cm/s. Higher temperature led to poor alignment, with S = 0.504 at 50 °C and S = 0.385 at 100 °C, which were both lower than the S value (0.546) at room temperature. The faster solvent evaporation may lead to less shear force, due to the lack of solvent flow during the alignment process. Consequently, room temperature is observed to be the optimal temperature condition for best NW alignment.

Number of coats and pressing between coats: To understand the relationship between coating cycle and NW alignment, as well the effect of pressing between coats, preferentially aligned NW electrodes were fabricated with and without mechanical pressing after each coat with a NW solution concentration of 3 mg/ml. The orientational order parameter, S, was calculated after each NW coating cycle for both samples and shown in table 3.2.

Table 3.2 Alignment comparison of preferentially aligned nanowire films with and without mechanical pressing after each nanowire coat

Coating cycle	*S* value (with mechanical pressing)	*S* value (without mechanical pressing)
After 1st coat	0.546	0.546
After 2nd coat	0.534	0.477
After 3rd coat	0.516	0.434
After 4th coat	0.495	0.394

It can be seen from table 3.2 that *S* values drop after each NW coating either with or without mechanical press, indicating that alignment degrades by multiple coatings. Coats negatively affect the alignment of subsequently coated layers because of their surface roughness, which impedes NW rotation. However, in case of the mechanical pressing, the *S* value drops much less than that of samples fabricated without mechanical pressing. These findings may be because pressing helps maintain the alignment as it improves adhesion of the NWs to the substrate and limits their rotation during the subsequent coating process. Pressing also aids in the alignment of subsequent coatings since it reduces the surface roughness of the NW film.

Figure 3.6(a) and (b) show SEM images of aligned AgNWs by Mayer rod coating with higher and lower NW density, respectively. The *S* value beneath each image quantifies the extent of alignment. The samples in figure 3.6(a) and (b) were deposited in the same direction for all four and three coats, respectively, using the same NW solution concentration. A rolling speed of 2 cm/s was used and mechanical pressing was applied after each coat to maintain alignment when subsequent layers were coated.

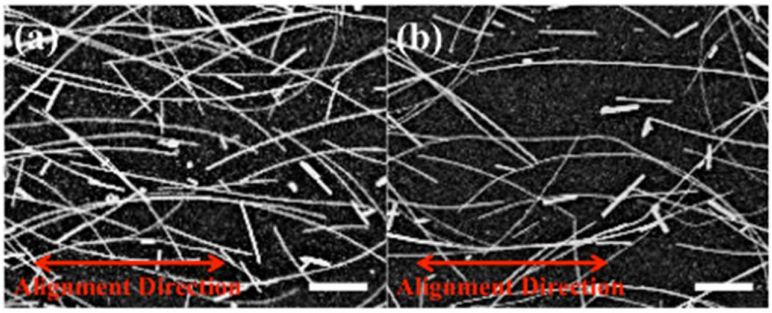

Figure 3.6 SEM images of (a) aligned silver nanowires by Mayer rod coating with a higher density and (b) a lower density along the horizontal direction (scale bar: 10 µm) The *S* parameter below each image quantifies the extent of alignment.

It can be seen that there is a slight preferential alignment of the NWs along the horizontal direction due to the shear force provided by rod coating and the capillary forces of solvent evaporation. In more detail, the Mayer rod coating can impart a slight alignment to the NWs due to the shear force of solvent flow, similar to microfluidic NW alignment [72]. The shear forces cause the NWs to rotate and preferentially align in the direction of the moving rod. After the rod rolling process, further AgNW alignment is facilitated by the capillary force induced by solvent evaporation, similar to capillary printing [90]. Even though the solvent evaporates out-of-plane, the liquid evaporation at the contact line (i.e. substrate-solvent-air interface) generates a net force to the NWs in the direction perpendicular to the contact line and inline with the alignment direction [127].

The alignment in figure 3.6(b) is slightly better than that in 3.6(a) since one less coating layer was required compared to 3.6(a). As discussed above, coats negatively affect the alignment of subsequently coated layers. With the optimum conditions, an alignment quality of S~0.5 can be achieved.

The alignment achieved by Mayer rod coating is not as high as that achieved by

other previous commonly used alignment methods [50][72][79][84] and by the substrate stretching technique described in chapter 3.2. However, it may be suitable in instances where rod-coating is already used to deposit NWs and imparting a modest alignment during coating, without the need for any additional steps, can provide some benefit. It is suitable for transparent electrode applications specifically, since a film of perfectly aligned AgNWs would not be conductive. Furthermore, this alignment method is advantageous for transparent electrodes because of its low cost, large area scalability, and roll-to-roll process compatibility. Most importantly, rod coating is already a standard method of AgNW electrode deposition so no extra steps are required to implement this strategy. In chapter 4, the alignment achieved during Meyer rod coating is exploited to increase the AgNW electrode transparency to linearly polarized light.

3.4 Conclusions

Aligning NWs by stretching PVA substrates is a simple, low-cost, large-area NW alignment method that can be used for both metallic and semiconductor NWs that are synthesized either in solution or on a substrate. Because PVA can be stretched up to 450% and does not retract after stretching, the method is both highly effective and convenient, which does not need a second stretching to achieve a supreme alignment result, with *S* values great as 0.97 achievable. Using poly[oxy(methyl-1,2-ethanediyl)] as a lubricant significantly reduces NW breakage which solves a persistent problem with shear force-based alignment methods.

A slight preferential alignment was achieved during Mayer rod coating, making it a simple, large-area, cost effective method as well, which is further compatible with roll-to-roll processes and does not require any extra steps since it is a common method for depositing NW films. It was found that sparser NWs deposited at a rolling speed of 2 cm/s at room temperature, with mechanical pressure applied between each coat led to the best NW film uniformity and alignment.

Both NW alignment techniques provide researchers in nanoscience and nanotechnology with simple, low-cost, and large-area methods for obtaining aligned NWs in large-area flexible electronics. Both techniques may also be applicable to in aligning other elongated nanostructures such as nanotubes and nanorods. The techniques are used in the following studies (chapter 4-5) to achieve NW alignment for applications.

Chapter 4 Exploiting both optical and electrical anisotropy in nanowire electrodes for higher transparency

Part of this work was published in a first-author publication [68].

4.1 Introduction

4.1.1 Traditional transparent electrodes

Transparent electrodes are films that are both electrically conductive and optically transparent. These electrodes are a crucial part of many electronic and optoelectronic devices such as touch panels, LCDs, OLEDs, solar cells, and transparent heaters. Electrical conductivity and optical transparency are two essential factors to evaluate the performance of transparent electrodes. In general, a good transparent electrode must have both a high conductivity and transparency, which can be evaluated by the FoM introduced in chapter 1.3.2.

ITO is currently the material most often used for commercial transparent electrodes. However, ITO films are not suitable as next generation transparent electrodes due to several limitations. First, indium is a rare earth material in scarce supply and the deposition of ITO requires complicated equipment and complex processes (e.g. elevated temperature and high vacuum conditions), both which cause the electrodes to be costly [128]. Second, ITO is not mechanically flexible, with strains as low as 3% causing it to crack. This makes it unsuitable for next-generation flexible electronic devices [129]. Third, ITO has a high refractive index (~1.9), which

is unfavorable for display applications since it reflects light [130]. Fourth, the ITO bandgap is about 4 eV, which leads to large absorption of light at wavelengths below 300 nm. Transparency of light with wavelengths above 1000 nm is also low due to plasma oscillations [131]. Thus, ITO is not suitable for the applications where a high transparency of UV or infrared light is required.

A replacement material for ITO with characteristics such as low cost, simple fabrication, mechanical flexibility and light weight is highly desired. This could have a huge economic impact, given that the transparent electrode market is currently $4.1 billion, as well as enable new devices such as flexible optoelectronic devices [132].

4.1.2 Random silver nanowire transparent electrodes

To overcome the drawbacks of ITO films, AgNW networks have been recently introduced as a promising alternative material [133][134]. Figure 4.1 shows an AgNW transparent electrode and an SEM image of its structure on a micrometer scale.

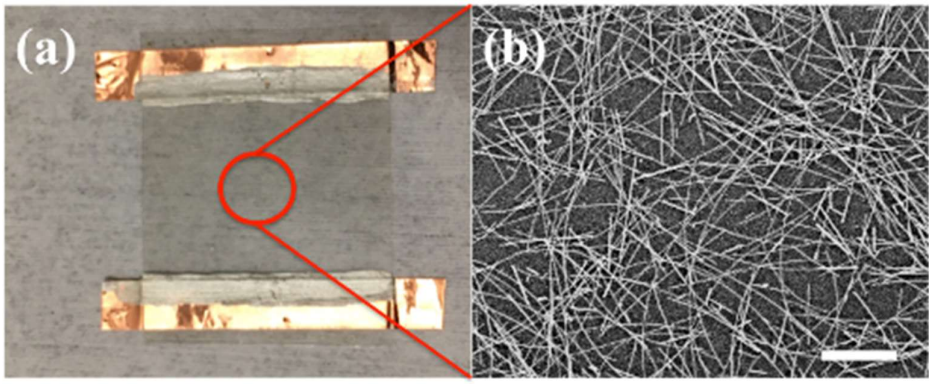

Figure 4.1 (a) Photograph and (b) SEM image of a silver nanowire transparent electrode. (Scale bar: 20 μm)

Random meshes of AgNWs show great potential to replace ITO as next generation transparent electrodes [135]. They have high transparency up to 90% with

a sheet resistance below 10 Ω/sq, which is similar to that of ITO electrodes [36]. AgNWs can be easily synthesized in solution using a scalable technique [21], and then deposited directly on a large-area transparent substrates such as PET or glass to create a random conductive network. AgNW films can be deposited in atmosphere using simple and inexpensive solution-deposition methods like spin coating [136], spray coating [137], and Meyer rod coating [36]. And the films can be fabricated either at room temperature [138], or at low annealing temperatures [36], making them compatible with plastic substrates to achieve flexible electrodes. These films are similar to an alternatively studied material, carbon nanotube films, except in this case all wires are metallic unlike batches of carbon nanotubes which usually contain a portion of less conductive semiconducting nanotubes. And because metal junctions can be sintered, the NW-NW junction resistances can also be much lower than for carbon nanotubes. This results in much higher conductivities for a given transparency compared to carbon nanotube electrodes. Regarding their optical properties, AgNW films are much more transparent in the infrared range than ITO which makes them more suitable for multi-junction solar cells, smart windows and other applications where transparency in the IR is required [134]. Although Ag is an expensive material, so little of it is used, resulting in a material cost less than half that of ITO [37]. And unlike ITO, AgNW transparent electrodes are very mechanically flexible and thus can be used in flexible device technologies [66].

AgNW transparent electrodes have attracted worldwide attention from both academia and industry. More than 200 research papers on the topic of AgNW

electrodes have been published, and these electrodes have been successfully integrated into devices including touch screens, OLEDs, solar cells, and smart windows [37][139][140][141]. Touch screens are the most likely first widespread application of AgNW electrodes, with several large companies currently developing AgNW electrodes for their touch screen devices. This is a large market; the global touch screen market was US$6B in 2016 and is expected to grow to US$20B by 2025 [142]. Thus, a small performance improvement of AgNW electrodes could lead to a tremendous contribution.

4.1.3 Aligned silver nanowire transparent electrodes

Up to now, the majority of the studies focus on electrodes where the AgNWs are randomly oriented in a mesh, such as in figure 4.1(b). However, aligning the AgNWs can improve the electrode properties, as this can lower sheet resistance while maintaining transparency [90][143]. Despite the advantages, only a few studies have discussed aligned NW electrodes. This is due in part because of the lack of inexpensive, large-area NW alignment methods.

Jagota et al developed a computational model to analyze the electrical conductivity of both random and partially aligned metal NW networks [143]. Partial alignment is the situation where the alignment quality is higher than that of no alignment and lower than that of perfect alignment, as shown in figure 4.2.

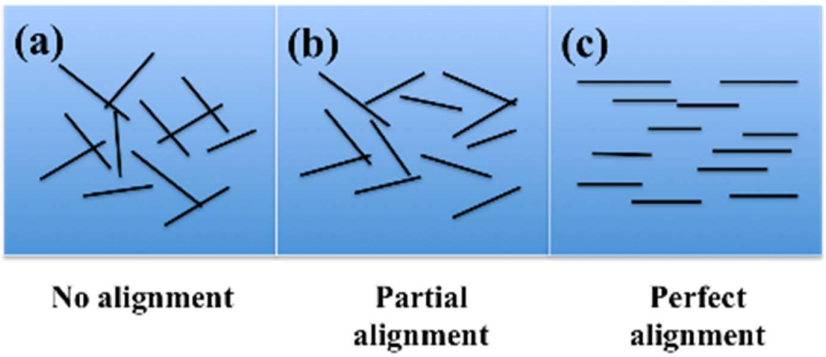

Figure 4.2 Schematics of nanowire networks with (a) no alignment, (b) partial alignment and (c) perfect alignment.

The simulation results show that the conductivity along the alignment direction increases at first but then decreases with increasing the alignment quality. This phenomenon can be explained by the result of two competing effects. As the alignment increases beyond a random orientation, the number of NW-NW junctions the current must travel through to cross the film decreases. Because the resistance of NW junctions is far higher than the resistance along the NW themselves [144], having pathways with less junctions leads to lower sheet resistance. On the other hand, as alignment increases less NWs are connected in the network since alignment reduces their probability of overlapping with other NWs. In the extreme case of perfect alignment (figure 4.2(c)), no NWs are overlapping one another. A lower number of connected NW means a lower number of NWs conducting current, and thus the sheet resistance increases. The model showed that an optimized extent of alignment can be found and is dependent on NW length and density. It was shown that conductivity can be improved by approximately 20% compared to the isotropic state [143].

Ko's group showed an experimental study on the relation between alignment and transparent electrode sheet resistance, where the AgNWs were aligned by capillary

printing [90]. From their results (figure 4.3), the aligned AgNW films showed significantly lower sheet resistance at the same NW surface density in comparison with those of random AgNW films.

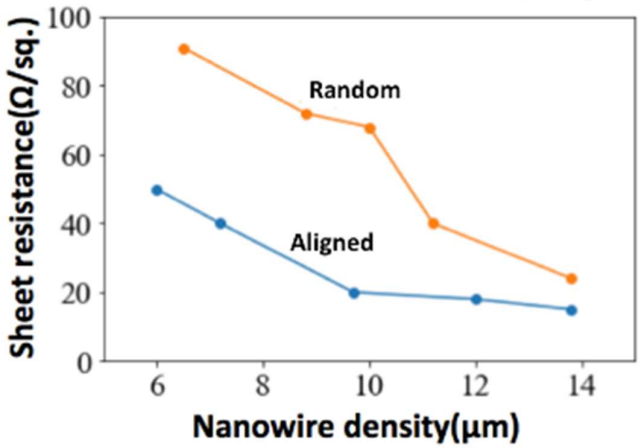

Figure 4.3 Sheet resistance for silver nanowire networks with aligned and randomly oriented geometries as a function of nanowire linear density. Data from [90].

Both of the studies above indicate that preferential alignment of NWs can increase their conductivity along the alignment direction compared to randomly oriented AgNW networks. However, NWs possess not only electrical anisotropy, but optical anisotropy as well, and no studies have yet investigated the ability to exploit their optical anisotropy to improve the transparency of NW transparent electrodes [90][143]. Furthermore, the alignment methods used to align AgNW films for electrodes in past studies are complicated and not compatible with roll-to-roll processes [77][90]. In this chapter, both the electrical and optical properties of aligned AgNW films are investigated and used to improve NW transparent electrode properties. FoM values are calculated to compare the performance of aligned and random transparent electrodes. The alignment is achieved through rod coating, which is simple and compatible with roll-to-roll processes.

4.1.4 Liquid crystal displays

An LCD is a flat panel display which uses the light modulating properties of liquid crystals. The working principle of an LCD is based on controlling the alignment of liquid crystal molecules using an electric field [145]. A schematic of a basic LCD is shown in figure 4.4.

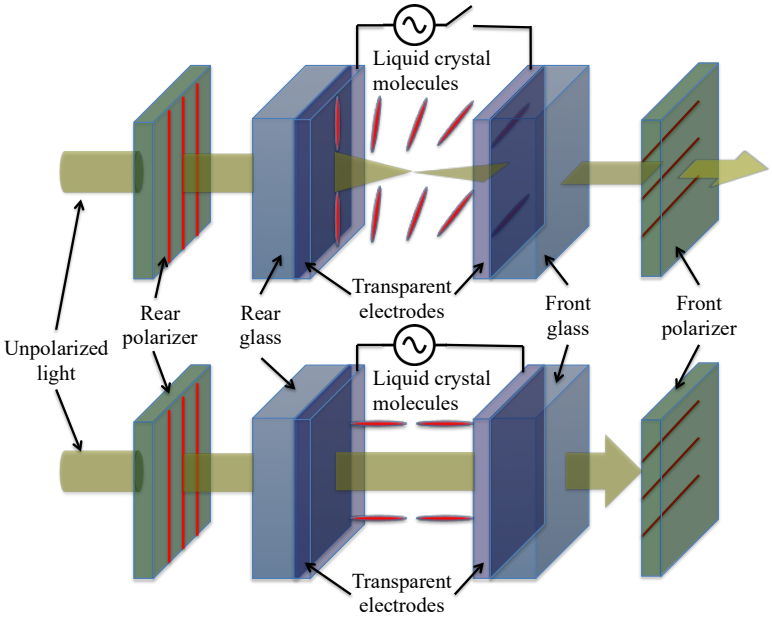

Figure 4.4 Structure of a liquid crystal display showing the OFF state (upper) and the ON state (lower).

As in figure 4.4, an LCD consists of 6 main parts: a light source, a rear polarizer, an ITO coated glass electrode, twisted nematic liquid crystals, a second glass substrate with ITO, and a front polarizer that is rotated 90° in relation to the rear polarizer [146]. In the OFF state, the liquid crystals are twisted by 90° when no external field is present. The polarization of the light emanating from the rear polarizer is rotated 90° when it passes through the twisted liquid crystals and thus is able to pass through the front polarizer. In the ON state, the crystals realign themselves with the field. In this

case, the polarization of the light emanating from the rear polarizer is unaffected, and the light is thus blocked by the front polarizer [147]. The transparent electrodes on the front/rear glass need to provide good conductivity as well as very high transparency to light. While the benefits of increased transparency is obvious, good conductivity is beneficial in minimizing the voltage drop across the electrode and to ensure fast switching times [37]. Unlike solar cells or OLEDs, transparent electrodes used for LCDs only need to be transparent to linearly polarized light rather than random light. In the case of LCDs, light wavelengths of 450 nm (i.e. blue light), 550 nm (i.e. green light), and 630 nm (i.e. red light) are mostly concerned, corresponding to the backlight wavelengths.

4.1.5 Metal nanowire polarizer

Aligned metallic NW arrays using photo/nanoimprint lithography techniques have attracted considerable interest for light polarization ranging from UV to infrared light [148][149][150]. Up to now, metal NWs such as gold, copper, aluminum, and Ag NW arrays have been used for polarizing light, and their optical properties have already been well studied [151][152].

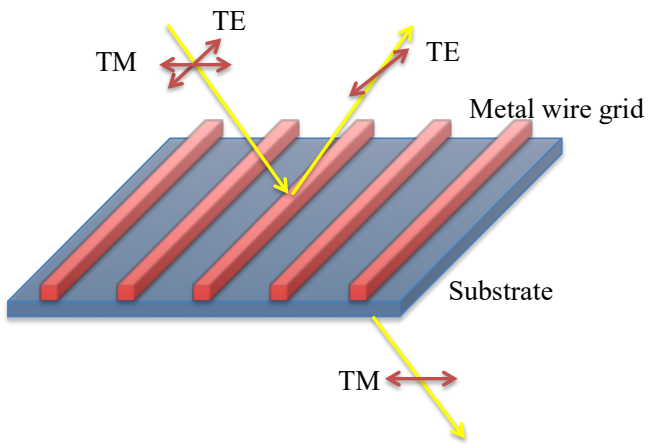

Figure 4.5 The working principle of a metal wire grid polarizer. TE represents TE-mode light (electric vector parallel to the grid lines), and TM represents TM-mode light (electric vector perpendicular to the grid lines).

Figure 4.5 shows the working principle of a metal wire grid polarizer. The thickness of the grid lines and their period should be sub-wavelength [153]. For light waves with their electric field parallel to the metallic NW arrays (i.e. parallel-polarized light), the movement of electrons along the length of the NW arrays can be induced. Since the electrons are free to move in this direction, the wave is reflected backwards along the incident beam, which is similar to continuous metal film when reflecting light. For waves with electric fields perpendicular to the NW arrays (i.e. perpendicular polarized light), electrons cannot oscillate with the field because the NW diameters are less than the wavelength and therefore the wave passes through. Since electric field components parallel to the NW arrays are reflected, the transmitted wave has an electric field purely in the direction perpendicular to the NW arrays [153].

Several studies have utilized the optical anisotropy of aligned AgNWs for polarizers, which provide higher transparency to perpendicularly polarized light than

parallel-polarized light. However, because the focus was on light polarization and not as their use as an electrode, the films are not conductive. Furthermore, the polarizers only operate at infrared wavelengths (wavelengths greater than 1000 nm) [92][154]. This is because the polarization inversion point of previously fabricated AgNW polarizers lies in the visible range.

In this work, I do not aim to use aligned AgNW films as a polarizer for LCDs because, even if the wavelength range is applicable (i.e. in the visible), commercially used LCD polarizers made by stretched iodine-doped PVA films have better performance and lower cost. However, the fact that aligned AgNW films have been shown to be more transparent to one type of polarized light is an interesting property which could be exploited to make NW transparent electrodes more transparent.

4.2 Motivation

In some device applications that employ transparent electrodes, the electrode should be isotropically transparent and conductive. However, in many other applications this is not the case. In LCDs, for which AgNW films would be the common electrodes, electrodes only need to be transparent to one kind of linearly polarized light. Additionally, in active-matrix LCDs, the most popular type of high-resolution LCDs [155], electric current only needs to flow along one direction of the transparent electrode. Similarly, the transparent electrodes used for touch sensors existing on top of LCDs, such as the touch screens on many cell phones, monitors and tablets, also generally need to only be transparent to one type of linearly polarized light as well as

require electrical conduction in only one direction. Furthermore, due to the common configuration of the metal contact bars acting as voltage suppliers or current collectors, organic solar cells, e-paper, smart windows, and OLED displays would benefit if the conductivity of the transparent electrode can be made higher in one direction even if conductivity in the other direction is compromised [156][157][158].

Unlike a conductive oxide film, which has the same properties in all in-plane directions, it was seen in subchapters 4.1.3 and 4.1.5 that films of NWs have anisotropic electrical and optical properties if the NWs are aligned. The anisotropic properties can be exploited to better design NW electrodes for applications where isotropic transparency or conductivity is not required such as LCDs and touch screens. Overall, NW alignment can be employed to both increase transparency in applications where polarized light is used as well as increase transparency for devices in which conductivity in one direction is more important than the other.

Even though substrate stretching (chapter 3.2) can achieve a better alignment quality than Mayer rod coating (chapter 3.3), it is not appropriate for electrode applications because a highly aligned AgNW network has low conductivity (as explained in chapter 4.1.3). And alignment achieved through Mayer rod deposition is very attractive for electrodes since it is already a standard method to deposit AgNW electrodes [36] so it doesn't require any extra steps, and it is roll-to-roll compatible.

In this chapter, the properties of preferentially aligned AgNWs are used to achieve a higher transparency to polarized light within the visible range, while also reducing the sheet resistance in one direction compared to typical random AgNW

electrodes. This is the first time preferentially-aligned AgNW networks has been used to increase transparency to polarized light in the visible range, allowing for electrodes to have higher transparencies for display applications and the touchscreens on top of them. Furthermore, although previous studies have shown that preferentially-aligned AgNWs can lead to higher conductivities in one direction, their alignment methods are complicated or are not compatible with roll-to-roll processes [77][90]. The performance improvements here are achieved using no extra processing steps which makes this an attractive strategy for AgNW transparent electrodes for touch screen, LCD, organic solar cell, e-paper, smart window, and OLED display applications.

4.3 Experimental

4.3.1 Fabrication of electrodes

AgNWs dispersed in ethanol were purchased from Novarials (Woburn, MA) with an average diameter and length of 70 nm and 50 μm. PET films with a thickness of 127 μm purchased from Tekra Inc. (New Berlin, WI), were sonicated in isopropanol alcohol for 60 s then DI water for 30 s, followed by drying in nitrogen. The AgNW solution was then deposited on the PET films using Mayer rod coating. A moderate NW alignment was achieved during Mayer rod coating, which is elaborated in chapter 3.3. The AgNW solution concentration, coating times, and rolling speed are different for different electrodes, which will be discussed in chapter 4.4.2. To fuse the overlapping NW junctions and thus reduce the electrode sheet resistance, mechanical pressure was applied at room temperature using an electric rolling press machine

(MSK-HRP-01, MTI Corporation, Richmond, CA) [159]. The pressure can also maintain the NW alignment when subsequent layers were deposited, as mentioned in chapter 3.3.3. For randomly aligned electrodes, pressing was only done after all coats were completed. Pressing once rather than multiple times does not make an obvious difference on sheet resistance (e.g. 0.6% difference between pressing once and four times). For each pressing round, the electrodes were first pressed with a roller spacing of 80 μm, and then rolled again with a spacing of 60 μm to better weld the NW joints. The rolling speed was 5 mm/s. Ag paste and strips of copper tape were applied on the two ends of each electrode.

4.3.2 Characterization of transparent electrodes

The electrode sheet resistance was measured through a 2-point probe measurement method using a multimeter (IP54, AccuRemote Corporate, San Clemente, CA). The multimeter probes were placed on the strips of copper tape at the two edges of a sample to obtain the resistance. The sheet resistance was then calculated by multiplying this resistance by the ratio of width to the length of the film (W/L). Past results from our group showed that the numbers from two-point measurement method are similar to those from a 4-point probe measurement [160].

Transparency spectra to parallel-polarized light, perpendicularly polarized light, and non-polarized light were measured with a UV-2501PC Shimadzu spectrophotometer. Linear polarized light was obtained using a polarizer purchased from Edmund Optics Inc. (Tokyo, Japan).

4.3.3 Simulation of aligned silver nanowire optical properties

Simulation work was done to understand the optical anisotropy of aligned AgNWs as well as interpret the experimental results. A finite difference time domain method was employed to calculate the transparency of aligned AgNWs to parallel and perpendicularly polarized light using Computer Simulation Technology (CST) Microwave Studio [161]. A mesh was built in the simulation environment, appropriate boundary conditions are applied and then a plane wave source is incident on the structure. Based on the mesh, Maxwell's equations at each point in the mesh was solved. Transparency can thus be calculated by deriving the power out divided by the input power from the plane wave source.

4.4 Results and discussion

4.4.1 Simulation

Figure 4.6 shows the simulated optical transparency of aligned AgNWs to perpendicularly (red line) and parallel (black line) polarized light as a function of wavelength. A unit cell boundary condition is applied in the (x-y) plane to generate a model composed of an infinite number of parallel infinitely long Ag cylinders with diameters of 70 nm and a period of 280 nm on a PET substrate. The alignment is perfect (i.e. S = 1). The simulation uses the optical properties of bulk Ag obtained from Palik's 1985 handbook which is the most commonly used Ag optical data used for simulation studies [162], and the surrounding medium is vacuum. Incident polarized light is applied normally to the PET substrate. Perpendicularly polarized

light is defined as light whose polarization direction is perpendicular to the NW long axes, while parallel-polarized light has a polarization direction parallel to the NW long axes. A dip in the NW transparency to perpendicularly polarized light was observed at wavelengths between 300 - 400 nm, which is mainly attributed to transverse surface plasmon resonances (SPRs) that are induced by electron oscillations along the NW diameters. However, across the visible wavelength range, the NW film is around 97% transparent to perpendicularly polarized light, far higher than the transparency to parallel-polarized light. This is because the NWs are only 70 nm thick along the direction of the electric field in the perpendicular polarization case, which is smaller than all visible wavelengths. Transverse electrons oscillation cannot occur and thus little light is absorbed or reflected. The parallel-polarized light, on the other hand, can induce electron oscillation along the NW long axes, allowing for longitude SPRs and thus a decrease in their transparency across the visible range.

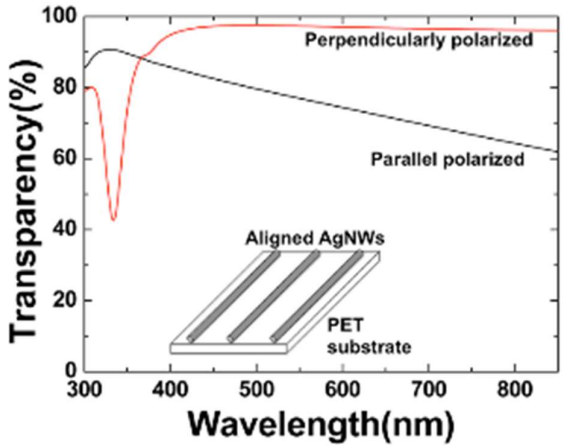

Figure 4.6 Simulated transparency vs. wavelength graph of aligned silver nanowires to both perpendicularly (red line) and parallel (black line) polarized light. (Inset: schematic of the unit cell used in the model).

For electrode applications where transparency to only one kind of linearly

polarized light is needed in the visible range, higher transparency can be achieved if a higher-than-average fraction of the NWs are aligned such that their long axes are perpendicular to the electric field of the polarized light compared to random alignment. In this work, the NWs are not perfectly aligned like in the simulation, but even for NWs that are rotated somewhat, their cross-sections to the electric field of perpendicularly polarized light is still less than visible wavelengths and thus less light will be absorbed or reflected. As mentioned previously, some misalignment is necessary to achieve a conductive film since NWs aligned perfectly to one another do not contact one another.

4.4.2 Aligned silver nanowire electrodes

Figure 4.7(a) and (b) compare 16 Ω/sq electrodes with more random and more aligned AgNWs, respectively. For the sample in figure 4.7(a), a NW solution with a concentration of 3.25 mg/ml is used for their deposition. In order to achieve a randomly aligned NW network, the NWs were coated in four orthogonal directions with a higher rolling speed of 4.0 cm/s. The sample was then mechanically pressed after applying all coats, but not pressed between each coat. The sample shown in figure 4.7(b) is deposited in the same direction for all four coats using a NW solution with a concentration of 3.0 mg/ml to achieve alignment (S = 0.495). A rolling speed of 2 cm/s was used and mechanical pressing was applied after each coat to maintain their alignment when subsequent layers were coated. It can be seen that there is a slight preferential alignment of the NWs along the horizontal direction due to the shear

force of the rod coating. Furthermore, different NW solution concentrations were used for randomly and preferentially aligned NW electrodes so that transparency could be compared for electrodes with the same sheet resistance. When the same NW concentration is used, the sheet resistance of the randomly aligned NW electrode is about 10 percentage points higher than that of the preferentially aligned NW electrode in the direction parallel to NW alignment.

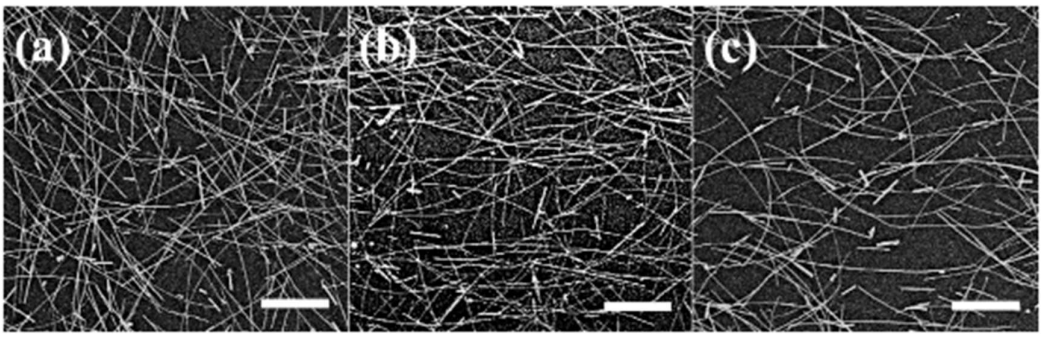

Figure 4.7 SEM images of a (a) 16 Ω/sq electrode with randomly oriented silver nanowires, (b) 16 Ω/sq electrode with a slight preferential alignment of silver nanowires along the horizontal direction, and (c) a 26 Ω/sq electrode with a slight preferential alignment of nanowires along the horizontal direction. (Scale bar: 20 μm).

Figure 4.7(c) shows the alignment result of a 26 Ω/sq electrode. The alignment (S = 0.517) is slightly better than in figure 4.7(b) since one less coating layer was required compared to (b). As discussed in chapter 3.3.3, coats negatively affect the alignment of subsequently coated layers and thus an electrode realized with less coating cycles has slightly better alignment.

4.4.3 Transparency and conductivity enhancement of aligned nanowires

The transparency spectra of the randomly and preferentially aligned AgNW films shown in figure 4.7(a) and (b) respectively are plotted in figure 4.8 (these same

transparency trends were observed among several samples). It should be noted that these are specular transparencies and they do not include diffusive light; if the latter is included, as is the case for many other reports [36], the transparencies would be 9.0 percentage points higher for the 16 Ω/sq electrode and 8.5 percentage points higher for the 26 Ω/sq electrode.

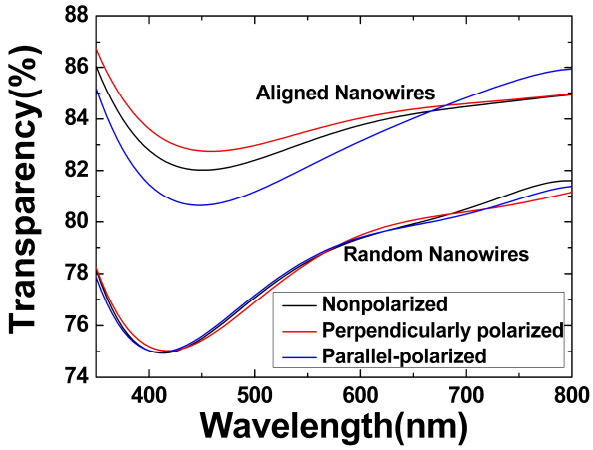

Figure 4.8 Transparency comparison between preferentially and randomly aligned silver nanowire transparent electrodes with the same sheet resistance of 16 Ω/sq to perpendicularly (red line) and parallel polarized light (blue line), and non-polarized light (black line).

Firstly, as shown with the two black curves, the transparency of the preferentially aligned NW electrode to non-polarized light is significantly higher than that of the random NW network. This is because a lower NW density is required to achieve a 16 Ω/sq sheet resistance between the two ends of the electrode when the NWs are preferentially aligned in the direction connecting the two ends. As listed in table 4.1(a), at 450 nm the transparency difference is 6.5 percentage points, which is higher than the experimental results reviewed in chapter 4.1.3 where NW alignment was also used to maximize conductivity along one direction [90]. In that latter study, the

transparency difference between aligned NWs and random NWs at 450 nm is less than 5 percentage points. In another study where NW alignment was achieved by water-bath dip coating, the transparency difference between aligned NWs and random NWs at 450 nm is only 2 percentage points [77]. In regards to FoM, which is calculated in table 4.1(b), the FoM of the preferentially aligned 16 Ω/sq electrode to non-polarized light is 27.1×10^{-3} Ω^{-1} compared to 17.2×10^{-3} Ω^{-1} of the randomly-aligned electrode. It should be noted for the calculation of FoM, total (diffusive + specular) transparency was used instead of specular transparency only.

Table 4.1 (a) Transparency comparison of randomly and preferentially aligned silver nanowire transparent electrodes to non-polarized and perpendicularly polarized light.

Sample	T_nonpolarized (450 nm)	T_ perpendicularly polarized (450 nm)
Random, 16 Ω/sq	75.5%	75.5%
Aligned, 16 Ω/sq	82.0%	82.8%
Random, 26 Ω/sq	83.0%	83.1%
Aligned, 26 Ω/sq	85.7%	86.4%

Table 4.1 (b) Figure of merit comparison of randomly and preferentially aligned silver nanowire transparent electrodes based on non-polarized and perpendicularly polarized light.

Sample	FoM (10^{-3} Ω^{-1}) (Nonpolarized)	FoM (10^{-3} Ω^{-1}) (Perpendicularly polarized)
Random, 16 Ω/sq	17.2	17.2
Aligned, 16 Ω/sq	27.1	28.6
Random, 26 Ω/sq	17.4	17.4
Aligned, 26 Ω/sq	28.1	28.7

The alignment compromises the sheet resistance in the orthogonal direction; in this case it is increased to 18 Ω/sq. Similarly, the orthogonal sheet resistance increases to 34 Ω/sq for the sample shown in figure 4.7(c), which has a sheet resistance of 26

Ω/sq in the direction parallel to NW alignment. However, for many applications conductivity along one direction is far more important than the other and in these cases preferentially aligning the NWs allows for superior transparency or alternatively, a higher conductivity in a given direction at the same transparency.

Regarding the transparency to polarized light, figure 4.8 shows that the randomly aligned AgNW electrode is nearly equally transparent to polarized and non-polarized light, as expected. The preferentially aligned NW electrode, on the other hand, is more transparent to perpendicularly polarized light than to non-polarized light for wavelengths less than 670 nm, which includes the 450 - 630 nm range that is of interest for LCDs and the touchscreens on top of them. At the wavelength of 450 nm, for example, the boost in transparency is 0.8 percentage points For the purposes of comparing to the simulation results in figure 4.6, this corresponds to a transparency difference between perpendicularly polarized light and parallel-polarized light (rather than perpendicularly polarized light to non-polarized light) of 2.2 percentage points. This is lower than the simulated case because of the non-perfect alignment. However, it is still advantageous for applications such as touch screens and LCDs to preferentially align NWs such that their long axes are perpendicular to the direction of light polarization. In this example, the total transparency enhancement due to both the increased conduction in one direction and increased transparency to polarized light is 7.3 percentage points, and the FoM became $28.6 \times 10^{-3}\ \Omega^{-1}$ (from $17.2 \times 10^{-3}\ \Omega^{-1}$ for the random electrode), a significant increase particularly for a simply implemented strategy.

In figure 4.8, we can observe that the transparency trend between perpendicularly and parallel polarized light reverses at a wavelength of 670 nm, known as the polarization inversion point. As mentioned in chapter 4.1.3, previous studies on aligned AgNW polarizers can only operate at infrared wavelengths because the polarization inversion point of these polarizers lies in the visible range. In this work, a sparser film of NWs than that of polarizers [92][154] was used, leading to a film with a smaller metal fraction on the PET substrate. The film thus has a lower average plasma frequency, causing the polarization inversion to occur at higher wavelengths than visible range. More details of this polarization inversion phenomenon can be found in the literature [149][152][163].

Different applications have different electrode sheet resistance requirements, so the consequence of preferential alignment on more resistive and transparent electrodes was also studied. The transparency of randomly and preferentially aligned NW films with a sheet resistance of 26 Ω/sq is shown in table 4.1(a). The total transparency increase due to alignment is 3.4 percentage points at a wavelength of 450 nm. The difference in FoM between random and aligned 26 Ω/sq electrodes to nonpolarized light (i.e. 28.1×10^{-3} Ω^{-1} versus 17.4×10^{-3} Ω^{-1}) is larger than that for 16 Ω/sq electrodes (i.e. 27.1×10^{-3} Ω^{-1} versus 17.2×10^{-3} Ω^{-1}). This is both because the NWs are better aligned in the more resistive electrode, and also because alignment reduces the sheet resistance more in sparser NW networks as can be seen in figure 4.3. The latter is because reducing the number of junctions in the pathways is more important when there are fewer pathways. The aligned electrodes FoM increase

between polarized and non-polarized light, however, is more modest for the 26 Ω/sq electrodes than the 16 Ω/sq electrodes because of the higher starting transparency of the former. Overall, because of these two effects, the final FoM of the preferentially-aligned 26 Ω/sq electrode nearly matches that of the 16 Ω/sq electrode with respect to polarized light.

It is interesting to postulate what the ideal alignment (i.e. ideal *S* value) would be to maximize the FoM. Perfect alignment ($S = 1$) is best for maximizing the film's transparency to polarized light. But the FoM would be 0 due to the infinite sheet resistance that would result. If FoM was plotted versus *S*, it would first increase with *S* but then decrease at larger values of *S*, as is the case when discussing the effects of alignment on sheet resistance alone (section 4.1.3). However, adding in the effect of alignment on the network's transparency to polarized light, the peak would occur at a higher *S* value. This optimized *S* would be dependent on NW length and density. Experimentally determining FoM versus *S* was not done here as the maximum *S* obtainable with rod-coating is lower than the *S* required for maximal FoM

4.4.4 Transparency enhancement of highly aligned nanowires

The transparency spectrum of a highly aligned AgNW film with an *S* value of 0.89 is plotted in figure 4.9. In this case, AgNWs dispersed in ethanol were purchased from Blue Nano Inc. (Charlotte, NC) with an average diameter and length of 90 nm and 16 μm, respectively. A NW solution with a concentration of 2.0 mg/ml was coated on a PVA substrate in the same direction for all four coats, followed by substrate stretching

to achieve good alignment.

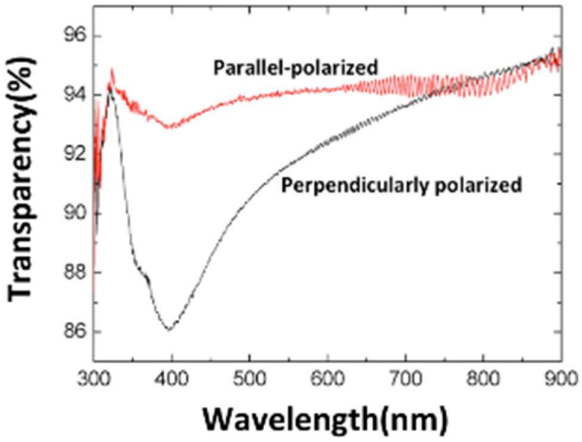

Figure 4.9 Transparency spectrum of more highly aligned silver nanowires. The red line represents transmittance to parallel-polarized light, and the black line represents transmittance to perpendicularly polarized light.

In the case of this highly aligned AgNW film, the transparency difference between two kinds of polarized light at 450 nm is 5.1 percentage points, compared to the 2.2 percentage point difference of the less aligned AgNW film at 450 nm in figure 4.8. As expected, better NW alignment boosts transparency to one kind of polarized light and is more similar to the simulation results in figure 4.6. However, this highly aligned AgNW film is not electrically conductive due to low NW-NW overlap, and thus it cannot be applied for electrode applications.

4.5 Conclusions

This is the first time preferentially-aligned AgNWs are used to achieve a higher transparency to polarized light within the wavelength range of 450 to 630 nm compared to randomly aligned AgNW electrodes, allowing for electrodes to have higher transparencies for display applications. A transparency boost of 7.3 percentage

points and a FoM increase to 27.1 × 10^{-3} Ω^{-1} from 17.2 × 10^{-3} Ω^{-1} for a 16 Ω/sq electrode was achieved. Since less NWs are needed to obtain a given sheet resistance along the alignment direction, preferentially aligning the NWs in a transparent electrode not only increases their transparency to polarized light, but to non-polarized light as well. The alignment technique used is cheap and scalable, compatible with roll-to-roll processes, and most importantly does not require extra processing steps, as rod coating is already a standard process for AgNW electrode fabrication. Compared to previously investigated and commercialized 2D isotropic transparent electrodes, transparent electrodes with preferentially aligned NWs are superior for touch screen and LCD applications where both optical and electric anisotropy is advantageous, as well as for organic solar cell, e-paper, smart window, and OLED display applications where conductivity is more important in one direction than the other. Increased transparencies will lead to better device performance, ranging from higher solar cell efficiencies to energy savings in displays.

Chapter 5 Metal nanowire interconnects in semiconductor nanowire networks

5.1 Introduction

Semiconductor NW devices have been extensively investigated and have shown their applications in numerous fields such as FETs [38][58], chemical sensors (e.g. pH, gas, ions) [164][165][166], biosensors (e.g. proteins, DNA) [42][56][167], mechanical sensors [62][168], and photon detectors [169]. Their popularity and wide applicability is due to a large number of reasons. First, growth techniques have been developed to enable the synthesis of semiconductor NWs of virtually any material, composition and geometry at large volumes [164], and very small feature sizes can be obtained without lithography. Unlike thin-films, single-crystalline NWs can be grown on or easily transferred to untraditional substrates like glass, plastics and textiles without the requirement for a potentially expensive lattice-matched single-crystalline substrate. NWs can be dispersed in an ink to be printed or deposited using high-throughput solution-deposition techniques at atmospheric conditions. Devices made from semiconductor NWs can be mechanically flexible and optically transparent. For sensing applications, the very high surface area-to-volume ratio and the similar diameter sizes to biological and chemical species are advantageous. Other technologically useful properties that NWs possess include large piezoresistance and high thermoelectric conversion efficiency.

As discussed in chapter 1.3, NW devices can be classified as single NW devices, mesh devices, and aligned NW devices with metal pads, from the perspective of the device structure. Single NW devices are mainly used for studying NW properties, but not suitable for low-cost large-area device applications. The device reliability based on a single NW is another issue. NW mesh devices solve the above issues, however, they suffer from high semiconductor-semiconductor NW junction resistance. Aligned NW devices with evaporated metal pads as interconnects were designed to reduce this junction resistance. But the NW-metal pad contact can't tolerate even small bending, making them unsuitable for flexible electronics. Furthermore, the fabrication of metal pads involves lithography and evaporation which requires expensive facilities and complicated fabrication processes.

5.2 Motivation

A hybrid of the NW mesh and aligned NWs device approaches may be able to solve the problems mentioned above while maintaining the main benefits. In this project, the semiconductor NWs are still aligned, thereby permitting devices such as those based on piezoelectric phenomena, but metal NWs instead of lithographically defined pads are used to connect individual semiconductor NWs. This is intended to solve the problem of high junction resistance incurred in semiconductor NW mesh devices, as the junctions are instead metal-semiconductor rather than semiconductor-semiconductor. A large number of metals are available in a NW form (e.g. gold, silver, copper, platinum, palladium, nickel), so ideally a metal that forms an

Ohmic contact with the semiconductor in question should be chosen [170]. The deposition of the metal NWs is inexpensive as it not require lithography or vacuum as in the case of metal pads and thus the easy fabrication of the NW mesh approach is maintained. And compared to metal pads which cannot incur strains greater than 3%, metal NWs are very flexible, tolerating strains as high as 40% [171]. Thus this approach is appropriate for flexible devices. Lastly, the metal NWs, along with the semiconductor NWs, can be optically transparent which is required for some applications.

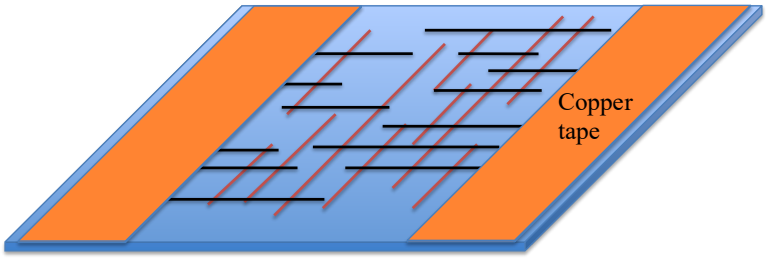

Figure 5.1 Schematic of metal nanowire/semiconductor nanowire grids. Black lines indicate aligned semiconductor nanowires, red lines indicate aligned metal nanowires which are perpendicular to the semiconductor NWs, and orange strips indicate copper tape used as main electrodes.

Figure 5.1 presents the device structure. Aligned semiconductor NWs are first deposited on a substrate, then metal NWs aligned perpendicularly to the semiconductor NWs are deposited on top. In this arrangement, as can be seen in figure 5.1, current cannot flow from one end of the film to the other exclusively through a semiconductor NW path nor a metal NW path. Because NWs of each type are parallel to one another, there are minimal semiconductor-semiconductor junctions and current will flow through metal from one semiconductor NW to another semiconductor NW. In this device, semiconductor NWs are used as the active region

and metal NWs are used as interconnects between one semiconductor NW to the next to avoid large semiconductor-semiconductor junction resistances. The device current is measured across the larger common electrodes (labelled 'Copper tape' in Figure 5.1) at the device ends. For example, if ZnONWs and AgNWs are used to fabricate a UV sensor, the conductivity of each ZnONW would increase under UV light illumination and the corresponding larger current flowing through all the ZnONWs connected in the network can be measured at the common electrodes at the device ends.

This device structure was attempted using several different semiconductor NW types including ZnO and copper oxide (CuO). Ag was used as the metal NW material. Ultimately, due to various reasons as will be discussed below, a working device was not obtained. The experiments are described, and things learned from these experiments, particularly the requirements of the alignment method and the NW samples, are summarized and suggestions to improve upon the device approach are given.

5.3 Experimental

5.3.1 Semiconductor nanowire deposition and alignment

Substrate-grown ZnONWs (with an average length of 1 μm) synthesized by Dr. Marwa Abd-Ellah using a hydrothermal method were transferred and aligned on 3 × 3 cm PET films using contact printing, an alignment method described in chapter 1.4. Substrate-grown CuONWs (with an average length of ~30 μm) synthesized by Dr. Marwa Abd-Ellah using a thermal oxidation method were also transferred and aligned

on 3 × 3 cm PET films using contact printing. ZnONWs in powder form (with an average length of 9.9 μm) were purchased from Novarials Corporation (Woburn, MA). To make the latter ZnONWs uniformly dispersed in solution (i.e. eliminating NW agglomeration), different solvents, NW concentrations, sonication time, and other chemical methods were tested. PVP with different average molecular weights purchased from Sigma-Aldrich (Saint Louis, MO) were also employed to assist with NW dispersion. Well-dispersed ZnONW solution was deposited on 3 × 5 cm PVA films using Mayer rod coating. To remove the PVP residues, the films were rinsed in ethanol for 10 seconds. The ZnONWs were then aligned using the substrate stretching method described in chapter 3.2, however lubricant was not added as it may have negative effects on device conductivity.

5.3.2 Metal nanowire alignment

AgNWs dispersed in ethanol were purchased from Novarials Corporation (Woburn, MA) with an average diameter and length of 70 nm and 50 μm, respectively. AgNWs were either Meyer rod-coated directly on top of the semiconductor NWs in a perpendicular alignment direction (chapter 3.3) or aligned on a separate 3 × 5 cm PVA film using substrate stretching (chapter 3.2), followed by pressing it against the PVA film with pre-aligned semiconductor NWs such that the metal NWs were situated perpendicularly.

5.3.3 Device fabrication

To increase the physical contact at the metal-semiconductor NW junctions, the

crossed aligned devices were mechanically pressed (chapter 4.3). The films were then annealed at 150 °C for 30 mins in air. These annealing parameters were taken from a study in the literature where electrical contact was made between ZnO thin-films and AgNWs [172]. Higher temperatures cannot be used as neither the plastic substrate or AgNWs can tolerate it. Ag paste and strips of copper tape were applied at the two ends of each electrode.

5.3.4 Device characterization

SEM images were taken of the samples, which were coated with a 10 nm thick layer of gold to prevent electron charging. Dark-field optical microscopy images were also taken of the samples. The optical transparency was measured by a window tint meter at a wavelength of 550 nm (SRW2000, ShowRange Corporation, China). A voltage of 5 V was applied across the devices by a power supply and the resulting current was measured with a multimeter (IP54, AccuRemote Corporate, San Clemente, CA).

5.4 Results and discussion

5.4.1 Alignment of nanowires on substrates

Figure 5.2 shows the OM images representing the alignment of substrate-grown ZnO and CuO NWs using contact printing. The average length of ZnONWs after contact printing is 0.80 μm, which is 80% of their original length. The average length of CuONWs after contact printing is 14.5 μm, which is about 48% of their original length. This phenomenon of NW breakage has been reported in previous NW

alignment studies using contact printing [84].

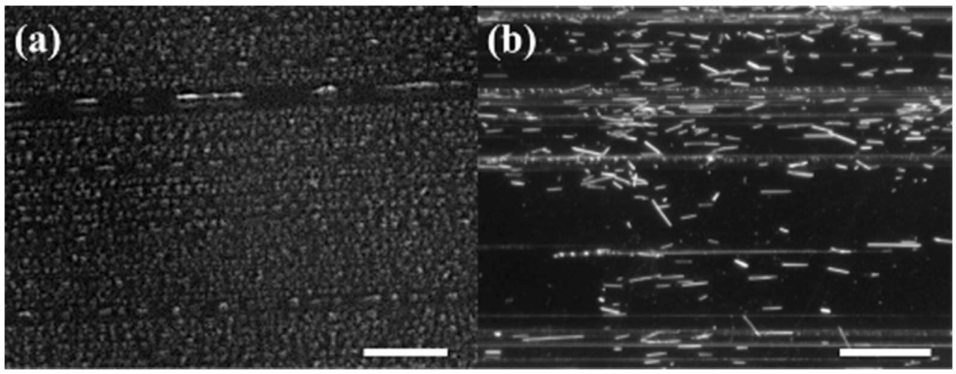

Figure 5.2 Optical microscopy images of (a) aligned substrate-grown zinc oxide nanowires on a polyethylene terephthalate film after contact printing (Scale bar: 25 μm), (b) aligned substrate-grown copper oxide nanowires on a polyethylene terephthalate film after contact printing. (Scale bar: 50 μm)

Because the ZnONW average length is very short, a very dense array of metal NWs would be required to achieve a connected network. I suggest that the spacing between metal NWs needs to be ~1/3 of the length of the semiconductor NWs for a high enough probability of overlap, which in this case is less than 0.3 μm. However, short circuits would easily happen with such a high density of metal NWs given that no NW alignment method is perfect. Furthermore, short NWs would lead to a high number of semiconductor-metal junctions which is undesirable due to the contact resistance. In figure 5.2(b), we see that the CuONW length is much larger than the NW spacing in some areas, however, there are almost no NWs at some other area. The poor CuONW density uniformity is not qualified for device application either.

5.4.2 Alignment of powder-form zinc oxide nanowires

To solve the NW length, density, and uniformity issues, powder-form ZnONWs purchased from Novarials with an average length of 9.9 μm (calculated by the image

processing method discussed in chapter 2.3) were dissolved in IPA with a concentration of 2.5 mg/ml and then deposited on PVA films. From 5.3(a), it is obvious that agglomeration occurs if no dispersion optimization is applied. I also found that powder-form ZnONWs purchased from Sigma-Aldrich suffers from the same issue, indicating that agglomeration is a common problem for ZnONWs in powder form.

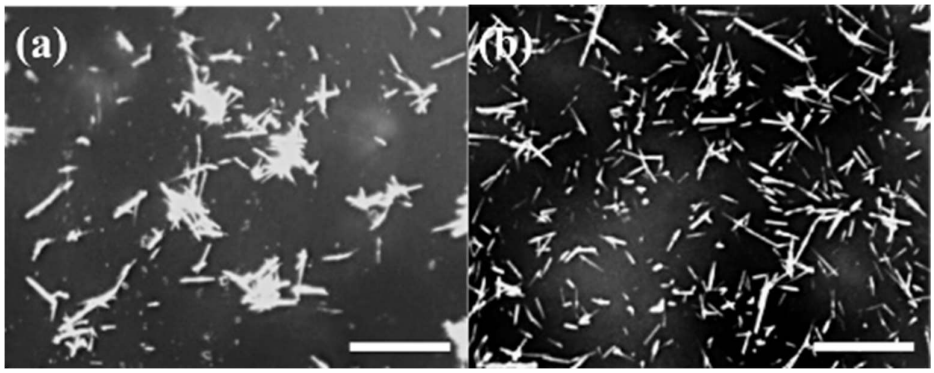

Figure 5.3 Optical microscopy image of (a) powder-form zinc oxide nanowires deposited on a polyvinyl alcohol film without dispersion optimization and (b) with dispersion optimization. (Scale bar: 50 μm)

To solve the dispersion issue of the powder-form ZnONWs, several methods were tested such as reducing the ZnONW solution concentration, increasing the sonication time, trying different solvents and adding chemicals (e.g. PVP) to the solution. Reducing the ZnONW solution concentration did not improve the NW dispersion. In addition, lower solution concentration is not desirable for device applications, since it requires more deposition steps to obtain the density needed. Increasing sonication time also did not solve the ZnONW agglomeration issue, and even worse, the ZnONWs break after a long period of sonication (e.g. 30 mins).

PVP with different molecular weights of 10000 and 40000 were added to the

ZnONW solution to improve the dispersion. PVP molecules, which bind to the surface of NWs, provide steric repulsion between polymer chains and help NWs be well separated [173]. It was found experimentally that ZnONWs with PVP are more uniformly dispersed in IPA than in ethanol. Because the substrate PVA is soluble in water, and acetone causes more NW agglomeration due to the low solubility of PVP in acetone, neither of these solvents are appropriate. Thus, IPA was chosen as the solvent. Different mass concentrations (1%, 5%, 10%) of PVP in the ZnONW solution were tested. Figure 5.3b shows the optimized results. In this case, ZnONWs were dissolved in IPA at a concentration of 2.5 mg/ml, with a 1% concentration of PVP with a moleculer weight of 10000. A short period (i.e. 10 mins) of sonication was applied for further dispersion improvement. It is seen from the image that most of the agglomeration was eliminated and ZnONWs were uniformly dispersed on the PVA films. PVP was then removed from the PVA films by rinsing with ethanol for 10 seconds [174]. Without the removal of PVP, it hardens and remains on the surface of PVA films during the ZnONW alignment process under heat, in which case ZnONWs cannot be accessed and thus it is not desirable for device applications.

It is found that the dispersion result is almost the same regardless of the PVP molecular weight and different PVP mass concentrations didn't lead to an obvious difference on the dispersion results either. PVP with a molecular weight of 10000 and a mass concentration of 1% was chosen for dispersion optimization because lower molecular weight PVP with a lower concentration can be more easily removed.

After dispersion optimization, ZnONW alignment was achieved using substrate

stretching, as shown in figure 5.4. To obtain a dense film, a ZnONW solution with a concentration of 5 mg/ml was used for deposition and the number of coats was 2. This was the highest density that could be used without a significant amount of NW agglomeration. The PVA film was stretched to 450% under heat and it can be seen that almost all the ZnONWs were aligned horizontally, with an *S* value of 0.91. No polymer lubricant was used in this project as was done in chapter 3, since the lubricant may degrade the conductivity.

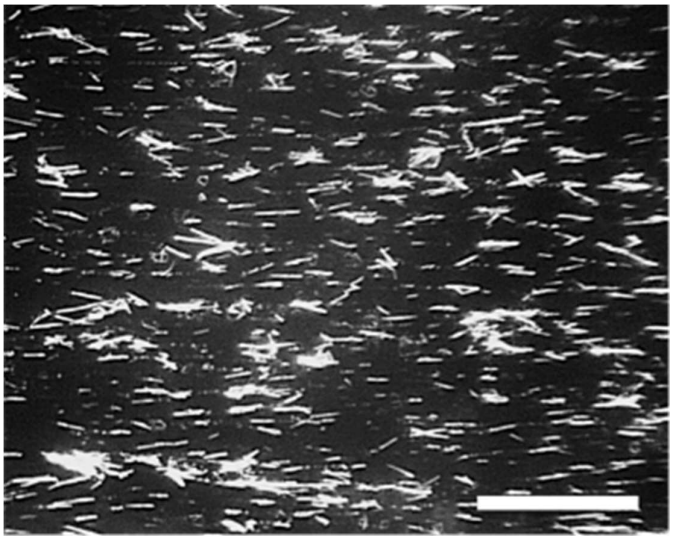

Figure 5.4 Optical microscopy image of aligned zinc oxide nanowires by substrate stretching after dispersion optimization. (Scale bar: 50 μm)

5.4.3 Silver nanowire alignment

To achieve a crossed Ag/ZnO NW structure, two alignment methods were used for the metal NWs. Firstly, AgNWs were aligned directly on top of pre-aligned ZnONWs using Mayer rod coating, perpendicular to the ZnONW alignment direction. Before AgNW alignment, mechanical pressing was applied to the pre-aligned ZnONWs to help maintain the alignment as it improves adhesion of the NWs to the substrate and

limits their rotation during the subsequent coating process, as discussed in chapter 3.3. AgNW solution with concentrations of 2 mg/ml and 3 mg/ml were deposited on the PVA films with pre-aligned ZnONWs and the AgNWs were subsequently aligned using Mayer rod coating, as shown in figure 5.5(a) and (b), respectively. The *S* values are 0.56 and 0.53 for the AgNW alignments. The crossed Ag/ZnO NW structure on PVA film was then mechanically pressed again followed by annealing to reduce the junction resistances.

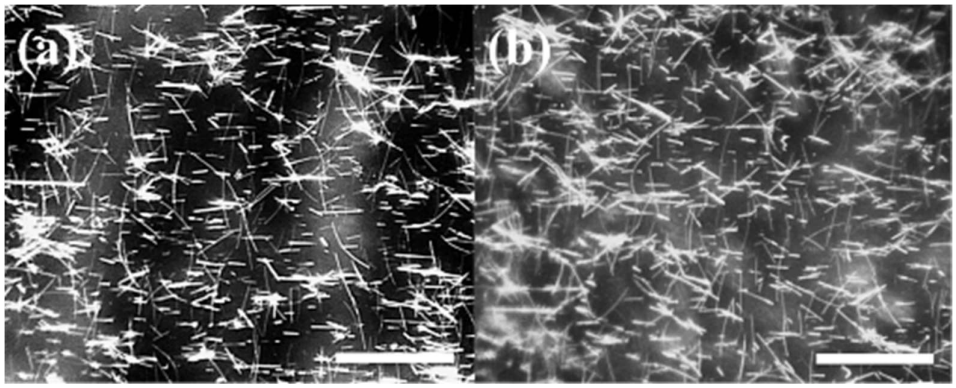

Figure 5.5 Optical microscopy image of crossed silver/zinc oxide nanowire structure with (a) sparser aligned silver nanowires and (b) denser aligned silver nanowires by Mayer rod coating. Zinc oxide nanowires are horizontally aligned and silver nanowires are perpendicularly aligned to the zinc oxide nanowires. (Scale bar: 50 μm)

From figure 5.5(a), the crossed Ag/ZnO NW network is not connected because the AgNW concentration is quite low. In an attempt to make it connected, AgNW with higher concentration was used for alignment, as shown in figure 5.5(b).

Other samples were prepared by aligning the AgNWs using substrate stretching. AgNW solution with a concentration of 3 mg/ml was deposited on another PVA film first with 2 coats, and the PVA film was stretched to 450% under heat to achieve a high-quality AgNW alignment. The PVA film with aligned AgNWs was mechanically pressed against the one with pre-aligned ZnONWs followed by an annealing. As

shown in figure 5.6, ZnONWs are horizontally aligned, and AgNWs are perpendicularly aligned. Due to the focal planes of the ZnONWs and AgNWs being different, it is impossible to get an optical microscopy image with crossed NWs in the same image. SEM imaging was not possible because all the NWs are embedded between PVA films and not exposed on the surface.

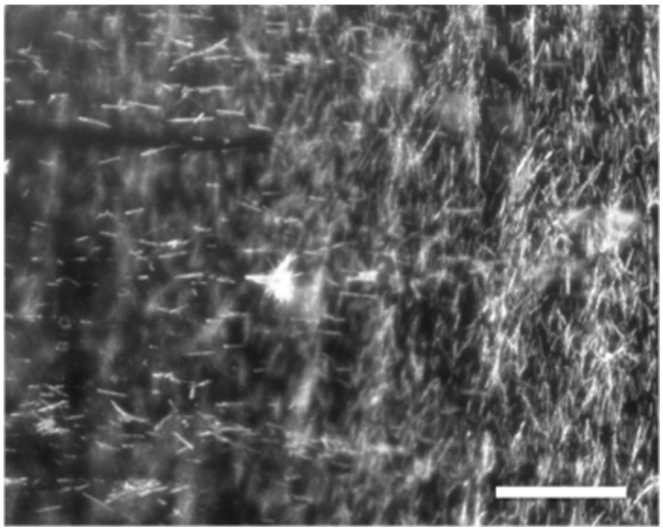

Figure 5.6 Optical microscopy image of crossed silver/zinc oxide nanowire structure where alignment were both achieved by substrate stretching. Zinc oxide nanowires are horizontally aligned and silver nanowires are perpendicularly aligned to the zinc oxide nanowires. (Scale bar: 50 μm)

5.4.4 Optical characterization

As can been seen in figure 5.7, the crossed Ag/ZnO NW network is highly transparent. This particular sample is the same as shown in figure 5.5(b). Its transparency at 550 nm is 89 %.

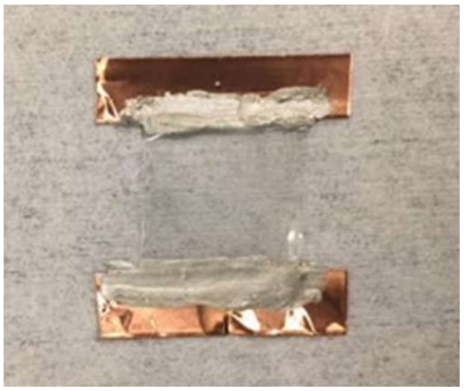

Figure 5.7 Photograph of a crossed silver/zinc oxide nanowire structure.

5.4.5 Electrical characterization

The electrical property of the above devices was measured using a multimeter with a sensitivity of 0.1 μA, but the signal was too small to be measured in all cases. As labeled in figure 5.8, there are many disconnections on the network which reduces the number of connected path ways of this network.

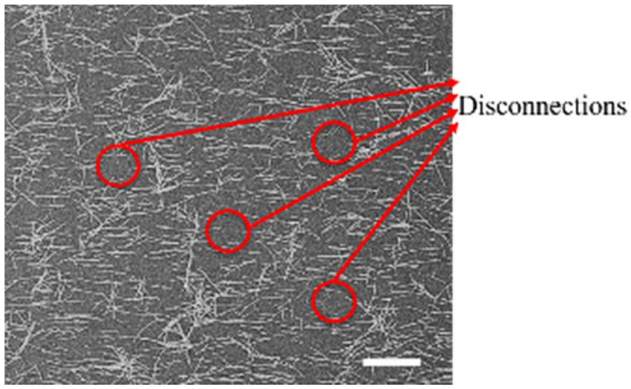

Figure 5.8 SEM image of a crossed silver/zinc oxide nanowire structure. Electrical disconnections in the network are indicated (Scale bar: 40 μm)

Compared with NW mesh devices, crossed NW devices have a much lower number of connected pathways which can be used to transmit electrical signals, which is the main reason that the electrical signal cannot be measured. It is mainly caused by the imperfect alignment method and the short average NW length. Neither substrate

stretching nor rod coating can provide a highly dense aligned NW array which is required to obtain many pathways. At very high densities, these methods lead to NW agglomeration and a decreased quality of NW alignment, the latter would cause short-circuits. Furthermore, the uniformity of the NW density is not ideal, and near-perfect areal uniformity is important to avoiding disconnections. Unfortunately, at this time, there does not exist any NW alignment method for solution-synthesized NWs that would have the alignment quality, density, and areal uniformity required for a quality semiconductor/metal crossed NW device. In regards to NW length, longer NWs are preferred. Long NW lengths would lead to more NWs being connected into pathways as well as reduce the number of ZnO-Ag NW junctions.

To further investigate the reason for the low current and the feasibility of this device structure, some estimated calculations were done. Figure 5.9 represents a schematic of a crossed ZnO/Ag NW device. The average length of ZnO and Ag NWs are 10 and 20 μm, which match the lengths in my experiment as seen in figure 5.5(b). The average spacing between ZnONWs and AgNWs is set to 10 μm, which also correlates to the experimental samples. The crossed NW devices have an effective width and length of 1 cm. For this width, the total number of parallel aligned ZnONWs at one end is about 1000. However, not all of these ZnONWs can contribute to the connected pathways because the chance AgNWs connect them into pathway is low due to the disconnections in a real device. Furthermore, even if a ZnONW is connected in a pathway, only part of its length will contribute to conduction as can be seen in the schematic. Overall, about 10% or less of the total length of ZnONWs can

contribute to conduction.

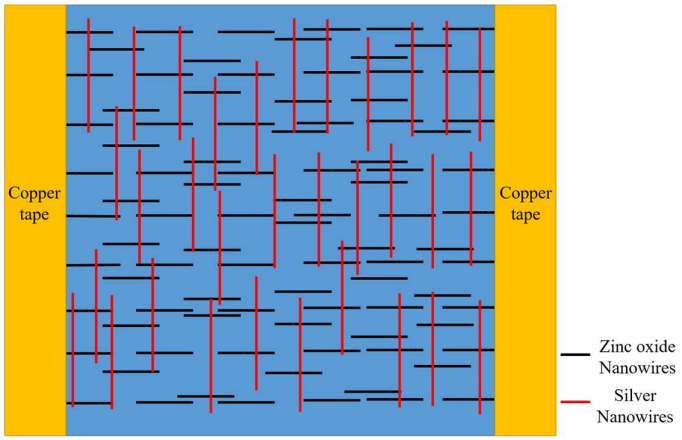

Figure 5.9 Schematic of a crossed silver/zinc oxide nanowire device fabricated by substrate stretching or rod coating. Black lines indicate aligned zinc oxide nanowires, red lines indicate aligned silver nanowires, and the orange strips indicate copper tape used as main electrodes.

Besides the low number of pathways, low doping of the ZnONWs used is another issue. The devices in this project were made from undoped ZnONWs. In comparison to intrinsic SiNWs, for example, intrinsic ZnONWs are inherently doped due to defects, but even still, intentionally doped NWs are better to achieve higher conduction. The resistivity is of an intrinsic ZnONW is about 0.26 Ω·cm [175]. Considering the percentage of ZnONW length which can contribute to the conduction, the current is only about 0.07 μA with an applied voltage of 5 V, which is lower than the limit of the multimeter. Furthermore, this calculation does not take the semiconductor-metal NW junction resistances into account which would lower the signal further. The semiconductor-metal NW junction resistance is likely high. To reduce the junction resistance, a higher annealing temperature is needed, which exceeds the thermal budget of AgNWs and plastic substrates.

Lastly, the semiconductor-metal NW junction resistance is likely high. To reduce

the junction resistance, a higher annealing temperature is needed, which exceeds the thermal budget of AgNWs and plastic substrates.

5.4.6 Perspectives on making a functional device

Semiconductor NWs can be densely grown on substrates with a long average length and good uniformity [84]. Long metal NWs can also be grown on substrates [176]. Contact printing is a potential alignment method for this application because it can achieve both a good alignment quality and a good areal density given substrate grown NWs. Figure 5.10 represents a schematic of a crossed Ag/ZnO NW device where alignment is achieved by contact printing. In the case of contact printing, the aligned semiconductor NW spacing can be 1 μm or less [84], and thus the total number of parallel aligned ZnONWs at one end is about 10^4/cm. Moreover, about 50% of the total length of ZnONWs can contribute to conduction due to their high density and good uniformity using the same AgNW density as used in my experiments above.

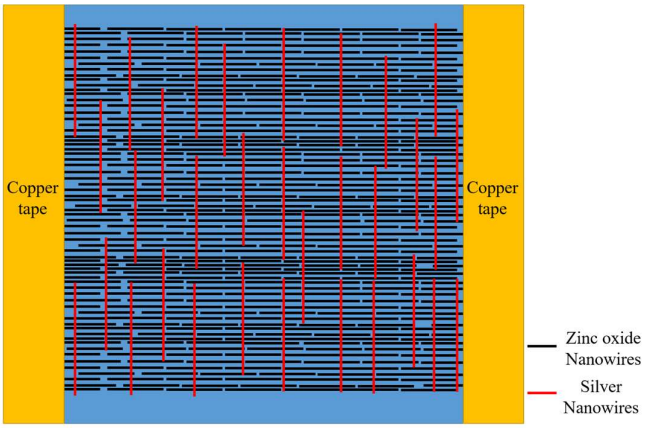

Figure 5.10 Schematic of a crossed zinc oxide/silver nanowire device fabricated by contact printing. Black lines indicate aligned zinc oxide nanowires, red lines indicate aligned silver nanowires, and orange strips indicate copper tape used as main electrodes.

If the ZnONWs are highly doped, the resistivity of a single NW is about 6.4 × 10^{-3} Ω·cm [177], which is 10^{-3} times that of intrinsic ZnONWs. Under the same applied voltage of 5 V, considering the higher number of NWs and their higher conductivity, the total current would be about 8.6 mA (not including junction resistances). This is 10^5 higher than that of devices made by aligned intrinsic ZnONWs using substrate stretching/rod coating. However, the downside of using contact printing is the high cost of growing NWs on substrates, more defects in substrate-grown metal NWs compared to solution-synthesized NWs, and NW breakage into short pieces.

A higher annealing temperature is required to reduce the semiconductor-metal NW junction resistance. This could be achieved by depositing or transferring the crossed semiconductor-metal NW film to a glass substrate, followed by a high-temperature annealing, and then a transfer back to PET or another flexible substrate. The drawbacks of this transfer process is the more complicated and expensive fabrication process. Also, metal NWs melt at lower temperatures than their bulk counterparts. For example, 90 nm diameter AgNWs can only tolerate 200 °C for 30 minutes before melting [37] and so annealing temperatures would still be limited. Once way to increase the thermal budget would be to use thicker NWs [134] as they have higher melting temperatures.

5.5 Conclusions

A crossed film structure consisting of semiconductor NWs aligned in one direction

and metal NWs perpendicularly aligned is postulated. The metal NWs are intended to act as interconnects to reduce semiconductor NW-NW junction resistances and these interconnects, unlike metal pads, are mechanically flexible and do not require expensive fabrication processes undesirable for large-area electronics such as lithography and metal deposition. The device fabrication process was developed and optimized: (i) The agglomeration issue of powder-form ZnONWs was solved using PVP and an appropriate solvent; (ii) the crossed Ag/ZnO NW structure was fabricated by aligning ZnONWs first using substrate stretching, followed by aligning AgNWs perpendicularly to them.

To make a working device, there are several requirements: (1) An alignment method which can achieve a high alignment quality, high NW density and good film uniformity is recommended for this application. This guarantees a large number of connected pathways for a larger electrical signal. Contact printing meets these requirements but is only useable for NWs grown on a substrate. (2) Substrate-grown semiconductor and metal NWs are required for contact printing. A good uniformity and long average length are recommended, since these can increase the chances of making connected pathways and a long average length can reduce the number of semiconductor-metal NW junctions as well. Dense substrate-grown semiconductor NWs are preferred. High density is to achieve a larger active area and thus higher signals. Metal NWs with a very high density wouldn't necessarily improve device performance as this could cause more semiconductor-metal junctions than needed, and high metal densities could also lead to short circuits due to non-perfect alignment.

(3) Highly doped semiconductor NWs are recommended because they can provide a lower resistivity compared to intrinsic semiconductor NWs. (4) A higher annealing temperature is required to reduce the semiconductor-metal NW junction resistance.

Although there are merits of the proposed device, and with the correct NW alignment methods and NW samples I believe it could work, the requirements of the NW alignment methods and samples are very high and specific. Reduction of semiconductor-metal NW junction resistance is another challenge of this project. Once these two problems are solved, I think this device could outperform NW mesh devices and aligned NW devices with metal pads and provides another template for large-area flexible electronics.

Chapter 6 Conclusion and future work

6.1 Conclusion and contribution to nanowire alignment

The purpose of this thesis is to research new NW alignment techniques and improved methods to quantify NW alignment, and apply aligned NWs in large-area flexible devices. The novel contributions of this thesis are listed below:

1. Developed a high-quality, large-area NW alignment method by a simple substrate stretching process. The alignment achieved was higher than all other substrate stretching/contracting methods in the literature, and a lubricant was employed for the first time to solve the NW breakage problem.

2. Demonstrated that NWs can be easily aligned during Mayer rod coating without any extra steps, and determined for the first time the pertinent parameters that lead to preferred alignment.

3. Developed two computer vision algorithms to realize automated NW object detection from microscopy images for the first time in the literature. This allows for quick, accurate alignment quantification that works for NWs of any material.

4. Developed two quantitative, statistical metrics for NW alignment quantification that are more precise and appropriate for alignment comparison within and across studies than previously used metrics.

5. Showed, for the first time, that imparting preferential alignment to the AgNWs in electrodes can increase electrode transparency to polarized light.

Highly aligned NWs (S=0.97) were achieved by stretching PVA films, which is scalable, simple, cheap, and compatible with industrial manufacturing processes. NW breakage, a common problem of shear force alignment, was solved by adding the lubricant poly[oxy(methyl-1,2-ethanediyl)] during alignment. In a second method, moderate, large-area, low-cost, and one-step NW alignment (S~0.50) was achieved during Mayer rod coating deposition, which is already a standard method for depositing solution-based nanomaterials on thin-film substrates and compatible with roll-to-roll manufacturing processes. NW transfer between large-area flexible substrates was developed using a rolling machine with NW alignment maintained, which is also compatible with roll-to-roll processes.

An automated, accurate, and fast computer vision algorithm based on an edge-detection convolution operation was developed for non-overlapping NW detection from microscopy images. To handle dense and overlapping NW networks, another computer vision algorithm based on a skeletonization convolution operation was developed. Two statistic alignment quantification metrics based on S and ODF were developed which provide quantitative methods to compare different alignment results.

Moderately aligned AgNWs achieved by Mayer rod coating were utilized as transparent electrodes, which achieved a higher transparency to polarized light within the visible wavelength range (i.e. 450 to 630 nm) and suitable for applications such as LCD and touch panels. Conductivity along the alignment direction is also enhanced compared with random AgNW electrodes.

A crossed semiconductor-metal NW device structure was postulated, where the metal NWs are intended to act as interconnects to reduce semiconductor NW-NW junction resistance while providing more mechanical flexibility than lithographically defined metal pads. The device fabrication process was developed and optimized. Suggestions for device improvement and an outlook for the future applicability of this device structure were given.

6.2 Future work

6.2.1 Percolation theory with alignment

There exists a study that makes use of NW alignment, alignment quantification and its application to transparent electrodes that I did not have the time to carry out, but I suggest it here as a future project. Networks of 1D nanoscale conductors such as AgNWs, copper NWs, and carbon nanotubes have been utilized as transparent electrodes to replace ITO thin films due to various advantages. Percolation theory is commonly used to describe the relationship between the conductivity of sparse networks composed of these 1D conductors and the network transparency. One critical parameter, the percolation threshold, represents the minimum density of 1D conductors needed to form a conductive network. Percolation theory is useful for transparent electrodes since it sheds light on how electrodes can be fabricated with an optimized figures of merit, which includes the properties of sheet resistance and transparency. It is particularly important for applications where the transparent electrode does not need to be highly conductive, such as for touchscreens and smart

windows. Up to now, percolation theory has only been considered for random nanoscale conductor networks. With the increased number of NW alignment studies and its usefulness in obtaining high-performing transparent electrodes (as shown in this thesis and by others), percolation theory taking alignment into account is needed since alignment can change, for better or worse, the NW density required for percolation. Aligned AgNW electrodes with different density and alignment quality can be fabricated using Mayer rod coating or substrate stretching as discussed in chapter 3. Alignment quality can be calculated and quantified using the *S* parameter as discussed in chapter 2, and sheet resistance and transparency can also be measured as discussed in chapter 4. This leads to a new relationship between sheet resistance and transparency where the *S* parameter takes effect. This new theory will be a more comprehensive one, which provides guidance for aligned NW transparent electrode fabrication. And the old percolation theory is a special case of the new theory at S=0 (i.e. random networks).

6.2.2 Alignment cascade

The following described experiment combines both alignment methods researched in this thesis to improve alignment quality. Substrate stretching can achieve a high alignment result, however, this method does not well-align NWs which are deposited on the substrate nearly perpendicularly to the stretching direction. To solve this issue, the deposition of NWs on the PVA substrate can be done by Meyer rod coating using the optimized alignment parameters discovered in chapter 3.3, to achieve a moderate

initial alignment as well as reduce the number of NWs deposited perpendicularly to the intended stretching direction. Substrate stretching would then be done afterwards as a so-called alignment cascade to achieve highly aligned NWs. The preferential alignment during rod-coating introduces no extra steps and should enhance alignment.

6.2.3 Alignment quantification deployment

One of the merits of the alignment quantification methods developed in this thesis is that it is widely applicable to NWs of any material, grown on either a substrate or in solution, and applicable to nanorods, nanotubes, and any other elongated nanostructures. Furthermore, in addition to alignment it also quickly calculates NW lengths in an image, which is still most commonly measured one-by-one by hand by NW and nanorod researchers around the world. However, use of the Python code written for this work requires setting up a Linux/Unix computational environment with Python and OpenCV installed by appropriate configurations, which is not user-friendly. The Python code runs by typing Linux command lines, which takes time for users to get used to. Therefore, a graphic user interface (GUI) was developed by an UWaterloo Nano-Engineering undergraduate student called Adrian Yabut. With his help, a user can run the code using the GUI on his PC without typing command lines, however, at this time it can't be shared with other researchers because the GUI was not set on a server that can be accessed through Internet. The ideal situation is that worldwide users can upload their images online, input minimal parameters, and receive the output with alignment as well as length results. For further deployment a

server which supports the required computational environment is required. Python and related packages are required to be installed on this server with appropriate configurations. An interface is needed which can solicit requests from users, trigger the Python code for alignment quantification at the back end and return results to users.

Letter of copyright permission

Title: Capillary Printing of Highly Aligned Silver Nanowire Transparent Electrodes for High-Performance Optoelectronic Devices

Author: Saewon Kang, Taehyo Kim, Seungse Cho, et al

Publication: Nano Letters

Publisher: American Chemical Society

Date: Dec 1, 2015

Logged in as:
Jianjin Dong
Account #:
3001276057

LOGOUT

PERMISSION/LICENSE IS GRANTED FOR YOUR ORDER AT NO CHARGE

This type of permission/license, instead of the standard Terms & Conditions, is sent to you because no fee is being charged for your order. Please note the following:

- Permission is granted for your request in both print and electronic formats, and translations.
- If figures and/or tables were requested, they may be adapted or used in part.
- Please print this page for your records and send a copy of it to your publisher/graduate school.
- Appropriate credit for the requested material should be given as follows: "Reprinted (adapted) with permission from (COMPLETE REFERENCE CITATION). Copyright (YEAR) American Chemical Society." Insert appropriate information in place of the capitalized words.
- One-time permission is granted only for the use specified in your request. No additional uses are granted (such as derivative works or other editions). For any other uses, please submit a new request.

If credit is given to another source for the material you requested, permission must be obtained from that source.

Reference

[1] Jiangtao Hu, Teri W. Odom, and Charles M. Lieber 1999 Chemistry and Physics in One Dimensions: Syntesis and Properties of Nanowires and Nanotubes *Acc. Chem. Res.* **32** 435–45

[2] Lieber C M 2001 The incredible shrinking consultant *Sci. Am.* **285** 58–64

[3] Lieber C M and Wang Z L 2007 Functional Nanowires *MRS Bull.* **32** 99–108

[4] Chockla A M and Korgel B A 2009 Seeded germanium nanowire synthesis in solution *J. Mater. Chem.* **19** 996

[5] Lu W and Lieber C M 2006 Semiconductor nanowires *J. Phys. D. Appl. Phys.* **39** 387–406

[6] Tang C, Bando Y, Liu Z and Golberg D 2003 Synthesis and structure of InP nanowires and nanotubes *Chem. Phys. Lett.* **376** 676–82

[7] Morral A F I 2011 Gold-free GaAs nanowire synthesis and optical properties *IEEE J. Sel. Top. Quantum Electron.* **17** 819–28

[8] Kim F, Sohn K, Wu J S and Huang J X 2008 Chemical Synthesis of Gold Nanowires in Acidic Solutions *J. Am. Chem. Soc.* **130** 14442–3

[9] Ye S, Rathmell A R, Chen Z, Stewart I E and Wiley B J 2014 Metal Nanowire Networks: The Next Generation of Transparent Conductors *Adv. Mater.* **26** 6670–87

[10] Banerjee S, Dan A and Chakravorty D 2002 Synthesis of conducting nanowires *J. Mater. Sci.* **37** 4261–71

[11] Cui Y, Duan X, Hu J and Lieber C M 2000 Doping and Electrical Transport in Silicon Nanowires *J. Phys. Chem. B* **104** 5213–6

[12] Dasgupta N P, Sun J, Liu C, Brittman S, Andrews S C, Lim J, Gao H, Yan R and Yang P 2014 25th anniversary article: Semiconductor nanowires - Synthesis, characterization, and applications *Adv. Mater.* **26** 2137–83

[13] Suzuki H, Araki H, Tosa M and Noda T 2007 Formation of Silicon Nanowires by CVD Using Gold Catalysts at Low Temperatures *Mater. Trans.* **48** 2202–6

[14] Chang P-C, Fan Z, Tseng W-Y, Chiou W-A, Hong J and Lu J G 2004 Characterization ZnO Nanowires Synthesized by Vapor Trapping CVD Method *Chemtry Mater.* **16** 5133–7

[15] Morales A M 1998 A Laser Ablation Method for the Synthesis of Crystalline Semiconductor Nanowires *Science (80-.).* **279** 208–11

[16] Liu J L, Cai S J, Jin G L, Thomas S G and Wang K L 1999 Growth of Si whiskers on Au/Si(111) substrate by gas source molecular beam epitaxy (MBE) *J. Cryst. Growth* **200** 106–11

[17] Halder A and Ravishankar N 2007 Ultrafine single-crystalline gold nanowire arrays by oriented attachment *Adv. Mater.* **19** 1854–8

[18] Chang Y, Lye M L and Zeng H C 2005 Large-scale synthesis of high-quality ultralong copper nanowires *Langmuir* **21** 3746–8

[19] Sun Y 2010 Silver nanowires – unique templates for functional nanostructures *Nanoscale* **2** 1626–42

[20] Sun Y, Gates B, Mayers B and Xia Y 2002 Crystalline Silver Nanowires by Soft Solution Processing *Nano Lett.* **2** 165–8
[21] Sun Y and Xia Y 2002 Large-Scale Synthesis of Uniform Silver Nanowires Through a Soft, Self-Seeding, Polyol Process *Adv. Mater.* **14** 833–7
[22] Sun Y, Mayers B, Herricks T and Xia Y 2003 Polyol synthesis of uniform silver nanowires: A plausible growth mechanism and the supporting evidence *Nano Lett.* **3** 955–60
[23] Haghi M, Thurow K and Stoll R 2017 Wearable devices in medical internet of things: Scientific research and commercially available devices *Healthc. Inform. Res.* **23** 4–15
[24] Cheng Y, Wang R, Zhai H and Sun J 2017 Stretchable electronic skin based on silver nanowire composite fiber electrodes for sensing pressure, proximity, and multidirectional strain *Nanoscale* **9** 3834–42
[25] Steudel S, De Vusser S, Myny K, Lenes M, Genoe J and Heremans P 2006 Comparison of organic diode structures regarding high-frequency rectification behavior in radio-frequency identification tags *J. Appl. Phys.* **99**
[26] Liu Z, Xu J, Chen D and Shen G 2015 Flexible electronics based on inorganic nanowires *Chem. Soc. Rev.* **44** 161–92
[27] Choudhry R and Garg K 2008 A Hybrid Machine Learning System for Stock Market Forecasting *World Acad. Sci. Eng. Technol.* **2** 315–8
[28] Maheshwari N 2016 *Silver Nanowire Coatings For Electrically Conductive Textiles* (Master Thesis, University of Waterloo, Canada)
[29] Lee C H, Kim D R and Zheng X 2011 Fabrication of nanowire electronics on nonconventional substrates by water-assisted transfer printing method *Nano Lett.* **11** 3435–9
[30] Cui Y, Zhong Z H, Wang D L, Wang W U and Lieber C M 2003 High performance silicon nanowire field effect transistors *Nano Lett.* **3** 149–52
[31] Gleskova H and Wagner S 2001 Electron mobility in amorphous silicon thin-film transistors under compressive strain *Appl. Phys. Lett.* **79** 3347–9
[32] Serre P, Mongillo M, Periwal P, Baron T and Ternon C 2015 Percolating silicon nanowire networks with highly reproducible electrical properties *Nanotechnology* **26** 15201
[33] Khaligh H H 2013 *Silver Nanowire Transparent Electrodes: Fabrication, Characterization, and Device Integration* (Master Thesis, University of Waterloo, Canada)
[34] Selzer F, Weiß N, Kneppe D, Bormann L, Sachse C, Gaponik N, Eychmüller A, Leo K and Müller-Meskamp L 2015 A spray-coating process for highly conductive silver nanowire networks as the transparent top-electrode for small molecule organic photovoltaics *Nanoscale* **7** 2777–83
[35] Finn D J, Lotya M and Coleman J N 2015 Inkjet printing of silver nanowire networks *ACS Appl. Mater. Interfaces* **7** 9254–61
[36] Hu L, Kim H S, Lee J-Y, Peumans P and Cui Y 2010 Scalable coating and properties of transparent, flexible, silver nanowire electrodes *ACS Nano* **4** 2955–63

[37] Khaligh H H, Liew K, Han Y, Abukhdeir N M and Goldthorpe I A 2015 Silver nanowire transparent electrodes for liquid crystal-based smart windows *Sol. Energy Mater. Sol. Cells* **132** 337–41
[38] Duan X, Huang Y, Cui Y, Wang J and Lieber C M 2001 Indium phosphide nanowires as building blocks for nanoscale electronic and optoelectronic devices. *Nature* **409** 66–9
[39] Chang Y-K and Hong F C-N 2009 The fabrication of ZnO nanowire field-effect transistors by roll-transfer printing. *Nanotechnology* **20** 195302
[40] Huang Y, Duan X, Cui Y, Lauhon L J, Kim K H and Lieber C M 2001 Logic gates and computation from assembled nanowire building blocks. *Science (80-.).* **294** 1313–7
[41] Cui Y and Lieber C M 2001 Functional nanoscale electronic devices assembled using silicon nanowire building blocks. *Science (80-.).* **291** 851–3
[42] Patolsky F, Zheng G and Lieber C M 2006 Nanowire sensors for medicine and the life sciences. *Nanomedicine* **1** 51–65
[43] Soci C, Zhang A, Xiang B, Dayeh S A, Aplin D P R, Park J, Bao X Y, Lo Y H and Wang D 2007 ZnO nanowire UV photodetectors with high internal gain *Nano Lett.* **7** 1003–9
[44] Huang M H, Mao S, Feick H, Yan H, Wu Y, Kind H, Weber E, Russo R and Yang P 2001 Room-temperature ultraviolet nanowire nanolasers. *Science (80-.).* **292** 1897–9
[45] Wang Z L and Song J 2006 Piezoelectric nanogenerators based on zinc oxide nanowire arrays. *Science (80-.).* **312** 242–6
[46] Feng X L, He R, Yang P and Roukes M L 2007 Very high frequency silicon nanowire electromechanical resonators *Nano Lett.* **7** 1953–9
[47] Kim E K, Lee H Y, Moon S E, Park J, Park S J, Kwak J H, Maeng S, Park K H, Kim J, Kim S W, Ji H J and Kim G T 2008 Electrical characterization of ZnO single nanowire device for chemical sensor application. *J. Nanosci. Nanotechnol.* **8** 4698–701
[48] Das S N, Kar J P, Choi J-H, Lee T Il, Moon K-J and Myoung J-M 2010 Fabrication and Characterization of ZnO Single Nanowire-Based Hydrogen Sensor *J. Phys. Chem. C* **114** 1689–93
[49] Ebrahimi N, McCullough K and Xiao Z 2013 Reliability of Sensors Based on Nanowire Networks Operating in a Dynamic Environment *IEEE Trans. Reliab.* **62** 908–16
[50] Xu F, Durham J W, Wiley B J and Zhu Y 2011 Strain-release assembly of nanowires on stretchable substrates *ACS Nano* **5** 1556–63
[51] Kim D J, Shin H I, Ko E H, Kim K H, Kim T W and Kim H K 2016 Roll-to-roll slot-die coating of 400 mm wide, flexible, transparent Ag nanowire films for flexible touch screen panels *Sci. Rep.* **6** 1–12
[52] Liu J, Park J, Park K H, Ahn Y, Park J-Y, Koh K H and Lee S 2010 Enhanced photoconduction of free-standing ZnO nanowire films by L-lysine treatment *Nanotechnology* **21** 485504
[53] Sysoev V V., Schneider T, Goschnick J, Kiselev I, Habicht W, Hahn H, Strelcov

E and Kolmakov A 2009 Percolating SnO2 nanowire network as a stable gas sensor: Direct comparison of long-term performance versus SnO2 nanoparticle films *Sensors Actuators, B Chem.* **139** 699–703

[54] Ternon C, Serre P, Rey G, Holtzinger C, Periwal P, Martin M, Baron T, Stambouli V and Langlet M 2013 High aspect ratio semiconducting nanostructure random networks: Highly versatile materials for multiple applications *Phys. Status Solidi - Rapid Res. Lett.* **7** 919–23

[55] Serre P, Ternon C, Stambouli V, Periwal P and Baron T 2013 Fabrication of silicon nanowire networks for biological sensing *Sensors Actuators, B Chem.* **182** 390–5

[56] Nguyen T T T, Legallais M, Morisot F, Cazimajou T, Mouis M, Salem B, Stambouli V and Ternon C 2017 On the Development of Label-Free DNA Sensor Using Silicon Nanonet Field-Effect Transistors *Proceedings* **1** 312

[57] Duan X 2008 Nanowire thin-film transistors: A new avenue to high-performance macroelectronics *IEEE Trans. Electron Devices* **55** 3056–62

[58] Legallais M, Nguyen T T T, Mouis M, Salem B, Robin E, Chenevier P and Ternon C 2018 An innovative large scale integration of silicon nanowire-based field effect transistors *Solid. State. Electron.* **143** 97–102

[59] Hsieh G W, Beecher P, Li F M, Servati P, Colli A, Fasoli A, Chu D, Nathan A, Ong B, Robertson J, Ferrari A C and Milne W I 2008 Formation of composite organic thin film transistors with nanotubes and nanowires *Phys. E Low-Dimensional Syst. Nanostructures* **40** 2406–13

[60] Ternon C, Serre P, Lebrun J M, Brouzet V, Legallais M, David S, Luciani T, Pascal C, Baron T and Missiaen J M 2015 Low Temperature Processing to Form Oxidation Insensitive Electrical Contact at Silicon Nanowire/Nanowire Junctions *Adv. Electron. Mater.* **1** 1–8

[61] Durham J W and Zhu Y 2012 Fabrication of functional nanowire devices on unconventional substrates using strain-release assembly *ACS Appl. Mater. Interfaces* **5** 256–61

[62] Ryu S Y, Xiao J, Park W Il, Son K S, Huang Y Y, Paik U and Rogers J a. 2009 Lateral buckling mechanics in silicon nanowires on elastomeric substrates *Nano Lett.* **9** 3214–9

[63] McAlpine M C, Friedman R S, Jin S, Lin K H, Wang W U and Lieber C M 2003 High-Performance Nanowire Electronics and Photonics on Glass and Plastic Substrates *Nano Lett.* **3** 1531–5

[64] Lee B H, Kim I G, Cho S W and Lee S-H 1997 Effect of process parameters on the characteristics of indium tin oxide thin film for flat panel display application *Thin Solid Films* **302** 25–30

[65] Sannicolo T, Lagrange M, Cabos A, Celle C, Simonato J P and Bellet D 2016 Metallic Nanowire-Based Transparent Electrodes for Next Generation Flexible Devices: a Review *Small* **12** 6052–75

[66] Liu C-H and Yu X 2011 Silver nanowire-based transparent, flexible, and conductive thin film. *Nanoscale Res. Lett.* **6** 75

[67] Song M, You D S, Lim K, Park S, Jung S, Kim C S, Kim D H, Kim D G, Kim J

K, Park J, Kang Y C, Heo J, Jin S H, Park J H and Kang J W 2013 Highly efficient and bendable organic solar cells with solution-processed silver nanowire electrodes *Adv. Funct. Mater.* **23** 4177–84

[68] Dong J and Goldthorpe I A 2018 Exploiting both optical and electrical anisotropy in nanowire electrodes for higher transparency *Nanotechnology* **29** 045705

[69] Wu J, Zang J, Rathmell A R, Zhao X and Wiley B J 2013 Reversible sliding in networks of nanowires *Nano Lett.* **13** 2381–6

[70] Duan S, Niu Q, Wei J, He J, Yin Y and Zhang Y 2015 Water-bath assisted convective assembly of aligned silver nanowire films for transparent electrodes *Phys. Chem. Chem. Phys.* **17** 8106–12

[71] Liu M, Wu Z, Lau W M and Yang J 2012 Recent Advances in Directed Assembly of Nanowires or Nanotubes *Nano-micro Lett.* **4** 142–53

[72] Huang Y, Duan X F, Wei Q and Lieber C M 2001 Directed assembly of one-dimensional nanostructures into functional networks *Science (80-.).* **291** 630–3

[73] Wang D, Chang Y L, Liu Z and Dai H 2005 Oxidation resistant germanium nanowires: Bulk synthesis, long chain alkanethiol functionalization, and Langmuir-Blodgett assembly *J. Am. Chem. Soc.* **127** 11871–5

[74] Tao A R, Huang J and Yang P 2008 Langmuir - Blodgettry of Nanocrystals and Nanowires *Acc. Chem. Res.* **41** 1662–73

[75] Liu X, Long Y Z, Liao L, Duan X and Fan Z 2012 Large-scale integration of semiconductor nanowires for high-performance flexible electronics *ACS Nano* **6** 1888–900

[76] Whang D, Jin S, Wu Y and Lieber C M 2003 Large-scale hierarchical organization of nanowire arrays for integrated nanosystems *Nano Lett.* **3** 1255–9

[77] Duan S, Niu Q, Wei J, He J, Yin Y and Zhang Y 2015 Water-bath assisted convective assembly of aligned silver nanowire films for transparent electrodes *Phys. Chem. Chem. Phys.* **17** 8106–12

[78] Yu G, Cao A and Lieber C M 2007 Large-area blown bubble films of aligned nanowires and carbon nanotubes. *Nat. Nanotechnol.* **2** 372–7

[79] Smith P A, Nordquist C D, Jackson T N, Mayer T S, Martin B R, Mbindyo J and Mallouk T E 2000 Electric-field assisted assembly and alignment of metallic nanowires *Appl. Phys. Lett.* **77** 1399–401

[80] Freer E M, Grachev O, Duan X, Martin S and Stumbo D P 2010 High-yield self-limiting single-nanowire assembly with dielectrophoresis. *Nat. Nanotechnol.* **5** 525–30

[81] Hangarter C M and Myung N V. 2005 Magnetic alignment of nanowires *Chem. Mater.* **17** 1320–4

[82] Hu Z, Fischbein M D, Querner C and Drndić M 2006 Electric-field-driven accumulation and alignment of CdSe and CdTe nanorods in nanoscale devices *Nano Lett.* **6** 2585–91

[83] Trotsenko O, Tokarev A, Gruzd A, Enright T and Minko S 2015 Magnetic field

assisted assembly of highly ordered percolated nanostructures and their application for transparent conductive thin films *Nanoscale* **7** 7155–61

[84] Fan Z, Ho J C, Jacobson Z A, Yerushalmi R, Alley R L, Razavi H and Javey A 2008 Wafer-scale assembly of highly ordered semiconductor nanowire arrays by contact printing *Nano Lett.* **8** 20–5

[85] Javey A, Nam S, Friedman R S, Yan H and Lieber C M 2007 Layer-by-layer assembly of nanowires for three-dimensional, multifunctional electronics *Nano Lett.* **7** 773–7

[86] Lee J, Sun F and Lee J 2013 Fabrication of large area flexible and highly transparent film by a simple Ag nanowire alignment. *J. Exp. Nanosci.* **8** 130–7

[87] Tang H, Lin Y and Sodano H A 2012 Enhanced energy storage in nanocomposite capacitors through aligned PZT nanowires by uniaxial strain assembly *Adv. Energy Mater.* **2** 469–76

[88] Ma X, Zhu X, You F, Feng J, Wang M-C and Zhao X 2014 Preparation and optical polarization of Ag/epoxy composite films with aligned Ag nanowires *J. Alloys Compd.* **592** 57–62

[89] Hsieh G-W, Wang J, Ogata K, Robertson J, Hofmann S and Milne W I 2012 Stretched contact printing of one-dimensional nanostructures for hybrid inorganic-organic field effect transistors *J. Phys. Chem. C* **116** 7118–25

[90] Kang S, Kim T, Cho S, Lee Y, Choe A, Walker B, Ko S J, Kim J Y and Ko H 2015 Capillary printing of highly aligned silver nanowire transparent electrodes for high-performance optoelectronic devices *Nano Lett.* **15** 7933–42

[91] Tao A R, Huang J and Yang P 2008 Langmuir-Blodgettry of nanocrystals and nanowires *Acc. Chem. Res.* **41** 1662–73

[92] Feng J, Ma X, Mao H, Liu B and Zhao X 2011 Ag/epoxy nanocomposite film with aligned Ag nanowires and their polarization property *J. Mater. Res.* **26** 2691–700

[93] Sun Y, Liu K, Miao J, Wang Z, Tian B, Zhang L, Li Q, Fan S and Jiang K 2010 Highly sensitive surface-enhanced raman scattering substrate made from superaligned carbon nanotubes *Nano Lett.* **10** 1747–53

[94] Jeon Y J, Kang H W, Ko S H and Sung H J 2013 Pattern analysis of aligned nanowires in a microchannel *Meas. Sci. Technol.* **24** 035303

[95] Fan G Y and Cowley J M 1985 Auto-correlation analysis of high resolution electron micrographs of near-amorphous thin films *Ultramicroscopy* **17** 345–55

[96] Dong J, Abukhdeir N M and Goldthorpe I A 2015 Simple assembly of long nanowires through substrate stretching *Nanotechnology* **26** 485302

[97] Dong J, Goldthorpe I A and Abukhdeir N M 2016 Automated quantification of one-dimensional nanostructure alignment on surfaces *Nanotechnology* **27** 235701

[98] Yao J, Yan H and Lieber C M 2013 A nanoscale combing technique for the large-scale assembly of highly aligned nanowires. *Nat. Nanotechnol.* **8** 329–35

[99] Bradski G and Kaehler A 2008 *Learning OpenCV: Computer vision with the OpenCV library* (Sebastopol, California, USA: O'Reilly Media, Inc.)

[100] NumPy https://docs.scipy.org/doc/numpy-1.13.0/reference/ (Accessed: 17 July

2018)
[101] Park J R 2011 *Algorithms for Image Processing and Computer Vision* (Indianapolis: Wiley Publishing, Inc.)
[102] Lecun Y, Bengio Y and Hinton G 2015 Deep learning *Nature* **521** 436–44
[103] Suzuki S and Abe K 1985 Topological structural analysis of digitized binary images by border following *Comput. Vision, Graph. Image Process.* **30** 32–46
[104] Fitzgibbon A W and Fisher R B 1995 A buyer's guide to conic fitting *Proceedings of the British Machine Conference* (Birmingham) pp 513–22
[105] Zannoni C 1988 Order parameters and orientational distributions in liquid crystals *Polarized Spectroscopy of Ordered Systems* (Berlin: Springer) pp 57–83
[106] Eppenga R and Frenkel D 1984 Monte Carlo study of the isotropic and nematic phases of infinitely thin hard platelets *Mol. Phys.* **52** 1303–34
[107] Liu X, Long Y Z, Liao L, Duan X and Fan Z 2012 Large-Scale Integration of Semiconductor Nanowires for High-Performance Flexible Electronics *ACS Nano* **6** 1888–900
[108] de Gennes P G and Prost J 1995 *The Physics of Liquid Crystals* (New York: Oxford University Press)
[109] Straley J P 1971 Liquid crystals in two dimensions *Phys. Rev. A* **4** 675–81
[110] Cuesta J and Frenkel D 1990 Monte Carlo simulation of two-dimensional hard ellipses *Phys. Rev. A* **42** 2126
[111] Buades A, Coll B and Morel J-M 2011 Non-Local Means Denoising *Image Process. Line* **1** 490–530
[112] Otsu N 1979 A Threshold Selection Method from Gray-Level Histograms *IEEE Trans. Syst. Man. Cybern.* **9** 62–6
[113] Haralick R M, Sternberg S R and Zhuang X 1987 Image Analysis Using Mathematical Morphology *IEEE Trans. Pattern Anal. Mach. Intell.* **9** 532–50
[114] Dougherty E R and Lotufo R A 2003 Hands-on Morphological Image Processing vol 71 (Washington, DC: SPIE Optical Engineering Press)
[115] Dan B, Irvin G C and Pasquali M 2009 Continuous and scalable fabrication of transparent conducting carbon nanotube films *ACS Nano* **3** 835–43
[116] Hu W, Niu X, Li L, Yun S, Yu Z and Pei Q 2012 Intrinsically stretchable transparent electrodes based on silver-nanowire–crosslinked-polyacrylate composites *Nanotechnology* **23** 344002
[117] Hibino K and Kimura Y 2000 Epoxy resin particles. I. Spontaneous particle formation by the polymerization reaction of epoxy resin in a stationary system using polyethers as organic media *Colloid Polym. Sci.* **278** 565–70
[118] Colin A C, Cancho S M, Rubio R G and Compostizo A 1997 Equation of State of Hydrogen-Bonded Polymer Solutions . Poly (propylene glycol) + n -Hexane and Poly (propylene glycol) + Ethanol *Macromolecules* **30** 3389–94
[119] Chen W and McCarthy T J 1998 Chemical Surface Modification of Po ly(ethylene terephthalate) *Macromolecules* **31** 3648–55
[120] Mohammadimasoudi M, Penninck L, Aubert T, Gomes R, Hens Z, Strubbe F and Neyts K 2013 Fast and versatile deposition of aligned semiconductor nanorods by dip-coating on a substrate with interdigitated electrodes *Opt. Mater.*

Express **3** 2045–54

[121] Mohammadimasoudi M, Penninck L, Aubert T, Gomes R, Hens Z, Strubbe F and Neyts K 2014 Polarized light emission by deposition of aligned semiconductor nanorods *PROCEEDINGS OF THE SOCIETY OF PHOTO-OPTICAL INSTRUMENTATION ENGINEERS* vol 9170 (San Diego) p 917013

[122] Han M H, Shin J K, Oh K Il, Lee Y J, Song D H, Sik Y, Lee Y R, Choi H G, Oh T H, Han S S and Noh S K 2010 Preparation of Recycled Poly (vinyl alcohol) (PVA)/ Iodine Polarizing Film *Polym. Polym. Compos.* **18** 391–6

[123] Azoz S, Exarhos A L, Marquez A, Gilbertson L M, Nejati S, Cha J J, Zimmerman J B, Kikkawa J M and Pfefferle L D 2015 Highly conductive single-walled carbon nanotube thin film preparation by direct alignment on substrates from water dispersions *Langmuir* **31** 1155–63

[124] Zhu S, Gao Y, Hu B, Li J, Su J, Fan Z and Zhou J 2013 Transferable self-welding silver nanowire network as high performance transparent flexible electrode. *Nanotechnology* **24** 335202

[125] Cheong H G, Triambulo R E, Lee G H, Yi I S and Park J W 2014 Silver nanowire network transparent electrodes with highly enhanced flexibility by welding for application in flexible organic light-emitting diodes *ACS Appl. Mater. Interfaces* **6** 7846–55

[126] Li B, Ye S, Stewart I E, Alvarez S and Wiley B J 2015 Synthesis and Purification of Silver Nanowires to Make Conducting Films with a Transmittance of 99% *Nano Lett.* **15** 6722–6

[127] Wayner P C, Tung C Y, Tirumala M and Yang J H 1985 Experimental study of evaporation in the contact line region of a thin film of hexane *J. Heat Transfer* **107** 182–9

[128] Hecht D S, Hu L and Irvin G 2011 Emerging transparent electrodes based on thin films of carbon nanotubes, graphene, and metallic nanostructures *Adv. Mater.* **23** 1482–513

[129] Kim E-H, Yang C-W and Park J-W 2011 The crystallinity and mechanical properties of indium tin oxide coatings on polymer substrates *J. Appl. Phys.* **109** 043511

[130] Kim H, Gilmore C M, Piqué A, Horwitz J S, Mattoussi H, Murata H, Kafafi Z H and Chrisey D B 1999 Electrical, optical, and structural properties of indium–tin–oxide thin films for organic light-emitting devices *J. Appl. Phys.* **86** 6451–61

[131] Mryasov O and Freeman A 2001 Electronic band structure of indium tin oxide and criteria for transparent conducting behavior *Phys. Rev. B* **64** 233111

[132] Transparent conductive films https://ocsial.com/en/application/films/ (Accessed: 17 July 2018)

[133] Khaligh H H and Goldthorpe I A 2013 Failure of silver nanowire transparent electrodes under current flow. *Nanoscale Res. Lett.* **8** 235

[134] Khaligh H H 2016 *Silver nanowire transparent electrodes for device applications* (PhD thesis, University of Waterloo, Canada)

[135] Nam S, Song M, Kim D-H, Cho B, Lee H M, Kwon J-D, Park S-G, Nam K-S, Jeong Y, Kwon S-H, Park Y C, Jin S-H, Kang J-W, Jo S and Kim C S 2014 Ultrasmooth, extremely deformable and shape recoverable Ag nanowire embedded transparent electrode. *Sci. Rep.* **4** 4788

[136] Kowalska D, Krajnik B, Olejnik M, Twardowska M, Czechowski N, Hofmann E and MacKowski S 2013 Metal-enhanced fluorescence of chlorophylls in light-harvesting complexes coupled to silver nanowires *Sci. World J.* **2013**

[137] Scardaci V, Coull R, Lyons P E, Rickard D and Coleman J N 2011 Spray deposition of highly transparent, low-resistance networks of silver nanowires over large areas *Small* **7** 2621–8

[138] Tokuno T, Nogi M, Jiu J and Suganuma K 2012 Hybrid transparent electrodes of silver nanowires and carbon nanotubes: A low-temperature solution process *Nanoscale Res. Lett.* **7** 1–7

[139] Jeon Y, Jin H B, Jung S, Go H, Lee I, Lee C, Joo Y K and Park K 2015 Highly flexible touch screen panel fabricated with silver nanowire crossing electrodes and transparent bridges *J. Opt. Soc. Korea* **19** 508–13

[140] Li J, Tao Y, Chen S, Li H, Chen P, Wei M Z, Wang H, Li K, Mazzeo M and Duan Y 2017 A flexible plasma-treated silver-nanowire electrode for organic light-emitting devices *Sci. Rep.* **7** 1–9

[141] Pathirane M K, Khaligh H H, Goldthorpe I A and Wong W S 2017 Al-doped ZnO/Ag-nanowire Composite Electrodes for Flexible 3-Dimensional Nanowire Solar Cells *Sci. Rep.* **7** 1–7

[142] Haptic Touchscreen Market https://www.prnewswire.com/news-releases/haptic-touchscreen-market-2025---2017-development-report-on-the-20-billion-industry-300542005.html (Accessed: 17 July 2018)

[143] Jagota M and Tansu N 2015 Conductivity of Nanowire Arrays under Random and Ordered Orientation Configurations. *Sci. Rep.* **5** 10219

[144] Bellew A T, Manning H G, Gomes da Rocha C, Ferreira M S and Boland J J 2015 Resistance of Single Ag Nanowire Junctions and Their Role in the Conductivity of Nanowire Networks *ACS Nano* **9** 11422–9

[145] Schadt M 1989 Plenary Lecture: The history of the liquid crystal display and liquid crystal material technology *Liq. Cryst.* **5** 57–71

[146] Castellano J A 2006 Modifying Light: Ubiquitous today, liquid-crystal displays are the outgrowth of more than a century of experimentation and development *Am. Sci.* **94** 438–45

[147]Schadt M 1997 Liquid Crystal Materials and Liquid Crystal Displays *Annu. Rev. Mater. Sci.* **27** 305–79

[148] Zhang J, Zhang L, Ye C, Chang M, Yan Y and Lu Q 2004 Polarization properties of ordered copper nanowire microarrays embedded in anodic alumina membrane *Chem. Phys. Lett.* **400** 158–62

[149] Pelletier V, Asakawa K, Wu M, Adamson D H, Register R A and Chaikin P M 2006 Aluminum nanowire polarizing grids: Fabrication and analysis *Appl. Phys. Lett.* **88** 211114

[150] Papalia J M, Adamson D H, Chaikin P M and Register R A 2010 Silicon nanowire polarizers for far ultraviolet (sub-200 nm) applications: Modeling and fabrication *J. Appl. Phys.* **107** 084305
[151] Ordal M A, Long L L, Bell R J, Bell S E, Bell R R, Alexander R W and Ward C A 1983 Optical properties of the metals Al, Co, Cu, Au, Fe, Pb, Ni, Pd, Pt, Ag, Ti, and W in the infrared and far infrared. *Appl. Opt.* **22** 1099–120
[152] Ehrenreich H and Philipp H R 1962 Optical Properties of Ag and Cu *Phy. Rev.* **128** 1622–9
[153] Feng J, Zhao Y, Lin X W, Hu W, Xu F and Lu Y Q 2011 A transflective nano-wire grid polarizer based fiber-optic sensor *Sensors* **11** 2488–95
[154] Pang Y T, Meng G W, Fang Q and Zhang L D 2003 Silver nanowire array infrared polarizers *Nanotechnology* **14** 20–4
[155] Kaneko E 1987 *Liquid Crystal TV Displays: Principles and applications of Liquid Crystal Displays* (KTK Scientific Publishers Tokyo)
[156] Solar cells: In the fast lane http://nature.com/am/journal/2011/201102/full/am201151a.html (Accessed: 8 July 2017)
[157] Different Type of OLED https://flexible-screen.wikispaces.com/Different+types+of+OLED (Accessed: 8 July 2017)
[158] PI Series (Projected Capacitive Touch Screen) http://gtouch.com.tw/products_panels_pi.html (Accessed: 8 July 2017)
[159] Khaligh H H and Goldthorpe I A 2014 Hot-rolling nanowire transparent electrodes for surface roughness minimization. *Nanoscale Res. Lett.* **9** 310
[160] Madeira A 2018 *Enhancing the performance of transparent electrodes through the design of new silver nanostructures* (PhD thesis, University of Waterloo, Canada)
[161] CST Microwave Studio, 492 Old Connecticut Path, Framingham, MA 01701, 2016
[162] Palik E D 1985 *Handbook of optical constants of solids* (Orlando: Academic Press)
[163] Pelletier V 2005 *Physics and Technology of Sheared Cylinder-Forming Diblock Copolymer Thin Films* (PhD Thesis, Princeton University, USA)
[164] Li Y, Qian F, Xiang J and Lieber C M 2006 Nanowire electronic and optoelectronic devices Electronic and optoelectronic devices impact many areas of society , from *Mater. Today* **9** 18–27
[165] Cui Y, Wei Q, Park H and Lieber C M 2001 Nanowire nanosensors for highly sensitive and selective detection of biological and chemical species. *Science (80-.).* **293** 1289–92
[166] Kuang Q, Lao C, Wang Z L, Xie Z and Zheng L 2007 High-sensitivity humidity sensor based on a single SnO2 nanowire. *J. Am. Chem. Soc.* **129** 6070–1
[167] Patolsky F and Lieber C M 2005 Nanowire nanosensors *Mater. Today* **8** 20–8
[168] Wang Z L 2010 Piezopotential gated nanowire devices: Piezotronics and piezo-phototronics *Nano Today* **5** 540–52

[169] Kerman A, Dauler E and Robinson B 2006 Superconducting nanowire photon-counting detectors for optical communications *Lincoln Lab. J.* **16** 217–24
[170] Yan F, Wang Y, Zhang J, Lin Z, Zheng J and Huang F 2014 Schottky or Ohmic metal-semiconductor contact: Influence on photocatalytic efficiency of Ag/ZnO and Pt/ZnO model systems *ChemSusChem* **7** 101–4
[171] Amjadi M, Pichitpajongkit A, Lee S, Ryu S and Park I 2014 Highly stretchable and sensitive strain sensor based on silver nanowire-elastomer nanocomposite *ACS Nano* **8** 5154–63
[172] Song M, Park J H, Kim C S, Kim D-H, Kang Y-C, Jin S-H, Jin W-Y and Kang J-W 2014 Highly flexible and transparent conducting silver nanowire/ZnO composite film for organic solar cells *Nano Res.* **7** 1370–9
[173] Perez Huertas S, Terpilowski K, Wisniewska M and Zarko V 2017 Influence of polyvinylpyrrolidone adsorption on stability of silica aqueous suspension - effects of polymer concentration and solid content *Physicochem. Probl. Miner. Process.* **53** 121–35
[174] Cui S, Liu H, Gan L, Li Y and Zhu D 2008 Fabrication of low-dimension nanostructures based on organic conjugated molecules *Adv. Mater.* **20** 2918–25
[175] Sakurai M, Wang Y G, Uemura T and Aono M 2009 Electrical properties of individual ZnO nanowires *Nanotechnology* **20**
[176] Xu J, Chen L, Mathewson A and Razeeb K M 2011 Ultra-long metal nanowire arrays on solid substrate with strong bonding *Nanoscale Res. Lett.* **6** 1–7
[177] Hsu C-H and Chen D-H 2010 Synthesis and conductivity enhancement of Al-doped ZnO nanorod array thin films *Nanotechnology* **21** 285603